UNIVERSITÀ DEGLI STUDI DI PADOVA

DIPARTIMENTO DI INGEGNERIA INDUSTRIALE
Corso di laurea Magistrale in Ingegneria Energetica

Tesi di laurea Magistrale in
Ingegneria Energetica

Design and Performance Evaluation of an Organic Rankine Cycle System Exploiting the Low Grade Waste Heat of the Main Engines in a LNG Carrier

Relatori: ***Prof. Christos A. Frangopoulos***[a]
Prof. Andrea Lazzaretto[b]

Correlatori: ***Ph.D. Giovanni Manente***[b]
Ph.D. Sergio Rech[b]

Laureando: ***Marco Soffiato***

[a] *National Technical University of Athens, Greece*
[b] *University of Padova, Italy*

ANNO ACCADEMICO 2013 – 2014

ABSTRACT

Organic Rankine Cycle (ORC) technology may represent an interesting way to exploit the low grade waste heat rejected by the ship power generating plant. This option has been investigated here to recover the heat available from three of the four engines of a real electrically driven Liquefied Natural Gas (LNG) carrier, when the electric power output is equal to 23,375 kW. A detailed analysis of the engines operation was first performed to create a reliable set of thermodynamic parameters that fulfil the energy balance of the engines. Heat associated with the jacket water, lubricating oil and charge air cooling of the engines has been considered to be available for the ORC, while the heat from the exhaust gases is already exploited to generate low pressure steam for ship internal use. Simple, regenerative and two-stage ORC configurations have been compared using six different organic fluids that were selected as the most suitable for this application. The thermal matching that maximizes the net power output of the total system including engine cooling circuits and ORC cycle is found by applying the Heatsep method, which allows the optimum heat transfer between thermal streams to be evaluated independently of the structure/number of the heat exchangers within the system. Three layouts of the cooling systems collecting the heat available from the engines have been compared. Results show that the maximum net power output (820 kW) that is achievable by the two-stage configuration almost doubles the simple cycle and regenerative ones (430÷580 kW). Economic feasibility has been studied taking into consideration the operation of the ORC system over the year.

RIASSUNTO

La tecnologia del ciclo Rankine a fluido organico (ORC) può rappresentare un'interessante opportunità per lo sfruttamento del calore a bassa temperatura usualmente rigettato all'ambiente dagli impianti di generazione di potenza a bordo navi. Quest'applicazione è stata investigata con riferimento ad una nave metaniera a trazione elettrica attualmente in esercizio, laddove tre dei quattro motori principali sono considerati operativi e forniscono complessivamente una potenza elettrica pari a 23,375 kW. Un'analisi dettagliata del funzionamento dei motori ha consentito di definire un insieme affidabile di parametri termodinamici che caratterizzano in quantità e in qualità i vari flussi termici disponibili e che soddisfano il bilancio energetico dei motori stessi. Il calore associato all'acqua di camicia, all'olio lubrificante, e quello legato al raffreddamento dell'aria di sovralimentazione è stato considerato quale sorgente calda per il ciclo ORC; il calore associato ai fumi di scarico è risultato essere non disponibile poiché riservato alla generazione di vapore a bassa pressione. Sono state confrontate tre differenti configurazioni per il ciclo ORC: ciclo semplice, ciclo rigenerativo e ciclo a due livelli di pressione. Sei fluidi organici sono stati selezionati e considerati nello studio quali sostanze di lavoro adatte alla particolare applicazione. L'accoppiamento termico che massimizza la potenza netta del sistema complessivo comprendente i circuiti di raffreddamento dei motori e il ciclo ORC è stato determinato attraverso l'applicazione del metodo Heatsep che consente di determinare il trasferimento di calore ottimale tra flussi termici caldi e freddi, indipendentemente dalla struttura/numero di scambiatori di calore necessari. Tre layout per i sistemi di raffreddamento dei motori sono stati definiti e confrontati. I risultati evidenziano come il massimo della potenza netta ottenibile con la configurazione a due livelli di pressione (820 kW) quasi raddoppia il valore delle soluzioni a ciclo semplice e rigenerativo (430 ÷ 580 kW). La fattibilità economica dei cicli ORC è stata studiata considerando il funzionamento del sistema nel corso dell'anno.

CONTENTS

NOMENCLATURE

Acronyms

AC	air cooler	HU	hot utility
CCC	cold composite curve	LO	lubricating oil
CU	cold utility	LOC	lubricating oil Cooler
EGB	exhaust gas boiler	M/E	main engine
FO	fuel oil	ODP	ozone depletion potential
FW	fresh water	ODS	ozone depletion substances
FWC	fresh water cooler	SF	size factor
FWG	fresh Water generator	SW	sea water
GWP	global warming potential	T/C	turbocharger
HCC	hot composite curve	VR	volumetric expansion ratio
HEN	heat exchanger network		

Symbols

b	specific fuel energy consumption	kJ/kWh
c_p	specific heat capacity	kJ/(kg·K)
h	specific enthalpy	kJ/kg
$\dot{H}$	energy flow	kW
$\dot{Q}$	thermal power	kW
H_u	lower heating value	kJ/kg
IRR	internal rate of return	%
NPV	net present value	k$
p_r	reduced pressure	-
PP	payback period	year
PWF	present worth factor	-
R	gas constant	J/(kg·K)
s	specific entropy	kJ/(kg·K)
T	temperature	K
t	time	s
V	speed	kn
$\dot{V}$	volumetric flow rate	m^3/s
$\dot{m}$	mass flow rate	kg/s
$\dot{W}$	electrical or mechanical power	kW

Greek letters

τ	reduced temperature by the value at the critical point
σ	molecular complexity
γ	specific heat capacity ratio
η	efficiency
Φ	effectiveness of the heat transfer
ξ	inverse of the saturated vapour curve slope on T-s diagram
χ	quality

Subscripts

a	air	lg	latent heat
A	engine-generator set model Wärtsilä 6L50DF	lo	lubricating oil
		m	mechanical
absorbed	absorbed	net	net
ac	air cooler	o	reference
B	engine-generator set model Wärtsilä 12V50DF	out	outlet
		p	propulsion
c	critical	pp	pinch point
con	condensing condition	pump	pump
d	distillate	r	radiation and convection losses
e	electric		
eg	exhaust gas	reg	regenerative
ep	except of propulsion	s	service
ev	evaporation condition	sub	subcritical
exp	expander	sup	superheating
f	fuel	spc	supercritical
fg	gaseous fuel	sv	saturated vapour
fl	liquid fuel	t	total heat recovery
in	inlet	th	thermal
is	isentropic	w	water
jw	jacket water		
lg	electric generator losses		

1 INTRODUCTION

The development of efficient ships has been attracted increasing interest in the last years because of economic and environmental reasons. The economic crises combined with the rising of the international crude oil prices have accentuated the keen global competition that characterized the shipping industries. Also, certain regulations have been introduced in order to reduce the pollution of oceans and seas [MARPOL (2002)]. In this context, several paths are under investigation in order to improve ships efficiency thus reducing fuel needs. They might be grouped under four main headings: ship design (i.e., efficiency of the scale, ballast reduction, use of optimum main dimensions), propulsion, machinery (i.e., auxiliary power generation, use of electric drives, waste heat recovery), operation & maintenance (i.e., speed of the vessel, hull cleaning) [Wärtsilä (2009)].

Despite of the wide availability of technologies, most of the ships do not integrate appropriate energy recovery systems on board. While sailing in water, less than 50% of the primary energy associated with the fuel is usually converted into mechanical or electric power and the remaining part is mostly rejected to the environment. Mainly, two types of waste heat recovery systems have been coupled with the main engines of a ship [Choi and Kim (2013)]: the first one consists in a power turbine exploiting the kinetic energy associated with the exhaust gas while the second one is based on a bottoming Rankine cycle which uses water as working fluid. However, other technologies including organic Rankine cycle (ORC) technology have been proposed for marine applications [Shu et al. (2013)]. In particular, the use of ORC systems is widely regarded as one of the most promising way for converting low temperature waste heat into power [Larsen et al. (2013)]; this is because the choice of the appropriate working fluid among all the possibilities allows the matching between thermal sources and thermodynamic cycle to be optimized thus increasing the overall efficiency even in case of low grade sources.

The first use of an ORC system aboard a ship has been found to be the module installed on a car-truck carrier [Öhman and Lundqvist (2013)]. The expectation was to obtain a 4÷6% fuel saving using R-236fa as working fluid [Tchanche et al. (2011)]. Only a few research papers are available in literature about ORC systems on ships [Choi and Kim (2013)], [Larsen et al. (2013)], but several other works concerning the coupling with internal combustion engines (ICEs) can be referred to as reference. In fact, thermal sources to be exploited on ships are mainly represented by the main engines exhaust gas and cooling flows. A certain amount of heat associated with these sources is usually used to produce fresh water (i.e., desalinated water) and low pressure steam required by auxiliary systems and for sanitary purposes [Dimopoulos and Frangopoulos (2008)]. Only

the residual quantity can be exploited by a recovery system because the needs of the vessel must always be satisfied first.

Sprouse and Depcik (2013) presented a review of ORCs for ICEs reporting that fluids R-245ca and R-245fa have been found to be suitable for waste heat recovery applications in case of turbine inlet temperature below 180°C. Wang et al. (2013) analysed the performance of an ORC system and suggested the best working fluids for various temperature level of the heat source. Baik et al. (2011) proposed a comparison between carbon dioxide and R-125 exploiting a low-grade heat source of about 100°C. Fluid R-125 has been suggested as the best choice due to the higher net power output. The same fluid showed high recovery efficiency and a good economic performance for utilization of a 90°C thermal source in Shengjun et al. (2011). Guo et al. (2011) investigated 27 working fluids to be used in the ORC section of a cogeneration system exploiting a 90°C temperature geothermal source. Fluids R-245ca and R-245fa showed high power output. Fu et al. (2013) presented a comparison between an ORC system and a Kalina cycle system exploiting a geothermal source of less than 140°C. Net power output of the Kalina cycle was higher than that of the ORC when the heat source temperature was above 100°C. However, the good performance of the Kalina cycle has been achieved by setting a very high evaporation pressure. As regards the ORC system, net power output achieved by using R-236fa as working fluid was higher than R-245fa. The superiority of fluid R-236fa over R-245fa has also been found by [Lazzaretto and Manente (2013)] in case of a 150°C temperature heat source. Branchini et al. (2013) presented the performance evaluation of various ORC configurations with respect to six thermodynamic indexes. In case of 200°C temperature heat source, fluid R-245fa showed best performance.

Vaja and Gambarotta (2010) analysed three different coupling between an ORC system and an ICE. The exhaust gas has been considered as thermal source for all the cases while the exploitation of the engine cooling water was investigated only to preheat the working fluid. Smolen (2011) proposed a two-stage ORC system exploiting both the thermal sources. In this cycle, the evaporation of the working fluid took place at two different pressure levels. A more complex solution is represented by the dual-loop bottoming ORC proposed by Wang E.H. et al. (2012) and Zhang et al. (2013). Working fluids for the high (HT) and low temperature (LT) loops were R-245fa and R-134a, respectively. A similar solution was the dual-loop Rankine cycle of Shu et al. (2013) where water was used as working fluid of the HT loop and six organic fluids have been investigated for the LT loop.

Several studies found in literature compare the performance of fluids and different ORC concepts when the layout of the heat exchanger network (HEN) that feeds the system itself is fixed first. This means that the exploitation of each thermal source fulfills a specific function in the heating process of the working fluid (i.e., preheating, evaporation or superheating) that is pre-defined. This approach simplifies the analysis of the system

by reducing the degrees of freedom of the coupling (ORC and thermal sources) but in some cases might not allow the optimal thermal matching to be obtained. A different approach based on the pinch analysis rules has been used by Desai and Bandyopadhyay (2009) that searched for the optimal integration of an ORC system with a “background process”. Analogous work has been proposed by Di Genova et al. (2013) exploiting the hot streams available from a Fischer Tropsch synthesis plant.

In the present work, the Heatsep method [Lazzaretto and Toffolo (2008)] is applied to the synthesis/design optimization of an ORC system exploiting the waste heat of a liquefied natural gas (LNG) carrier that is actually in operation. The method looks for the values of the ORC design parameters that allow the best thermal coupling between thermal sources and ORC itself to be obtained, thus optimizing the overall system. Three ORC concepts have been considered including single pressure level and two-pressure level design options. Both subcritical and supercritical cycles have been investigated.

2 FLUIDS FOR ORGANIC RANKINE CYCLES

2.1 Introduction

Several fluids have been proposed in literature to be used in Organic Rankine cycle (ORC) systems, especially for low grade waste heat recovery applications. Characteristics and properties of the fluids affect directly the performance of the ORC systems; a suitable fluid should present good physical, chemical, economic, environmental and safety properties.

This chapter is aimed to compare the working fluids under various point of view providing useful information that will be used for the selection of the suitable mediums for the system studied in the present work.

2.2 Definition and Classification

Most fluids used in Organic Rankine Cycles (ORCs) are called "organic" referring to their chemical structure. They are pure fluids or mixtures based on compounds that present bounds between atoms of carbon (C). In these molecules there is also the presence of a few other elements, mainly hydrogen, oxygen and nitrogen.

Carbon oxides (CO_x), carbonic acid (H_2CO_3) and carbonic salts such as calcium carbonate ($CaCO_3$) are excluded from this category and they are considered inorganic compounds.

The accepted definition for ORCs does not exclude the use of inorganic fluids in these systems, thus substances like ammonia NH_3 and carbon dioxide CO_2 can be considered as working mediums and the name of the cycle remains the same [Chen et al. (2010)]. Figure 2.1 presents some working fluids that are used in ORCs.

ORGANIC RANKINE CYCLES

Organic Fluids	Inorganic Fluids
R-143a	R-717
R-227ea	R-744
R-245fa	

Figure 2.1 Examples of working fluids.

The regulation ANSI/ASHRAE 34 (2007) proposes a method to classify the fluids on the basis of their chemical composition. The assigned name is composed of a prefix made up of letters and a suffix made up of digits. For refrigerants, the prefix is the letter “R”. The sets of digits that compose the suffix depend on the kind of compound or mixture and are presented in Table 2.1. In the case of isomers, the most symmetrical one is indicated by the combination of prefix and suffix. The others are indicated adding also a lowercase letter in the decreasing order of symmetry. Sometimes two letters are used, if required.

Table 2.1 Suffixes used to compose the name of the fluid.

Kind of fluid	Rule
Hydrocarbons and derivatives	The suffix is composed of four digits: W X Y Z. W number of unsaturated carbon-carbon bonds (omitted if equal to zero). X number of carbon atoms (C) minus 1 (omitted if equal to zero). Y number of hydrogen atoms (H) plus 1. Z number of fluorine atoms (F). Examples: R-134a, R-125.
Zeotropic mixture	The suffix is a number in the 400 series that is representative only of the components of the mixture (no information about the amount of each component). The number given to each fluid is decided by ASHRAE. Examples: R-407c, R-410a.
Azeotropic mixture	The suffix is a number in the 500 series. Example: R-502, R-500a.
Other organic compounds	The suffix is a number in the 600 series. Examples: isobutene R-600a.
Natural fluids	The suffix is a number in the 700 series. The last two digits are representative of the molecular mass. Examples: ammonia R-717, carbon dioxide R-744.

2.3 Categories of the Working Fluids

According to Hung et al. (1997), the classification of the working fluids can be based on the slope of the saturated vapour curve on T-s diagram. The defined categories are three: “dry fluids”, “isentropic fluids” and “wet fluids” in the case of positive, nearly infinite or negative slope, respectively (Figure 2.2). Through the parameter ξ, defined as the inverse of the slope, it is possible to quantify whether a fluid is dry, isentropic or wet ($\xi>0$, $\xi\approx0$, $\xi<0$):

$$\xi = \frac{ds}{dT} \tag{2.1}$$

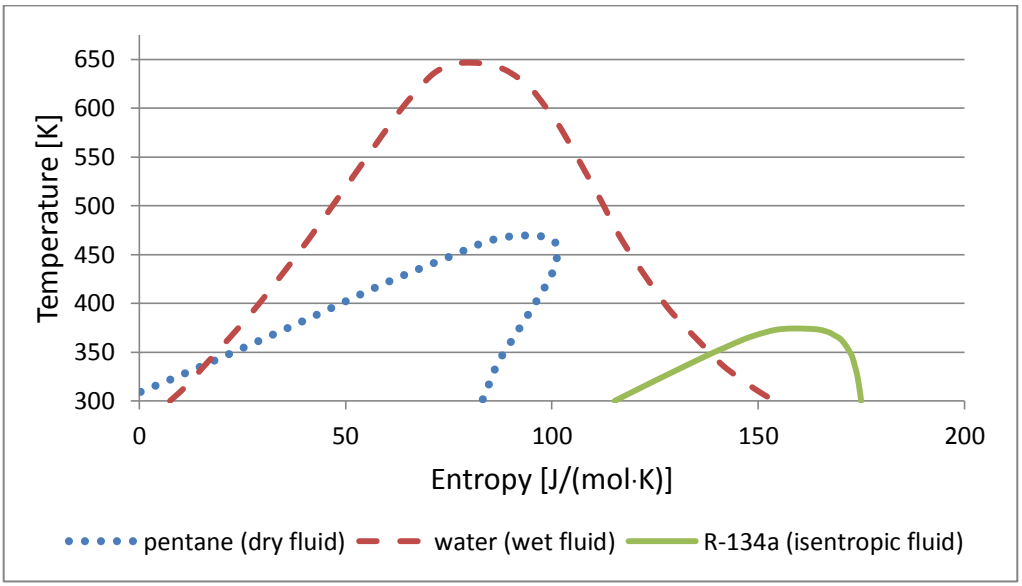

Figure 2.2 Three categories of the working fluids.

Liu (2002) derived Eq. (2.2) to evaluate ξ:

$$\xi = \frac{c_p}{T_{ev}} - \frac{\frac{n\cdot\tau_{ev}}{1-\tau_{ev}}+1}{T_{ev}^{\,2}}\cdot h_{lg} \tag{2.2}$$

where n is suggested to be 0.375 or 0.38, τ_{ev} denotes the reduced evaporation temperature by the critical temperature (T_{ev} / T_c), h_{lg} is the latent heat and c_p is the specific heat capacity.

Of course the type of each fluid is related to the chemical structure of the molecule (molecules in the case of mixture), however it was observed that the presence of hydrogen bonds interactions results in a higher latent heat and the fluid becomes “wet”.

Furthermore, regarding “wet fluids”, Hung (1997) stated that usually they have low molecular weights.

Because of the simplifications adopted to develop Eq. (2.2), Chen et al. (2010) noted that its use instead of the direct calculation of the slope through the entropy and temperature data, leads to a large deviation at off-normal boiling points and so they suggest to calculate ξ by direct application of Eq. (2.1), if possible.

In order to provide a few examples, fluids like R-125, R-143a and R-152a are wet. R-123, R-134fa are isentropic and R-236fa, R-600, R-600a are dry.

Another parameter that can give information about the slope of the saturated vapour line of a substance is the molecular complexity σ defined by Invernizzi et al. (2007) through Eq. (2.3):

$$\sigma = \frac{T_c}{R}\left(\frac{\delta s}{\delta T}\right)_{sv,\tau_{ev}=0.7} \tag{2.3}$$

where R is the gas constant and the subscription “*sv*” refers to the saturated vapour line. This coefficient is primarily a function of the heat capacity of the vapour and is related to the molecular structure of the fluid. For homologous fluids the molecular complexity rises with the number of atoms of the molecule.

Under the hypothesis of saturated vapour comparable to an ideal gas, Eq. (2.3) becomes [Invernizzi et al. (2007)]:

$$\sigma = \left[-\frac{1}{p_r}\left(\frac{dp_r}{d\tau}\right)_{sv} + \frac{\gamma}{\gamma - 1}\cdot\frac{1}{\tau}\right]_{sv,\,\tau=0.7} \tag{2.4}$$

where

- γ specific heat capacity ratio,
- p_r reduced pressure,
- τ reduced temperature,

and the other symbols have the same meaning of Eq. (2.3).

For simple molecules the slope of the saturated vapour line in the T-s diagram is negative and the term $-\left(dp_r/d\tau\right)_{sv}/p_r$ prevails on the positive term $\gamma/\left[\left(\gamma-1\right)\cdot\tau\right]$. With the increase of the molecular complexity, the slope of the saturated vapour line becomes positive (Figure 2.3).

The category of the working fluid used in an ORC cycle affects the choice and the arrangement of the components within the system as will be presented in the next chapter (Section 3.6).

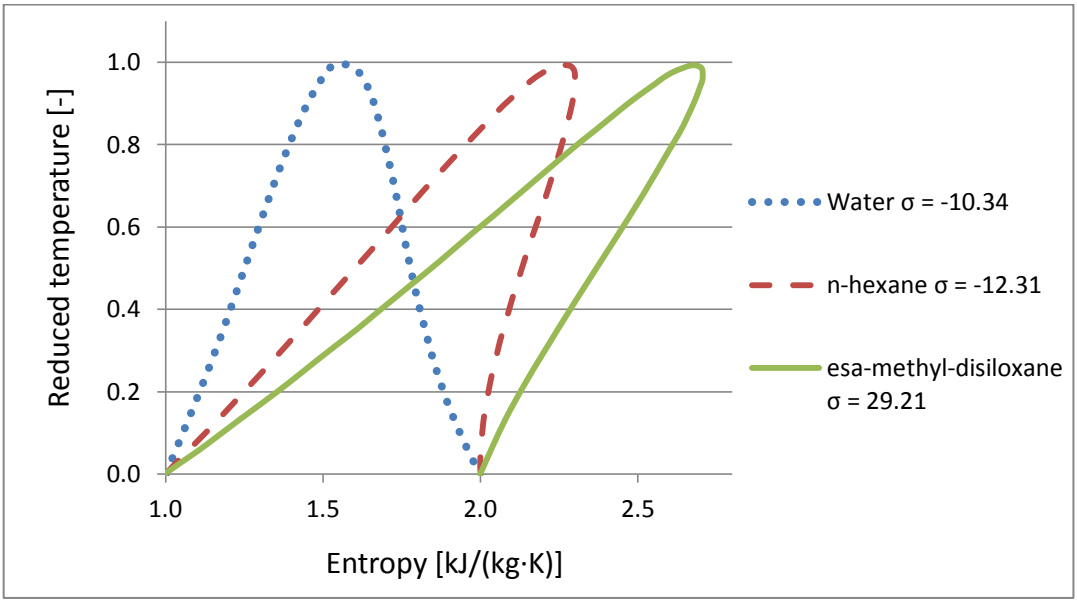

Figure 2.3 Relation between the molecular complexity and the slope of the saturated vapour line [Invernizzi et al. (2007)].

2.4 Critical Point of the Working Fluids

The critical point of a fluid is at the peak point of the fluid saturation line in the diagram Temperature-Entropy (T-s). This state is characterized by two parameters: the critical temperature T_c and the critical pressure p_c. They represent the highest values of temperature and pressure at which both a gaseous and a liquid phase of a fluid can coexist. The intensive properties (density, heat capacity, etc.) become equal for the two phases [McNaught et al. (1997)] and at this state, the heat of vaporization is zero. Moreover, an increase in pressure of a gas phase cannot form a liquid.

Angelino et al. (1984) considering seven alkanes, from normal-butane C_4H_{10} to normal-decane $C_{10}H_{22}$, noted the relation between molecular complexity and critical point. Being the molecular complexity a function of the number of atoms in the molecule, it was observed that while it grows from butane to decane, the critical pressure decreases and the critical temperature increases. The same observation regarding various fluids was made by Invernizzi et al. (2007).

Figure 2.4 presents the critical points of the aforementioned fluids.

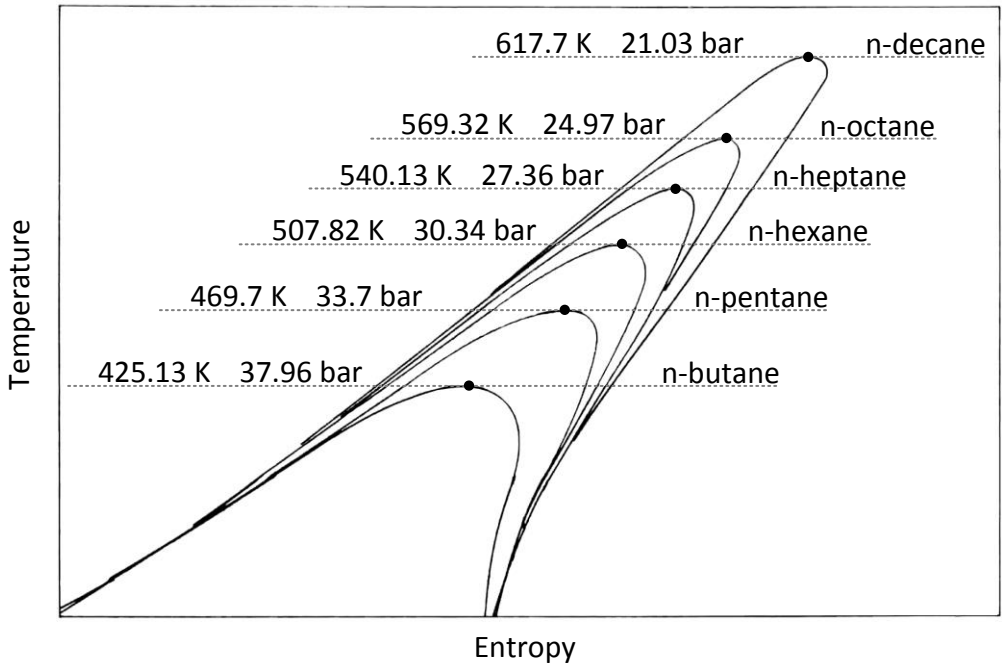

Figure 2.4: Critical point of some Alkanes [Angelino et al. (1984)].

2.5 Chemical Stability and Compatibility with Materials in Contact

Most organic fluids suffer chemical decomposition and deterioration at high temperatures and pressures. Because of this, it is important to check that they are operated well below the unstable conditions [Hung et al. (1997)].

The working fluids should be non-corrosive and compatible with materials and fluids that could come in contact, such as the metal of pipelines and the lubricating oil [Chen et al. (2010)]. Moreover, the products of the decomposition of certain organic fluids could be corrosive and this makes it necessary to pay attention at the conditions under which fluids are operated.

Calderazzi and Colonna di Paliano (1997) proposed a method and studied the thermal stability of R-134a, R-141b, R-1311, R-7146, and R-125 when they are in contact with stainless steel. Also Andersen and Bruno (2005) made studies in this field determining the decomposition reaction rate constant of four fluids at the temperature and the pressure of interest.

Providing an example about fluids compatibility with materials in contact, ammonia is corrosive and it cannot be used with copper heat exchangers.

2.6 Environmental Regulations

Due to the environmental issues and the concerns regarding the climate changes, in the recent years more attention was placed to the evaluation of effects of the emissions in the atmosphere. Certain regulations were then introduced to plan the phase out of the harmful fluids.

Certain parameters were defined and used to make comparison between different fluids and they are presented in the following sub-sections.

2.6.1. Ozone depletion potential

The ozone depletion potential (ODP) measures the effects of a compound upon the ozone layer [Wuebbles (1983)]. This parameter quantifies the global ozone losses due to the release of a particular molecule relative to a reference molecule that generally is R-11 ($CFCl_3$).

The ODP of a compound can be calculated by the use of the Eq. (2.5) [Solomon (1992)]:

$$ODP\ x = \frac{\sum_z \sum_\theta \sum_\tau \Delta O_3(z,\theta,t)_x \cdot \cos\theta}{\sum_z \sum_\theta \sum_\tau \Delta O_3(z,\theta,t)_r \cdot \cos\theta} \tag{2.5}$$

where

z altitude,

ϑ latitude,

t atmospheric lifetime,

ΔO_3 change in ozone at steady state per unit mass emission rate.

The numerator of the equation is referred to the considered compound "x" and the denominator refers to the reference molecule.

In order to provide a few examples, fluids like R-11, R-22, R-123 and R-124 are not utilizable due to the existing regulations. The first one is a chlorofluorocarbon and the others are hydrochlorofluorocarbons and they have already been phased out.

2.6.2. Global warming potential

The global warming potential (GWP) is a parameter that for a particular time horizon, expresses the relative contribution of a considered molecule to the greenhouse effect and to the global warming.

In fact it is defined as the ratio between the time-integrated radiative forcing from the instantaneous release of 1 kg of a substance to that of 1 kg of a reference gas [Houghton et al. (2001)]:

$$GWP\ x = \frac{\int_0^t a_x \cdot [x\ t\ ] \cdot dt}{\int_0^t a_r \cdot [r\ t\ ] \cdot dt} \tag{2.6}$$

where

- t time horizon for the calculation,
- a_x radiative efficiency due to a unit increase of the atmospheric abundance of the substance in question, [W/(m^2·K)],
- [x(t)] time-dependent decay in abundance of the instantaneous release of the substance.

The corresponding quantities in the denominator are those of the reference gas. Usually the considered reference substance r is carbon dioxide, CO_2, and the GWP can be given for different time horizons such as 20, 100, 500 years. In these cases usually the time horizon is indicated as a subscript: GWP_{20}, GWP_{50}, GWP_{100}. Table 2.2 provides the GWP_{100} value of various fluids.

Table 2.2 GWP_{100} of various fluids [Houghton et al. (2001)].

Fluid	GWP_{100}
R-125	3400
R-134a	1300
R-245fa	950

2.6.3. MARPOL 73/78 regulation

MARPOL 73/78 as the acronym of “Marine Pollution” is an international agreement for the prevention and reduction of pollution from ships that was signed on in 1973 and modified in the 1978. The convention considers in particular the various possible sources for marine pollution caused by ships and establish the way that has to be followed to reduce the environmental impact.

All ships registered in countries (flag state) that signed MARPOL have to respect it independently of the place where they are operated and each state is responsible for certifying their compliance with the convention.

MARPOL 73/78 is composed of six annexes (Annex I to annex VI) and the attention of the current work is focused on the last one. Particular interest is paid to the amended Regulation 12 that concerns ozone-depleting substances (ODS) such as chlorofluorocarbons (CFCs), hydro-chlorofluorocarbons (H-CFCs) and halons [MARPOL (2002)].

In summary, the use of ODS other than H-CFCs is forbidden on new ships since 2005. The use of H-CFCs shall be prohibited on new installations on or after the 1st January 2020. Moreover, each ship that uses ODS on rechargeable systems shall maintain an ozone-depleting substances record book or an electronic system where to note every activity about recharge, repair and maintenance of the interested equipment.

Other fluids nominated in the regulation are the Hydrofluorocarbons (HFCs). At first they have been developed as alternatives to CFCs and nowadays they are available in a wide variety of binary and ternary mixtures. HFCs are not affected by MARPOL, because they are not ozone depleting substances.

In Table 2.3 the frequently used ozone-depleting substances are reported. Substances belonging to Category 1 are forbidden in new installations since 2005 and those belonging to Category 2 are prohibited on or after the 1st January 2020. In both cases, "old installations may remain in use" and the meaning given to this word is "*The charging, topping up and removal of refrigerant from the system or equipment*".

Table 2.3 Frequently used ODS [MARPOL (2002)].

Category 1	Category 2
Halon, R-11 to R-13, R-111 to R-115, R-211 to R-217	R-21 to R-22, R-31, R-121 to R-124, R-131 to R-133, R-141 to R-142, R-151, R-221 to R-226, R-231 to R-235, R-241 to R-244, R-251 to R-253, R-261 to R-262, R-271, R-401, R-409a

The same regulation provides a list of the available refrigerants that have zero ODP and a low GWP_{100} value. They are reported in Table 2.4, where the presence of the symbol "*" denotes that the fluid is considered suitable for use in marine applications for refrigeration and air conditioning.

Table 2.4 Available refrigerants [MARPOL (2002)].

Refrigerant Number		Name	GWP_{100}
R-134a	*	1,1,1,2-Tetrafluoroethane	1300
R-744	*	Carbon dioxide	1
R-407A	*	Blend of R-32/125/134a	1770
R-407C	*	Blend of R-32/125/134a	1526
R-410A	*	Blend of R-32/125	1725
R-717	*	Ammonia	0
R-290	*	Propane	3
R-600	*	Butane	3
R-600a	*	Isobutane	3
R-718		Water	0
R-32		Difluoromethane	580
R-50		Methane	24.5
R-152a		1,1-Difluoroethane	140
R-30		Methylene chloride	15
R-170		Ethane	3

* Refrigerants considered suitable for marine applications for refrigeration and air conditioning.

2.6.4. European regulation

The European Parliament through Regulation (EC) No. 1005/2009 decided that the production of the “controlled substances” that are listed in “Annex I” shall be prohibited. Those fluids are HCFCs, halons and CFCs. Also, the placing on the market of products and equipment containing them shall be prohibited [Regulation (EC) 1005 (2009)].

This regulation is more restrictive than MARPOL (previous sub-section) and in accordance with the European Commission, it is applied to the ships that are registered in a country that is member of the European Community.

As regards this work, it is decided to not to take into consideration the use of HCFCs and CFCs.

2.7 Cost of the Fluid

The cost of the working fluid can vary in a very wide range. Hydrocarbons are usually cheap [Chen et al. (2010)] but several other fluids that are usually used are expensive. The cost of a fluid depends also on the way followed for its production and in certain cases a more massive production can make it cheaper.

2.8 Safety

The classification provided by the ANSI/ASHRAE Standard 34/2007 is a good indicator to evaluate the fluid's level of danger. Six different "safety groups" are defined on the basis of toxicity and flammability. Each of them is indicated by a letter (A or B) that regards relative toxicity and a digit (1, 2 or 3) that represents relative flammability [Calm and Hourahan (2001)].

It is also important to consider the maximum pressure at which fluids are operated, because sometime this value must be limited due to safety reasons. In particular, fluids that are used at a higher pressure than the critical value can present the main difficulties [Chen et al. (2010)].

2.8.1. Toxicity

Toxicity of a substance or a mixture is indicated on the basis of its "Threshold Limit Value", TLV, that is its maximum environmental concentration that can be tolerated by most of the people in everyday work, for all their life, without presenting health problems.

In particular, this parameter is used in the form of TLV-TWA with the meaning "time-weighted average" and indicates that the TLV value refers to the time-weighted average exposure of a 8-h workday and a 40-h work week [Mignini et al. (2004)]. In Table 2.5 the two categories are summarized.

Table 2.5 Categories of toxicity.

Category name	TLV-TWA	Meaning
-	ppm	-
A	> 400	low toxicity
B	< 400	high toxicity

2.8.2. Flammability

Standard ANSI/ASHRAE 34/2007 considers three groups to define the flammability of a fluid (Table 2.6). In particular it refers to the Lower Flammability Limit (LFL) [kg/m^3] that is the lowest concentration above which a flammable mixture of vapour or gas in air can be ignited under prescribed test conditions (temperature and pressure).

Table 2.6 Categories of flammability.

Category name	Meaning
1	Non-flammable fluids. Fluids that do not present flame propagation at the temperature of 21°C and atmospheric pressure.
2	Low flammable fluids. Fluids that have a Lower Flammability Limit (LFL) higher than 0.10 kg/m^3 at atmospheric pressure and temperature of 21°C, and present a lower heating value lower than 19 kJ/kg.
3	High flammable fluids. Fluids that have a LFL up to 0.10 kg/m^3 at atmospheric pressure and temperature of 21°C, and present a lower heating value higher or equal to 19 kJ/kg.

2.9 Fluids Review

Many authors presented comparison between fluids for organic Rankine cycles in various applications. In this section various works are taken into consideration in order to provide a review of the available information. If needed, reference will be made to various cycles and arrangements that are better explained in the Chapter 3. It is important to note that the best fluid for a particular application could not be the best in other cases. In fact, the choice of a fluid rather than another should consider the quality and the quantity of the heat to be exploited. The fact that the comparisons found in literature between fluids usually consider certain fixed conditions for the thermal sources justifies the differences obtained in results.

Dai et al. (2009) analysed the performance of 10 different working fluids in a simple subcritical Rankine cycle for low grade waste heat recovery. The system was composed of an evaporator, a turbine, a condenser and a pump. The use of an internal regenerator

was investigated as well. Under the hypothesis of waste heat source temperature of 145°C, they indicated R-236ea as the fluid that provides the higher exergy efficiency. They stated also that a regenerator cannot improve the performance of the system.

Chen et al. (2010) provided a review of 35 working fluids in subcritical and supercritical cycles. Their results suggest that wet fluids with low critical temperature such as R-32, R-125 and R-143a are promising for supercritical Rankine cycle. Isentropic fluids can be used in both subcritical and supercritical Rankine cycles without the superheating that instead is needed for wet fluids due to turbine issues. Fluids R-141b, R-123, R-21, R-245ca, R-245fa, R-236ea and R-142b are isentropic with critical temperature above 125°C. Their use is suggested in subcritical cycles rather than in supercritical cycles in case of low temperature heat sources. Dry fluids may be used in both subcritical and supercritical Rankine cycles. In the first case superheating is not recommended. Their work suggests also that isentropic and dry fluids are preferred in subcritical Rankine cycles.

Papadopoulos et al. (2010) presented a method to design and select the optimum working fluids for low temperature organic Rankine cycles, based on computer aided molecular design (CAMD). They considered a simple cycle where the evaporation and condensation pressure were the saturation pressure of the working fluid at the temperature of 80°C and 35°C, respectively. The selection criteria excluded fluids with too high values of the evaporation pressure, mass flow rate, flammability and toxicity. Their method showed that methyl-formate (R-611) is the highest performing molecule in economic terms. Well-known fluids that are indicated to be good choices are methanol and butane.

Lakew and Bolland (2010) considered R-134a, R-123, R-227ea, R-245fa, R-290 and n-Pentane as working fluids in a simple ORC cycle and evaluated their performance in exploiting a low temperature heat source. They calculated the required size of heat exchanger and turbine. The maximum power output in case of heat source temperature in the range 80 ÷ 160°C was obtained with R-227a but R-134 provides a similar value. R-245fa gave the highest work output in case of source temperature higher than 160°C. As regards as the surface of the heat exchangers, they found that R-134a requires the higher area.

Toffolo et al. (2010) presented the off-design model of an ORC system looking for the optimum operating parameters. A geothermal source in the range of 130 ÷ 180°C was considered as thermal source for the system. R-134a and isobutane were considered as working mediums. They confirmed the advantage at off-design conditions of the R-134a supercritical cycle over the isobutane subcritical cycle that has been found at design conditions.

Sauret and Rowalds (2011) investigated the use of five different fluids to exploit a geothermal heat source of 150°C: R-134a, R-143a, R-236fa, R-245fa and n-Pentane. They

have been selected on the basis of their theoretical thermodynamic performance and on a balance of various desired criteria: low flammability, low toxicity and relative inert behaviour. The best performing cycle was based on R-134a.

Shengjun et al. (2011) proposed a performance comparison of various fluids in optimized subcritical and transcritical cycle for a low temperature heat source of 80 ÷ 90°C. They noted that fluids in transcritical cycles provide lower thermal efficiency than that of fluids in subcritical ones. Best thermal and exergy efficiency were obtained with R-123, R-600, R-245fa, R-245ca and R-600a whereas high recovery efficiency was obtained with R-218, R-125, R-41 (with the note that this last fluid is flammable). R-152a, R-134a, R-600 and R-143a led to low heat exchanger area per unit of power output. The use of fluids R-152a, R-600, R-134a, R-143a, R-125 and R-141 has been pointed out to minimize the ratio between the system cost and total net power output.

Shu G. et al. (2012) studied a waste heat recovery system that combined a thermoelectric generator with an organic Rankine cycle. R-123 was used as working fluid of the ORC section because of its decomposition temperature that is beyond 600 K.

He et al. (2012) proposed a theoretical formula to calculate the optimum evaporation temperature of the working fluids to be used in a simple subcritical Rankine cycle. Net power output was considered as objective function. The temperature of the heat source was equal to 150°C. They investigates 22 different fluids and suggested R-114, R-245fa, R-123, R-601a, n-pentane, R-141b and R-113 as best choices.

Wang Z.Q. et al. (2012) presented a working fluid selection where the screening criteria were the heat exchanger area per power output unit and the heat recovery factor defined as the ratio between the exploited energy and the available energy of the heat source. They took into consideration 13 different fluids suggesting R-123 as the best choice in case of heat source temperature in the range of 100 ÷ 180°C and R-141b in case of temperature higher than 180°C.

Macián et al. (2013) studied a waste heat recovery system for heavy duty engines of vehicles. Water and R-245fa were considered as working fluids. R-245 was selected because it is suitable to exploit low temperature heat sources. The results indicated that water leads to a higher power output thanks to the possibility to exploit in a better way the high temperature heat provided by the exhaust gas. However, the cycle with R-245fa was considered as the most feasible solution because of the lower space requirements. The maximum evaporation temperature of the organic cycle was 150°C.

Quoilin et al. (2013) presented a summary of various working fluids recommended by other studies found in literature, reporting also the evaporation and condensation temperature at which they were been investigated. Fluids like R-123, R-124, ammonia, pentane, R-152a, R-245ca, R-290, R-600, could be suitable in case of evaporation temperature close to 100°C. R-113, R-227ea, R-236ea, R-245fa, n-hexane in case of

temperature close to 120°C whereas R-123, R-236ea, R-245ca, R-245fa were suggested in case of temperature of 150°C.

Table 2.7 presents the sources of the information reported in Table 2.8. This last table shows the thermodynamic properties (molar mass, critical temperature and pressure) and the environmental properties (ODP and GWP) of several fluids. Each fluid has been suggested in literature to be used to exploit a heat source at certain temperature levels. This information has been collected taking into consideration various works and is presented in Table 2.8. In particular, these temperatures are referred to the evaporation temperature of the working fluid when the source is Quoilin et al. (2013) (subscript "b" in the table) whereas the temperature levels are referred to the heat source in the other cases.

Table 2.7 Sources of the data presented in Table 2.8.

Symbol	Reference
a	Shengjun et al. (2011)
b	Quoilin et al. (2013)
c	Sauret and Rowlands (2011)
d	Chen et al. (2010)
e	Dai et al. (2009)
f	Shu et al. (2012)
g	Macián et al. (2013)
h	Papadopoulos et al. (2010)
i	He et al. (2012)
l	Wang Z.Q. et al. (2012)
m	Lakew and Bolland (2010)
n	EC (2009)
o	Houghton et al., eds. (2001)
p	Calm and Hourahan (2007)
q	Toffolo et al. (2010)
r	Lemmon et al. (2007)

Table 2.8 Properties of the fluids suitable for use in various temperatures of the heat source.

Substance				Molar mass	T_c	p_c	ODP	GWP_{100}	Category	ASHRAE Safety	Heat source Temperature [all but b] Evaporation Temperature [b]			
				kg/kmol	K	bar	-	-		group	< 100°C	~120°C	~150°C	> 150°C
Methane series														
R-11	Trichlorofluoromethane	CCl_3F	CFC	137.37	471.11	44.076	1	4600 [o]	Isen.	A1 [p]				
R-41	Fluoromethane	CH_3F	HFC	34.033	317.28	58.97	0	97 [o]	Wet [a]		a			
Ethane series														
R-113	1,1,2-Trichloro-1,2,2-Trifluoroethane	CCl_2FCCl_2	CFC	187.38	487.21	33.922	0.8 [n]	6000 [o]		A1		b	i	
R-114	1,2-Dichloro-1,1,2,2-Tetrafluoroethane	$CClF_2CClF_2$	CFC	170.92	418.83	32.57	1 [n]	9800 [o]		A1			i	
R-123	2,2-Dichloro-1,1,1-Trifluoroethane	$CHCl_2F_3$	HCFC	152.93	456.83	36.618	0.02 [n]	120 [o]	Isen. [a]	B1	a, b,	l	b, l	f, l
R-124	1-Chloro-1,2,2,2-Tetrafluoroethane	$CHClFCF_3$	HCFC	136.18	395.43	36.243	0.022 [n]	620 [o]		A1	b			
R-125	Pentafluoroethane	CHF_2CF_3	HFC	120.02	339.17	36.177	0	3400 [o]	Wet [a]	A1	a			
R-134a	Tetrafluoroethane	CF_3CH_2F	HFC	102.03	374.21	40.593	0	1300 [o]	Isen [a]	A1			c	q
R-141b	1,1-Dichloro-1-Fluoroethane	CCl_2FCH_3	HCFC	116.95	477.5	42.12	0.11	700 [o]					i	l
R-143a	1-1-1-Trifluoroethane	CF_3CH_3	HFC	84.041	345.86	37.61	0	4300 [o]	Wet [a]	A2			c	
R-152a	1,1-Difluoroethane	CHF_2CH_3	HFC	66.051	386.41	45.168	0	120 [o]	Wet [a]	A2	b			
Propane series														
R-218	Octafluoropropane	$CF_3CF_2CF_3$		188.02	345.02	26.4	0	8600 [o]	Isen. [a]	A1	a			
R-227ea	1,1,1,2,3,3,3-Heptafluoropropane	CF_3CHFCF_3	HFC	170.03	374.9	29.28	0	3500 [o]	Dry [a]	A1	m	b, m	m	
R-236ea	1,1,1,2,3,3-Hexafluoropropane	$CF_3CHFCHF_2$	HFC	152.04	412.44	35.02	0	1200 [o]	Dry [a]			b	b, e	
R-236fa	1,1,1,3,3,3-Hexafluoropropane	$CF_3CH_2CF_3$	HFC	152.04	398.07	32.0	0	9400 [o]	Dry [a]	A1			c	
R-245ca	1,1,2,2,3-Pentafluoropropane	$CHF_2CF_2CH_2F$	HFC	134.05	447.57	39.25	0	640 [o]	Dry [a]	A1	a, b		b	
R-245fa	1,1,1,3,3-Pentafluoropropane	$CF_3CH_2CHF_2$	HFC	134.05	427.16	36.51	0	950 [o]	Dry [a]	B1	a	b	b, c, g, i	m
R-290	Propane	$CH_3CH_2CH_3$		44.096	369.89	24.512	0			A3 [p]	b			
Miscellaneous compounds														
R-717	Ammonia	NH_3		17.03	405.4	113.33	0			B2 [p]	b			
R-170	Ethane	CH_3CH_3		30.069	305.32	48.722	0	~20 [a]	Wet [a]	A3				
R-744	Carbon Dioxide	CO_2		44.01	304.13	73.773	0	1 [o]	Wet [a]	A1				
R-600	n-Butane	CH_3-2(CH_2)-CH_3		58.122	425.13	37.96	0	~20 [a]	Dry [a]	A3	a, b, h			
R-600a	Isobutane	CH-3(CH_3)		58.122	407.81	36.29	0	~20 [a]	Dry [a]	A3	a			
R-601	n-Pentane	CH_3-3(CH_2)-CH_3		72.149	469.7	33.7	0			A3	b		i	
R-601a	Isopentane	$(CH3)_2CHCH_2CH_3$		72.149	460.35	33.78	0			A3 [p]			b, i	
	Benzene	C_6H_6		78.108	562.05	48.94	0		Dry					
	n-hexane	CH_3-4(CH_2)-CH_3		86.175	507.82	30.34	0					b		

2.10 Conclusions

A classification of the fluids used in ORC systems based on the chemical composition has been introduced in accordance with the regulation ANSI/ASHRAE 34 (2007). Three categories of fluids have also been defined by considering the slope of the saturated vapour curve on T-s diagram: “dry fluids”, “isentropic fluids” and “wet fluids”. The category of the fluid and critical temperature and pressure have been linked with its molecular weight. The issues of the chemical stability and the compatibility of the fluids with materials in contact have been introduced.

Two parameters have been used to define the environmental impact of the fluids. They are the ODP and the GWP which are referred to the degradation of the ozone layer and the greenhouse effect, respectively. The use of certain fluids has been found to be limited or prohibited by the MARPOL regulation and the European regulation.

Safety issues related to the use of the fluids have been taken into consideration; the “safety group” defined by ANSI/ASHRAE Standard 34/2007 has been introduced to measure the toxicity and flammability of the fluids.

A literary review of the fluids used in ORC systems has been presented. The use of each fluid has been suggested for a certain temperature level of the heat source according to the information that has been collected.

3 ORGANIC RANKINE CYCLES

3.1 Introduction

Various arrangements for ORC systems have been proposed in literature to optimize the exploitation of different heat sources. Many alternatives have been found even for the same application. As regards the recovery of the waste heat of internal combustion engines, both single pressure level and dual pressure level ORC and both single and dual loop ORC have been investigated. These alternatives with other aspect that regard ORC systems are presented in the chapter. The choice of the operating parameters such as the maximum pressure of the cycle and the eventual superheating is discussed taking into consideration the behaviour of fluids belonging to the different categories presented in Chapter 2. Appropriate parameters are introduced in order to compare the performance of different couples cycle-organic fluid.

3.2 Concept of Rankine Cycle

A Rankine cycle is a thermodynamic cycle that transforms heat into mechanical or electrical power. The concept is realized by four components: an evaporator, a turbine, a condenser and a pump (Figure 3.1). A working fluid circulates through these components. First, it enters the evaporator in the liquid state to be heated and transformed in the vapour state by the heat source. Then it passes through the expander generating mechanical or electrical power. Finally, it rejects low grade heat in the condenser and its pressure is increased by the pump.

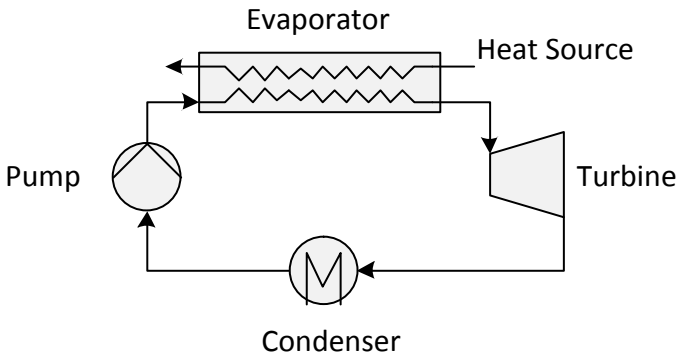

Figure 3.1 Arrangement of a simple Rankine cycle.

Traditionally the working fluid operating in Rankine cycles is water and several modifications are then introduced in order to obtain a higher thermal efficiency. Other fluids (organic fluids) can be taken into consideration, especially when the temperature of the heat source is low.

3.3 Rankine Cycles Applied to Low Grade Heat Recovery

Low grade heat cannot be converted efficiently into electric or mechanical power by conventional methods and because of this it is usually wasted. In fact, recovery systems based on Rankine cycle technology where water is used as working fluid may not be competitive. Instead, Organic Rankine cycles allow a better exploitation of low temperature sources and lead to smaller systems than in case of the use of water [Yamamoto et al. (2001)].

Several advantages are commonly credited to these systems. Working fluids usually do not need to be superheated to avoid the risk of corrosion of the turbine blades and to extend the lifetime of this component. Small size of the components that is due to the high density of the working fluid leads to low cost of the system. Generally, operating pressures do not exceed 30 bar leading to a simpler construction of the components than in case of the use of water. [Quoilin et al. (2013)].

3.4 Efficiency

The word “efficiency” is commonly used to indicate the parameter that measures the performance of a system or a cycle. It is important to pay attention to its definition especially when a comparison between results of different works is attempted.

In the present work, two efficiencies are used to compare the performance of the cycles that are investigated. Their definition is presented in the following sub-sections.

3.4.1. Thermal efficiency

The thermal efficiency is defined as the ratio between the net power output and the heat absorbed by the cycle. With reference to the simple organic Rankine cycle proposed in Figure 3.2, this parameter is given by:

$$\eta_{th} = \frac{\dot{W}_{net}}{\dot{Q}_{absorbed}} = \frac{(h_3 - h_4) - (h_2 - h_1)}{(h_3 - h_2)} = 1 - \frac{(h_4 - h_1)}{(h_3 - h_2)} \tag{3.1}$$

where the specific enthalpy difference (h_3 - h_4) is related to the power output of the turbine, (h_2 - h_1) is related to the power need of the pump and (h_3 - h_2) is the increase of specific enthalpy due to the heating process. Note that in the figure the working fluid is superheated at turbine exit.

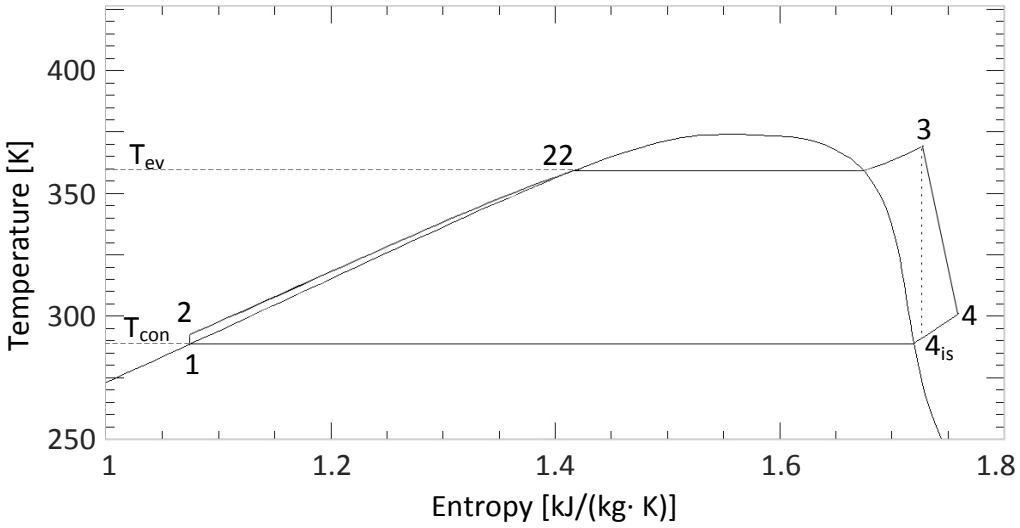

Figure 3.2 Simple organic Rankine cycle.

Wang et al. (2011) reported that for a given value of the reduced condensation temperature τ_{con}, the thermal efficiency η_{th} is strongly dependent on the reduced evaporation temperature τ_{ev}. Figure 3.3 shows the trends of the thermal efficiency of the simple ORCs operating with R-134a and R-245fa as working fluids, as a function of the reduced evaporation temperature. Two values for the reduced condensation temperature are considered. The thermal efficiency is calculated assuming constant values for the performance of the pump and of the turbine. Critical temperatures of the fluids are equal to 374.21 K and 427.16 K for R-134a and R-245fa, respectively.

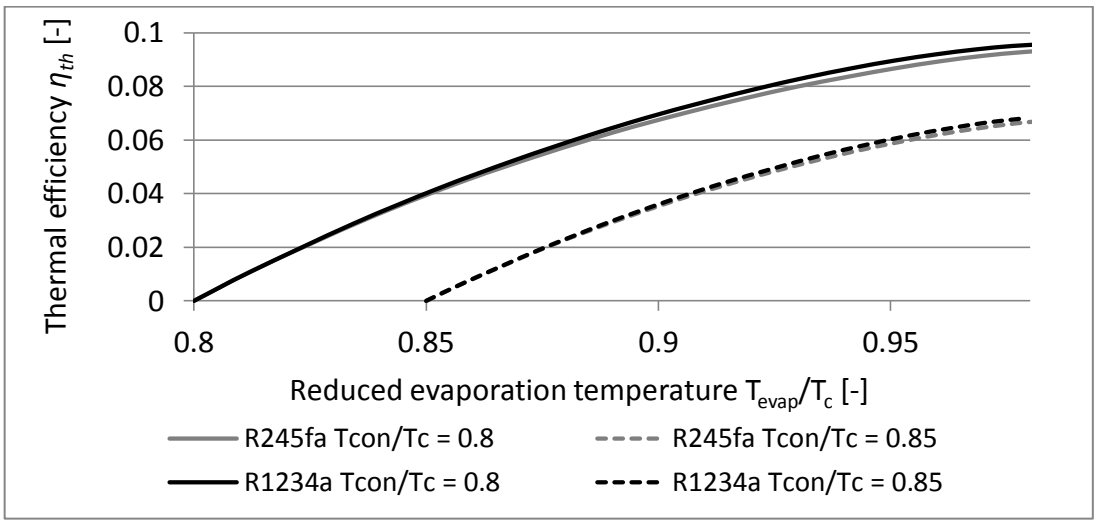

Figure 3.3 Dependence of η_{th} on the reduced evaporation temperature τ_{ev}.

3.4.2. Total heat recovery efficiency

The only concept of "thermal efficiency" is not satisfactory for measuring the performance of a system whose aim is to exploit a particular heat source. In certain cases, a recovery system characterised by a relatively high thermal efficiency might not exploit all the available heat. A less efficient cycle might improve this exploitation thus leading to a higher output and making this solution more suitable. In these cases, the introduction of an additional parameter is required and useful to compare different cycles. Liu et al. (2004) defined the "total heat recovery efficiency" as:

$$\eta_t = \frac{\dot{W}_{net}}{\dot{Q}_{available}} \tag{3.2}$$

where

$\dot{W}_{net}$ net power output of the cycle,

$\dot{Q}_{available}$ available heat.

The "total heat recovery efficiency" can also be related with the "thermal efficiency" of the cycle:

$$\eta_t = \Phi \cdot \eta_{th} \tag{3.3}$$

where

η_{th} thermal efficiency

Φ heat recovery factor.

Φ is the ratio between the heat that is absorbed by the cycle and of the thermal available, Eq. (3.4). Vaja and Gambarotta (2010) proposed the definition of Eq. (3.5) for the parameter Φ.

$$\Phi = \frac{\dot{Q}_{absorbed}}{\dot{Q}_{available}} \tag{3.4}$$

$$\Phi = \frac{h_{in} - h_{out}}{h_{in} - h_2} \tag{3.5}$$

In Eq. (3.5), h_{in} and h_{out} are the specific enthalpy of the fluid exploited as heat source, at the inlet and outlet conditions, respectively. h_2 is the minimum value for the

specific enthalpy that is reached at the outlet condition in case of maximum exploitation of the heat source (Figure 3.4).

Under fixed conditions for the available heat to be exploited, the maximization of the "total heat recovery efficiency" leads to the maximization of the net power output of the recovery system. The corresponding operating point does not necessarily corresponds to that of maximum thermal efficiency.

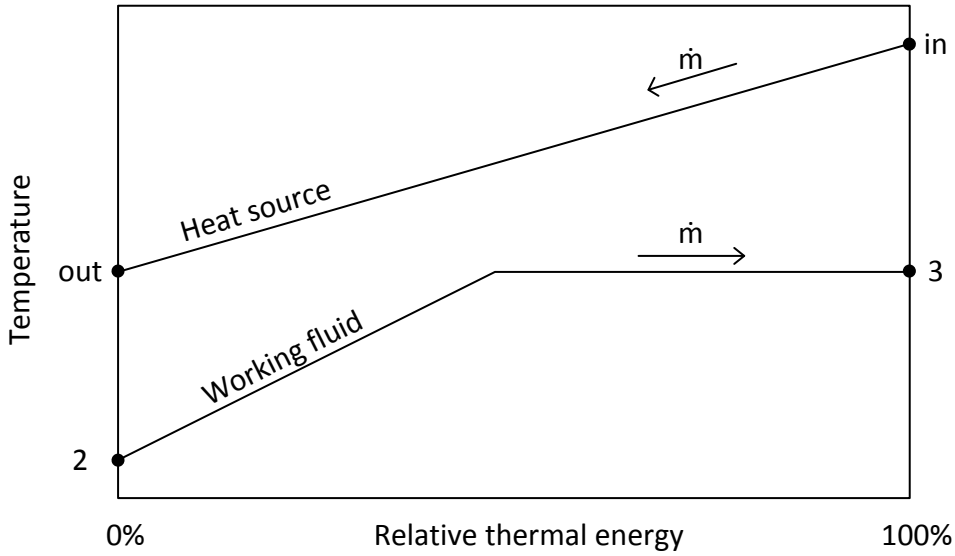

Figure 3.4 Schematic representation of the matching of waste heat and heating phase of the working fluid.

3.5 Subcritical and Supercritical Rankine Cycles

Based on the maximum value for the pressure that is reached by the working fluid, it is possible to distinguish between subcritical and supercritical cycles. In the first case, after the condenser the fluid is pumped up to a value for the pressure that is lower than the critical value (Figure 3.5). The fluid is then heated, evaporated and eventually superheated.

Working fluids with a relatively low critical pressure can be pumped up to a pressure that is higher than the critical value. In this case, the following heating process takes place in a unique phase in which the properties of the fluid change progressively and the transformation of the liquid into the gas form occurs without discontinuities (Figure 3.5). (See also Section 2.4).

Karellas and Schuster (2008) made a comparison between a subcritical and a supercritical ORC, noting that in the first case the specific enthalpy drop at the turbine (h_3-h_4) is lower than the value ($h_{3'}$-$h_{4'}$) of the second case, Figure 3.5. They stated that the

higher specific work that is needed by the pump in the case of supercritical cycle is low so that the thermal efficiency of a supercritical cycle is generally higher. Also, they suggested the use of a cycle operating in supercritical conditions in order to maximize the total heat recovery efficiency.

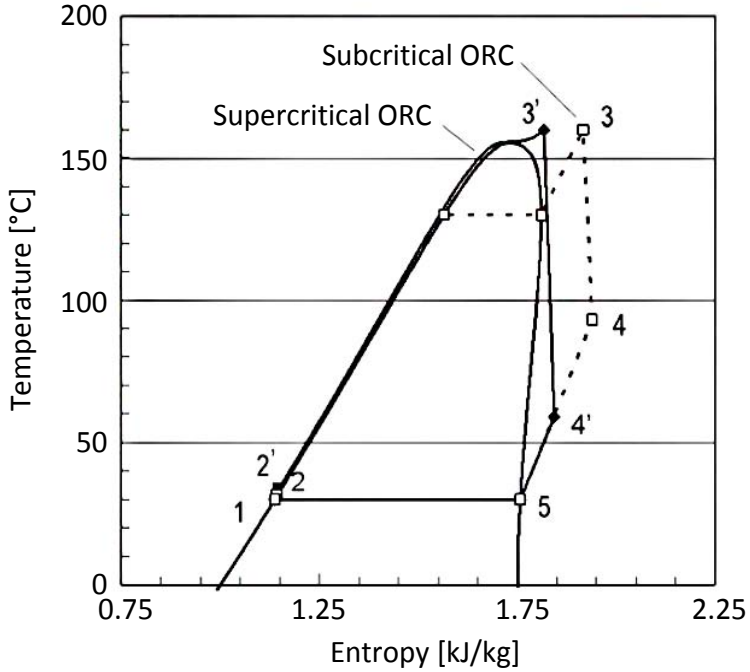

Figure 3.5 Examples of subcritical and supercritical ORC [Schuster et al. (2010)].

It is important to note that a high value for the evaporation pressure, which might be required to operate in supercritical conditions, leads to the use of stronger and more expensive components than in case of subcritical conditions. The benefit of a more efficient cycle might not be justified from the economic point of view. Also, Mikielewicz and Mikielewicz (2010) pointed out that supercritical cycles require a bigger size for the heat exchanger used to heat the fluid than in case of subcritical cycle.

As regards the heating profile of the fluid and the thermal match with a heat source, Figure 3.6 shows the comparison between a generic fluid operating in subcritical conditions (left) and one operating in supercritical conditions (right). Considering a sensible heat source, the isothermal evaporation does not allow for a complete exploitation of the available heat quality resulting in high irreversibility [Schuster et al. (2010)]. On the contrary, the supercritical cycle matches in a better way the heating profile of the working fluid and the heat source; the average temperature at which heat is supplied to the working fluid is higher. Both examples consider the same value for the minimum vertical distance between the two curves (ΔT_{pp}).

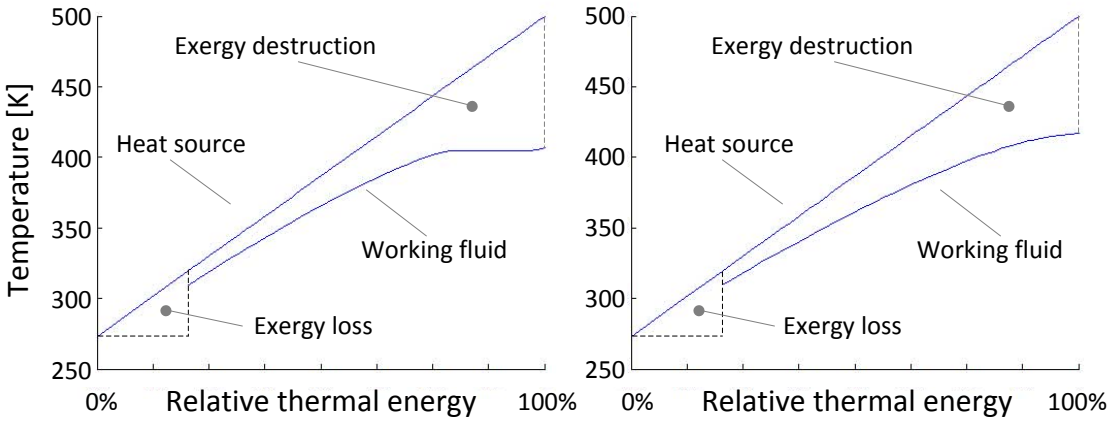

Figure 3.6 Thermal match in the heating process for optimized subcritical ORCs (left) and for optimized supercritical ORCs (right).

3.6 Dry, Isentropic and Wet Fluids in ORCs

Three different categories of working fluids have been defined in Section 2.3: dry, isentropic and wet fluids. Liu et al. (2002) stated that dry and isentropic fluids are more appropriate for ORC systems because after the expansion in the turbine they are superheated. On the opposite, wet fluids become saturated after they go through a large enthalpy drop in the turbine and the eventual impingement of liquid droplets on the turbine blades might cause damages. Wet fluids are usually superheated before the turbine in order to overcome this problem.

As regards the dry fluids, the energy associated with the superheating that occurs at turbine outlet can be exploited for preheating the working fluid coming from the pump. In this case, an additional heat exchanger called regenerator is introduced.

3.7 Effectiveness of the Superheating

Although superheating is commonly used in Rankine cycles operating with water in order to increase the thermal efficiency, this is not always the case with ORCs.

As presented in Section 3.6, wet fluids usually require to be superheated before the turbine whereas this is not the case of isentropic and dry fluids which are usually superheated at expander outlet [Saidur et al. (2012)].

Wang et al. (2011) reported that superheating could increase the thermal efficiency of the system, but it would be restricted by the thermal stability temperature. However, the optimum efficiency of a cycle is achieved when superheating does not take place in case of dry fluids.

Hung et al. (1997) found that the thermal efficiency of a cycle is a weak function of the inlet temperature of the turbine and an increase of superheating in the turbine does not lead to a significant increase in efficiency.

Chen et al. (2010) explained that the impact of superheating on the thermal efficiency is determined by the rate at which the constant pressure lines diverge on enthalpy-entropy diagram, Figure 3.7. Considering an increase in the degree of superheating from a reference point (saturated vapour state), they defined the incremental efficiency, Eq. (3.6):

$$\eta' = \frac{\Delta \dot{W}}{\Delta \dot{Q}} = \frac{\Delta h_1 - \Delta h_2}{\Delta h_1} \tag{3.6}$$

Superheating has a positive impact only if the incremental efficiency is higher than the thermal efficiency at the reference state. As a rule, thermal efficiency increases for wet fluids with the superheating while it decreases for dry fluids and it is not recommended in this case.

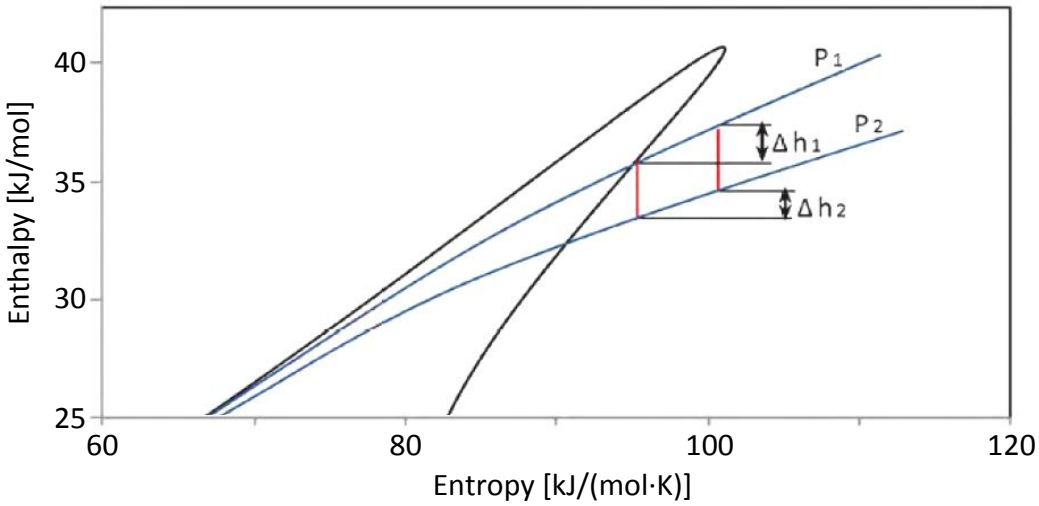

Figure 3.7 Enthalpy–entropy diagram of dry fluid pentane demonstrating the effect of superheating [Chen et al. (2010)].

3.8 Other Technical Aspects

3.8.1. Heat exchangers

Heat exchangers represent more than 90% of the capital cost of the ORC system [Papadopoulos et al. (2010)]. They are selected on the basis of the compatibility with

fluids in contact, the level of temperature and the operating pressures. The choice of the kind takes also into account the available space. The most common heat exchangers that are used in this field are of shell & tube or plate type. Plate exchangers are more compact and are preferred in small scale systems [Quoilin et al. (2013)].

With similar heat source to be exploited, different optimized organic Rankine cycles operating with different working fluids require a different size for the heat exchangers. For example, in case of high vapour density leads to a low volume flow rate and low pressure drops and the use of compact heat exchangers is allowed. Fluids which present low viscosity in both the liquid and vapour phases are preferred because they lead to low friction losses and high values for the heat transfer coefficients. This last result is obtained also in case of high thermal conductivity [Quoilin et al. (2013)].

As regards the eventual superheating of the vapour before turbine expansion, Schuster et al. (2009) stated that it requires very large and expensive heat exchangers to be realized due to the low heat transfer coefficient. Same issue occur in case of supercritical cycles [Mikielewicz and Mikielewicz (2010)].

3.8.2. Turbine

Angelino et al. (1984) defined four parameters related to the efficiency of an axial flow turbine stage. Two of them depend only on the properties of the considered fluid. These are the size factor (SF) and the volumetric expansion ratio (VR) which are given by Eqs. (3.7) and (3.8), respectively:

$$SF = \frac{\sqrt{\dot{V}_{out}}}{\Delta h_{is}^{1/4}} \tag{3.7}$$

$$VR = \frac{\dot{V}_{out}}{\dot{V}_{in}} \tag{3.8}$$

where

$\dot{V}_{in}$ volume flow rate of the working fluid at turbine inlet,

$\dot{V}_{out}$ volume flow rate at turbine outlet,

Δh_{is} isentropic enthalpy drop in the turbine.

The value of the SF factor is proportional to actual turbine size. Highest efficiencies are found for turbines with a high SF factor and a low VR ratio.

3.8.3. Diathermic oil

Several works found in the literature about energy recovery with bottoming ORCs use of an intermediate circuit where a fluid (thermal oil) is used to transfer heat indirectly to the organic fluid. This is applied when a high temperature heat source is exploited such as the exhaust gas of an internal combustion engine. This is done for safety reasons. In fact, many organic fluids are highly flammable and the exposure to high temperatures could lead to decomposition problems [Karellas (2012)]. However, note that the use of this additional circuit introduces further irreversibility in the heat transfer and causes a reduction of the global efficiency of the system [Vaja and Gambarotta (2010)].

Quoilin et al. (2013) stated that in case of direct thermal matching between working fluid and exhaust gas, deterioration problems could be higher during start-up phases and transients. Moreover, the controllability and the stability of the system are harder to achieve and to maintain so that most commercial ORC installations make use of an intermediate oil loop.

3.9 Synthesis of Organic Rankine Systems

Various configurations (syntheses) have been found in literature for organic Rankine cycles. In the following sub-sections they are presented together with the main characteristics of the considered heat source.

3.9.1. Single Loop Organic Rankine Cycles

Vaja and Gambarotta (2010) considered three different syntheses to realize a bottoming system of a co-generative internal combustion engine fuelled with natural gas. All of them are based on a simple subcritical ORC cycle where the working fluid is pumped to the high pressure value, is heated, passes through the turbine and condenses. The electric power output of the engine is 2928 kW. The temperature of the exhaust gas and the cooling water at engine outlet is 470°C and 90°C, respectively. Note that the quality of the available heat is similar to that found in the current work so that particular attention is paid to this study.

In the first case, the thermal source is made up only of the exhaust gas (Figure 3.8), whereas heat from the cooling system of the engine is not exploited. The second case add a preheater to the first ORC arrangement in order to allow the engine cooling flow (water flow) to be used, as shown in Figure 3.9. In the third case the ORC system is fed only by the exhaust gas but a heat exchanger (recuperator) is included in order to recover the desuperheating heat of the vapor leaving the turbine, Figure 3.10.

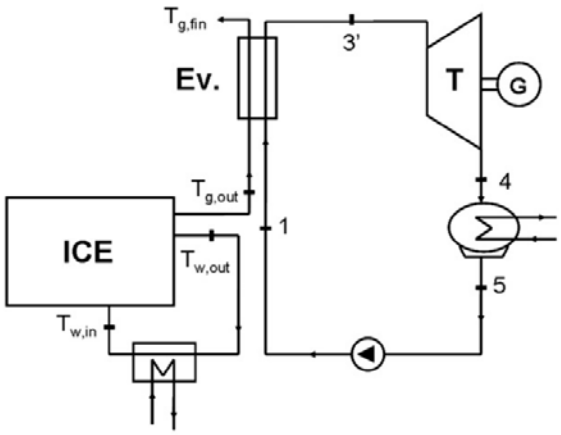

Figure 3.8 Simple cycle which exploit the heat associated with the exhaust gas [Vaja and Gambarotta (2010)].

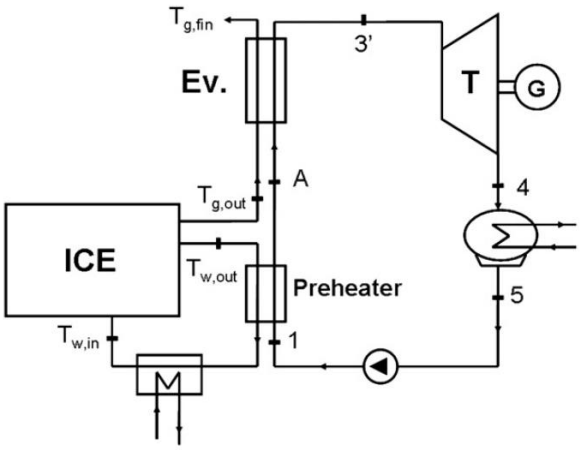

Figure 3.9 Simple cycle which exploit the heat associated with the exhaust gas and the cooling water flow of the engine [Vaja and Gambarotta (2010)].

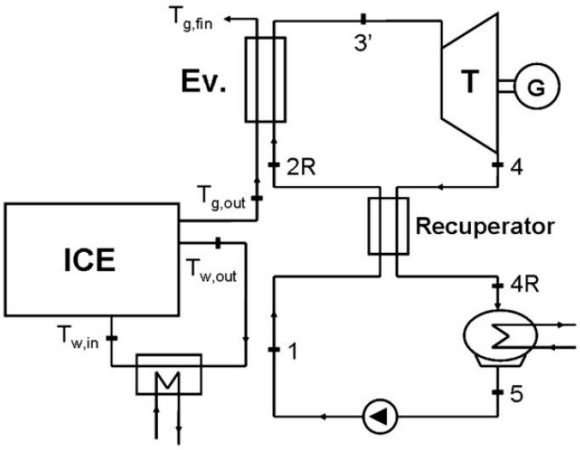

Figure 3.10 Simple cycle with a recuperator [Vaja and Gambarotta (2010)].

Three fluids have been considered in their work: benzene, R-11 and R-134a. They have been selected to represent the different behaviours of dry, isentropic and wet fluids,

respectively, in the *T-s* diagram (Section 3.5) whereas other aspects such as environmental friendliness, toxicity and flammability have not been taken into consideration.

As regards the first simple cycle (Figure 3.8), the highest thermal efficiency was obtained by benzene (20%) whereas R-11 and R-134a led to a thermal efficiency approximately equal to 17% and 9%, respectively. The exploitation of the relative low temperature heat associated with the water cooling flow (Figure 3.9) led to a significant increase of the net power output in the cases of fluids which present low critical temperature (R-11 and R-134a). The thermodynamic cycles were the same as in the first case so that the thermal efficiencies did not change. The higher output is justified by the better exploitation of the available heat: the higher heat recovery factors led to higher total heat recovery efficiencies. The third synthesis (Figure 3.10) can be applied only if the working fluid is dry. In this case the vapour is superheated at the end of the expansion and the heat associated with can be exploited to preheat the fluid after the pump. The heat flow rate that is transferred internally has been found to be about 10% of the total introduced heat rate. The mechanical power is increased of about 12.4% if compared to the first case.

The organic Rankine cycle section of the system has allowed the overall efficiency to be increased. The extra power output is in range of 4.8% ÷ 12.8%, where the first value is obtained in the cases of simple cycle operating with R-134a and regenerative cycle operating with benzene, respectively. The efficiency of the electric generator has been considered constant and equal for all the cases. They noted that the regenerative cycle requires the use of a liquid-gas heat exchanger (recuperator). The high exchange surface of this component leads to high space needs and high cost. Note that space requirements are a critical issue for marine installations so that this aspect has to be taken into account to evaluate the feasibility of the system. Conversely, the use of a liquid-liquid exchanger to exploit the heat of the engine cooling system is suggested due to the simplicity of this component.

Yu et al. (2013) analysed a bottoming organic Rankine cycle for a Diesel engine using R-245fa as working fluid. Both the jacket water and exhaust gas were considered as heat sources. Note that the power of the engine was very low (258.3 kW) compared with that of the engines lower in this work but the temperature level of the jacket water is practically the same. The proposed ORC cycle was equal to the one presented in Figure 3.9. A diathermic oil loop was used to transfer heat from the exhaust gas to the organic fluid. They obtained a maximum thermal efficiency of 9.4% for the cycle and an increment of 6.1% in thermal efficiency of the overall system.

Wang et al. (2011) proposed a simple cycle similar to the one in Figure 3.9 with the difference that preheating was carried out by circulating the working fluid of the ORC in the engine block, in order to obtain a better exploitation of the heat quality. This

arrangement seems to be difficult to be applied, especially in engines with high power, and it will not be considered in the choice of the system here.

Smolen (2011) presented a two-stage bottoming organic Rankine cycle for heat recovery from a combustion engine. Thermal sources exploited by the working fluid R-245fa were the cooling water and the exhaust gas, Figure 3.11. Note that two different expanders were used for the high and low pressure stages: they are a turbine and a screw

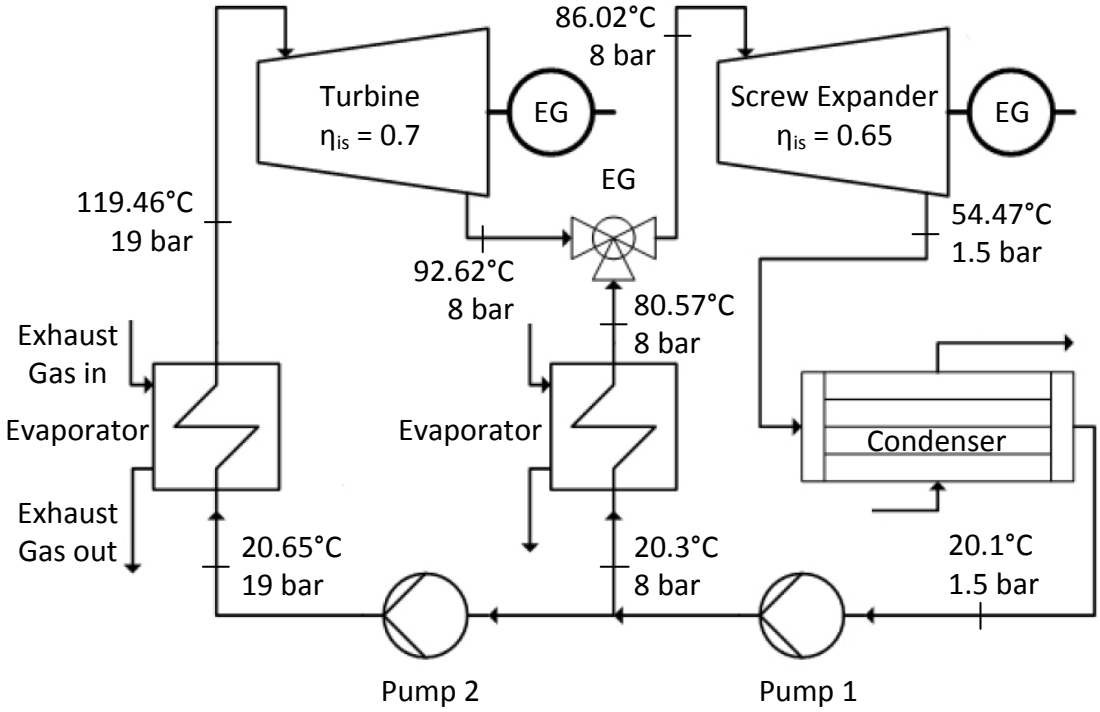

Figure 3.11 Arrangement of the two-stage ORC [Smolen (2011)].

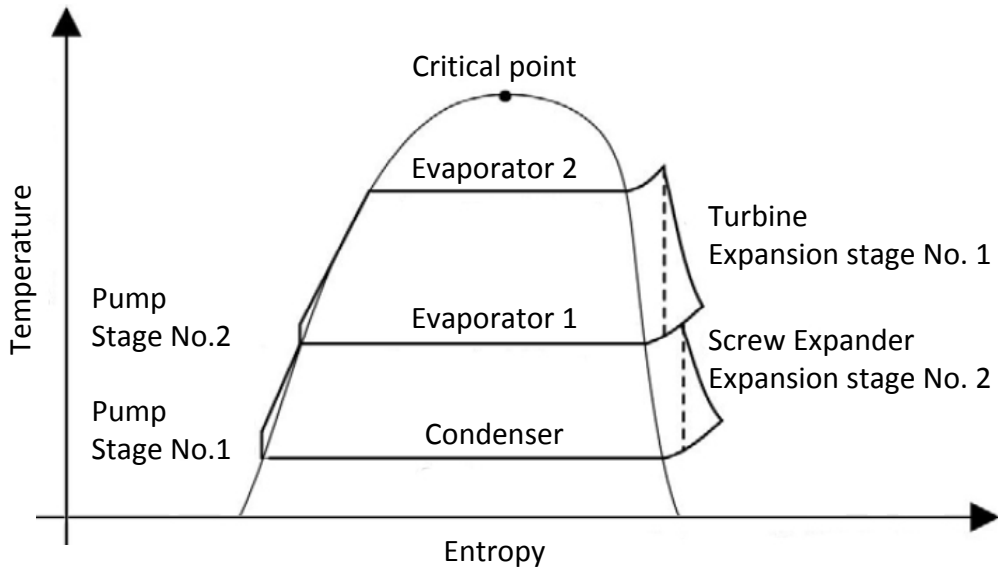

Figure 3.12 Simplified view of the two-stage ORC process on a T-s diagram [Smolen (2011)].

expander. Pressure and temperature values of the main states of the cycle are presented in the figure. The maximum temperature of the working fluid was around 120°C, while no justification is provided to explain this choice; this value is relatively low if it is considered that the thermal flow transferred to the HT circuit comes from the exhaust gas. Considering temperature, pressure and efficiency values presented in Figure 3.11, the thermal efficiency was 7.5%. Figure 3.12 shows the simplified diagram T-s of the cycle.

3.9.2. Dual Loop Organic Rankine Cycles

Wang E.H. et al. (2012) proposed a dual loop bottoming organic Rankine cycle for a gasoline engine.

Figure 3.13 shows the arrangement of the cycle whereas Figure 3.14 presents the T-s diagram with the thermodynamic transformations. Working fluids for low and high temperature loops were R-134a and R-245fa, respectively; which have been selected because of their environmental properties and for safety reasons as for R-245fa. In that cycle, the high temperature circuit (HT) exploited the engine exhaust gas to heat the working fluid up to the temperature of 131.5°C (pressure of 24 bar). After the expansion of the vapour, the condensation took place at the temperature of 80°C by transferring the extracted heat to the low temperature (LT) circuit through a heat exchanger. This heat was used to preheat and to partially evaporate LT circuit working fluid (R-134a) at a pressure of 21.17 bar (70°C). The evaporation was completed and the fluid was superheated by absorbing the heat associated with the engine cooling water flow. The condensation of the R-134a took place at the temperature of 30°C. A screw expander was considered to be installed in the LT circuit because of its good performance in small-scale applications.

Even though the exhaust gas is exploited as heat source and the heat associated with is high in quality, it is noted that the evaporation pressure of the working fluid of the HT circuit is set to be relatively low. No explanation is provided for this choice. Also, note that Evaporator 1 transfers heat directly from exhaust gas to the working fluid, while several works found in the literature suggest the use of an intermediate circuit, in order to better control the temperature of the ORC working fluid (see Sub-section 3.8.3). The authors stated that the proposed arrangement is particularly interesting when the heat flow rates associated with exhaust gas and cooling water are significantly different to each other.

Zhang et al. (2013) presented a similar work on a light-duty engine, following the same procedure. The same fluids were considered and the values of the operating parameters were close to those of the previous work. Two single screw expanders were adopted for the two circuits.

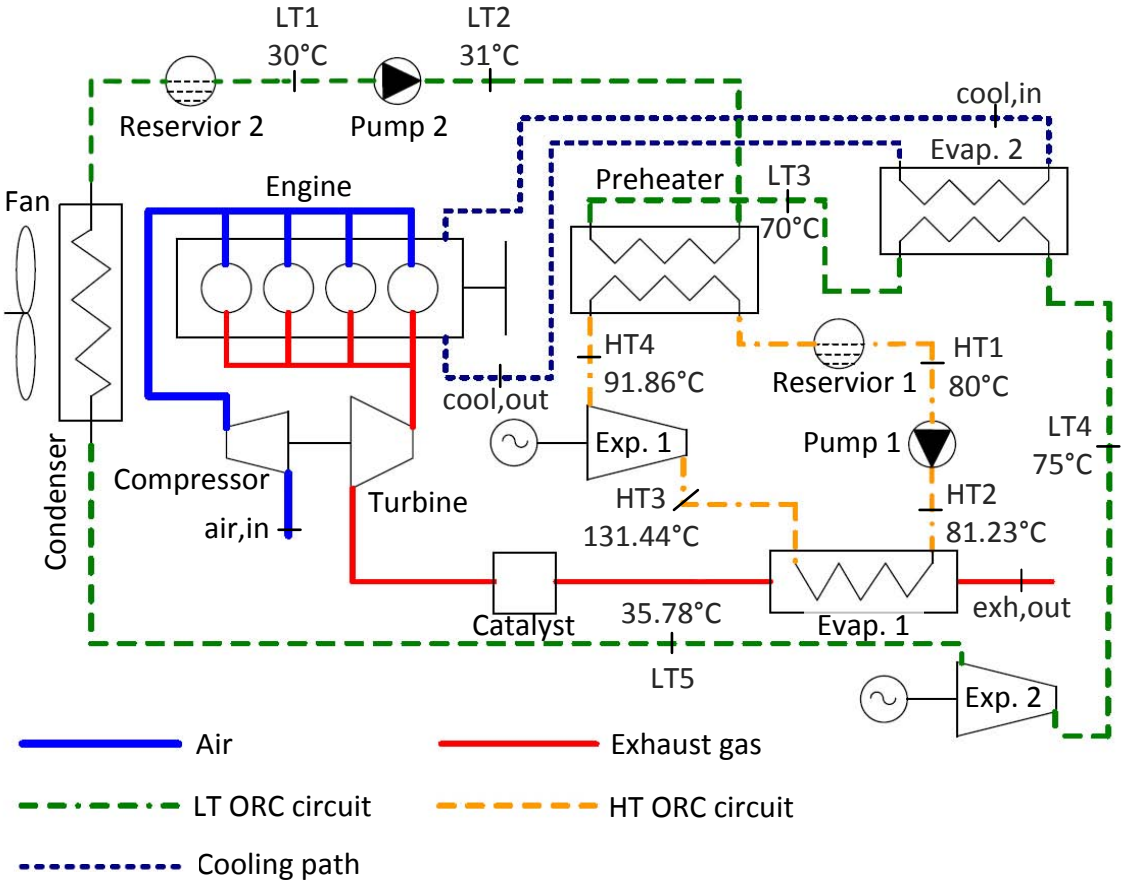

Figure 3.13 Dual loop ORC [Wang et al. (2012)].

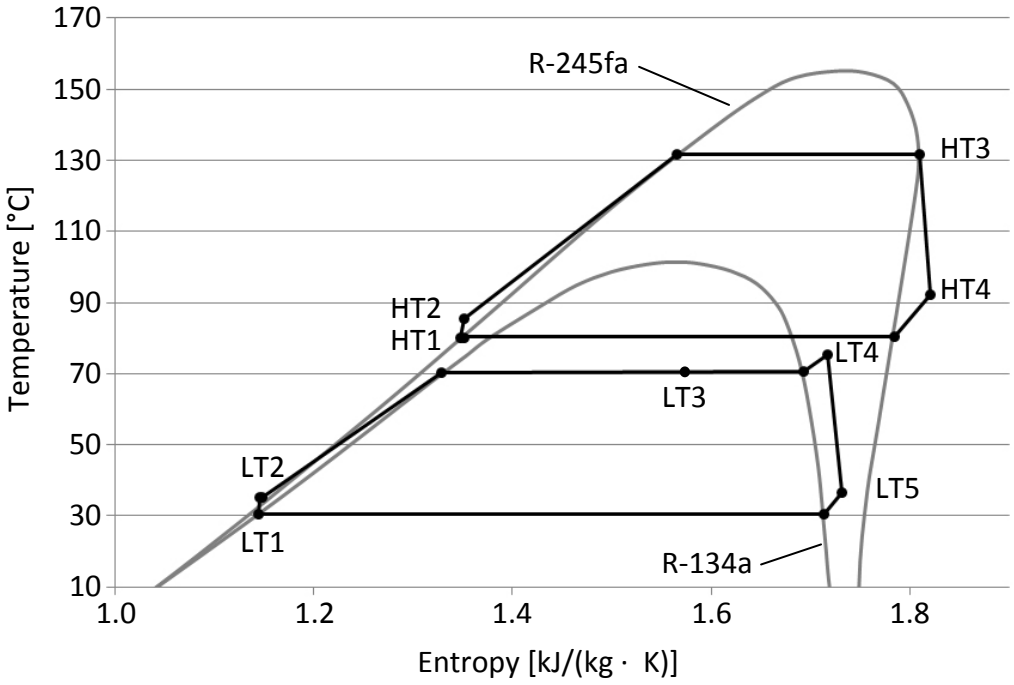

Figure 3.14 T-s diagram of the dual loop ORC [Wang et al. (2012)].

3.10 Conclusions

Various configurations for organic Rankine cycles have been proposed in literature and presented in this chapter. Particular attention has been paid to ORCs exploiting low temperature heat sources and coupled with internal combustion engines.

Two parameters have been introduced to compare the performance of different cycles and fluids: they are the thermal efficiency η_{th} and the total heat recovery efficiency η_t. Two factors that are related to the isentropic efficiency of the expander have been presented: the “size factor” (*SF)* and the “volumetric expansion ratio” (*VR)*.

Both subcritical and supercritical cycles have been considered and presented together with related advantages and disadvantages. The behaviour of fluids belonging to the different categories presented in Chapter 2 has been discussed as well as the issue of the superheating effectiveness. It has been found that superheating has a positive impact on wet fluids and allows to avoid damages to the turbine that are due the presence of liquid droplets. Dry fluids are usually superheated at turbine outlet and the associated heat can be exploited by the addition of a regenerator.

Heat recovery from different sources could result in different best solutions for the arrangement and the operating parameters of the system. This requires to conduct the design process considering various alternatives simultaneously. Also, other technical aspects should be taken into consideration depending on the particular application (i.e., naval application), objective of insertion of the ORC system, characteristics of the thermal flows to be exploited (i.e., kind of fluids and temperature level). When the energy and exergy quantities of the thermal sources are of the same level, a simple or a regenerative ORCs might be good choices according to the simplicity of their arrangement. However, in other cases, these kind of systems might not be suitable to exploit all the available heat and more complex configurations shall be investigated like a two-stage system or a dual loop one.

4 ENERGY SYSTEMS OF THE SHIP

4.1 Introduction

The LNG carrier under study can be considered an integrated energy system where various equipment operates simultaneously. This chapter presents the electric power generating plant, the fresh water generators (FWGs) and the boilers for steam production that are installed aboard the ship. Each component is described and its operation and performance in design and off-design conditions is presented according to the available information.

4.2 Electrical Power Generating Plant

The “Machinery Operating Manual” of the ship provides information regarding the composition of the electric power generating plant (such as number of engines, type, electric power, etc.). Data that can be used to perform the energy balance of the engines are provided as well. Further information is provided by the “Energy and steam balance of the ship” [Energy and steam balance of the ship]. The “Product guide” of the engines [Wärtsilä (2012)] supports the comprehension of the engines cooling systems and gives certain information that is useful in interpreting the other documents.

The plant is composed of four Dual Fuel Diesel Electric engines (DFDE) that supply electric power to the ship. No. 1 and No. 4 Diesel engines are Wärtsilä 12V50DF type, and No. 2 and No. 3 are Wärtsilä 6L50DF type. All the engines are four-stroke turbocharged inter-cooled ones and the pumps of the cooling systems are of the engine driven type. Each engine can be fuelled either with natural gas or with heavy fuel oil (HFO). In case of natural gas, a small amount of Light Fuel Oil (LFO) is required as pilot injection. Wärtsilä 6L50DF is a six cylinders in-line engine and Wärtsilä 12V50DF is a twelve cylinders V engine. Figure 4.1 gives a cross section view of the engines.

The design main characteristics of the two different engines are presented in Table 4.1. Most of the information that is reported is taken from the “Product guide” of the engines. The “Electric output” is provided by the “Energy and steam balance of the ship”. Note that the efficiency of the electric generators is approximately equal to 96.5%. Considering the composition of this plant and the data of Table 4.1, the maximum available electrical power at generators outlet is 33000 kW.

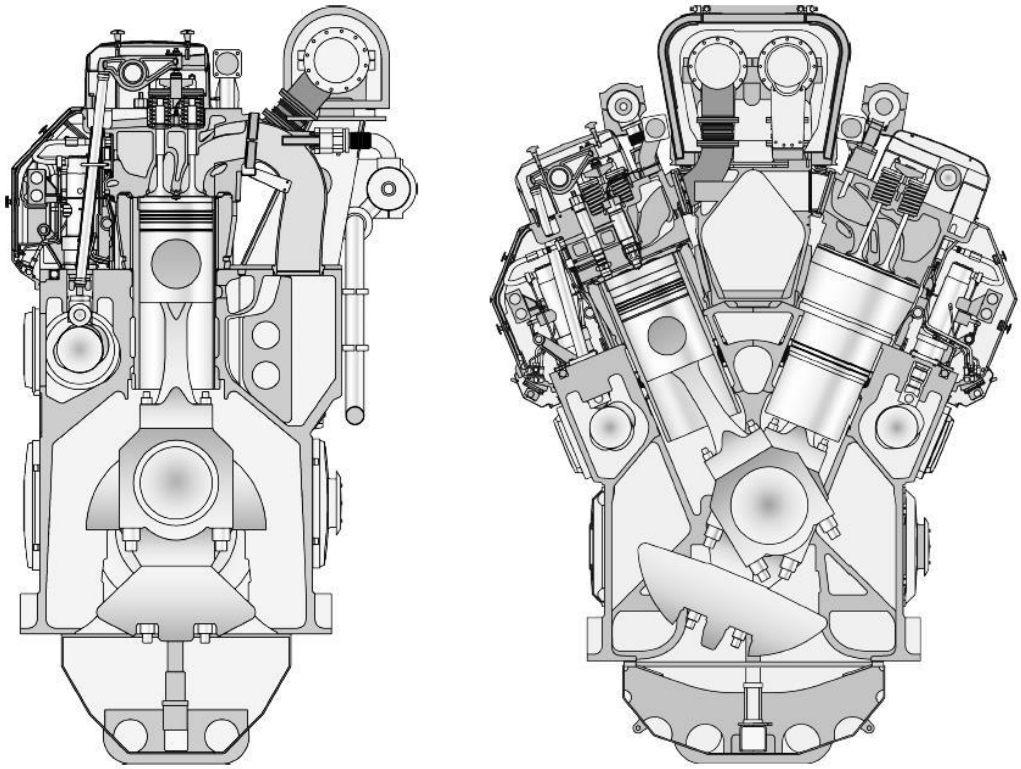

Figure 4.1. Cross section of the in-line engine (left) and of the V engine (right) [Wärtsilä (2012)].

Table 4.1 Main characteristic of the Diesel generator engines, [Wärtsilä (2012); Energy and steam balance of the ship].

	Unit	12V50DF	6L50DF
[Wärtsilä (2012)]			
Mechanical output	kW	11400	5700
Cylinder bore	mm	500	500
Stroke	mm	580	580
Engine speed	rpm	500	500
Mean piston speed	m/s	9.7	9.7
Mean effective pressure	bar	20	20
[Energy and steam balance of the ship]			
Electric output	kW	11000	5500
Generator efficiency	%	96.49	96.49

4.2.1. Energy balance of the main diesel generators

In this sub-section the first law energy balance of the two different types of engines is performed, considering that the boundaries of the systems include the conversion of the mechanical power into the electrical form. The balance will describe how the primary energy of the fuel is exploited in order to produce the desired output (electric power).

First the general procedure is discussed and then the calculations are performed and presented for both Diesel generators.

ISO conditions are considered as reference conditions. The reference temperature T_o is equal to 25°C, the total barometric pressure p_o is 1 bar and the relative humidity of the air is equal to 30%. The charge air coolant temperature is 25°C [Wärtsilä (2012)].

As explained at the beginning of the section, the engines are Dual fuel type. However, the operating mode with heavy fuel oil (HFO) will not be considered in the present work according to the information that has been collected about the real operation of the engines. Note that the natural boil-off gas has to be removed from the tanks to keep constant storage pressure. Due to the fact that the ship has not a liquefaction plant, this quantity of natural gas would be oxidized (burned) if not used by the engines. So, it is assumed that the engine-generator sets are fuelled with natural gas and with the needed small quantity of light fuel oil (LFO) for the pilot injection. In case of steady-state conditions, Eq. (4.1) expresses the energy balance:

$$\dot{H}_f + \dot{Q}_a = \dot{W}_e + \dot{Q}_{lo} + \dot{Q}_{jw} + \dot{Q}_{ca,HT} + \dot{Q}_{ca,LT} + \dot{Q}_{eg} + \dot{Q}_r + \dot{W}_{lg} \tag{4.1}$$

where

- $\dot{H}_f$ energy flow rate of the fuels,
- $\dot{Q}_a$ energy flow rate of the air,
- $\dot{W}_e$ electric power,
- $\dot{Q}_{lo}$ heat flow rate rejected to the lubricating oil,
- $\dot{Q}_{jw}$ heat flow rate rejected to the jacket water,
- $\dot{Q}_{ca,HT}$ heat flow rate at the high temperature charge air cooler,
- $\dot{Q}_{ca,LT}$ heat flow rate at the low temperature charge air cooler,
- $\dot{Q}_{eg}$ heat flow rate associated with the exhaust gas,
- $\dot{Q}_r$ radiation and convection losses,
- $\dot{W}_{lg}$ electric generator losses.

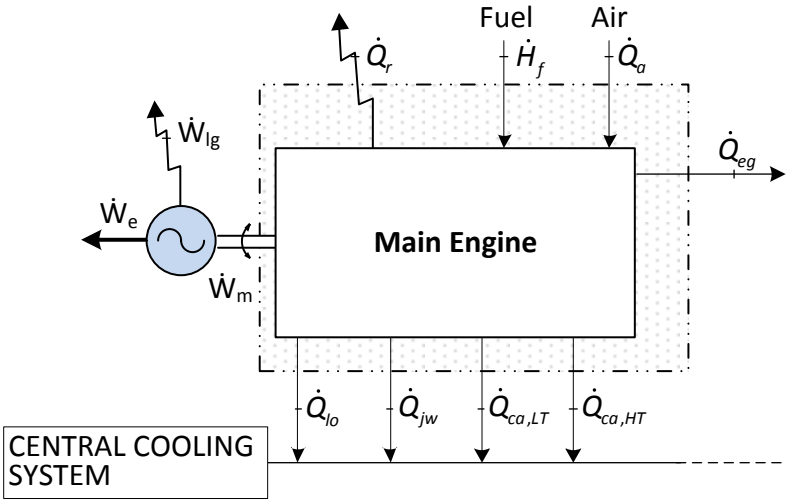

Figure 4.2 Energy balance of the Main Engines.

The energy flow rate $\dot{H}_f$ depends on the energy flow rate of the two fuels (natural gas $\dot{H}_{fg}$ and LFO $\dot{H}_{fl}$) as expressed by Eq. (4.2). In particular, lower heating value H_u and inlet temperature T_f should be considered for each of these two fuels, Eqs. (4.3) and (4.4):

$$\dot{H}_f = \dot{H}_{fg} + \dot{H}_{fl} \tag{4.2}$$

$$\dot{H}_{fg} = \dot{m}_{fg} \cdot [H_{u,fg} + c_{p,fg} \cdot (T_{fg} - T_o)] \tag{4.3}$$

$$\dot{H}_{fl} = \dot{m}_{fl} \cdot [H_{u,fl} + c_{p,fl} \cdot (T_{fl} - T_o)] \tag{4.4}$$

The terms $\dot{m}_{fg}$ and $\dot{m}_{fl}$ of Eqs. (4.3) and (4.4) are the mass flow rate of the two fuels, natural gas and LFO, respectively. $H_{u,fg}$ and $H_{u,fl}$ are the lower heating values, $c_{p,fg}$ and $c_{p,fl}$ are the specific heat capacities. T_o is the reference temperature.

Equation (4.5) is preferable than Eqs. (4.1), (4.2) and (4.3) to evaluate the term $\dot{H}_f$ because it considers directly the value of the total specific fuel energy consumption b_f that is an information provided by the documents. It represents the overall consumption of primary energy that is needed to make available the mechanical power $\dot{W}_m$. The total energy flow rate associated with the fuels becomes:

$$\dot{H}_f[\text{kW}] = b_f[\frac{\text{kJ}}{\text{kWh}}] \cdot \dot{W}_m[\text{kW}] \cdot \frac{h}{3600\,s} \tag{4.5}$$

The enthalpy flow of the air $\dot{Q}_a$ is defined by Eq. (4.6) where T_{a1} is the inlet temperature of the air and T_o is the reference temperature. This work considers that the inlet conditions (temperature and pressure) of the air are equal to the ISO ones. In this way the term $\dot{Q}_a$ is equal to zero.

$$\dot{Q}_a = \dot{m}_a \cdot c_{p,a} \cdot (T_{a1} - T_o) \tag{4.6}$$

The mechanical power $\dot{W}_m$ depends on the output electrical power $\dot{W}_e$ of the generator and on the electrical losses that occur in the conversion of mechanical power into electrical form $\dot{W}_{\text{lg}}$, Eq. (4.7). If the values of these last two terms are not available, they can be evaluated by Eqs. (4.8) and (4.9), respectively, considering the efficiency of the electrical generator η_e.

$$\dot{W}_m = \dot{W}_e + \dot{W}_{\text{lg}} \tag{4.7}$$

$$\dot{W}_e = \dot{W}_m \cdot \eta_e \tag{4.8}$$

$$\dot{W}_{\text{lg}} = \dot{W}_m \cdot (1 - \eta_e) \tag{4.9}$$

As stated before, Eq. (4.1) expresses the energy balance of the Diesel generator in steady-state conditions that has to be satisfied. Since the provided documents specify all the terms except of $\dot{Q}_{eg}$, this last term can be evaluated as the difference:

$$\dot{Q}_{eg} = \dot{H}_f + \dot{Q}_a - \dot{W}_e - \dot{Q}_{lo} - \dot{Q}_{jw} - \dot{Q}_{ca,HT} - \dot{Q}_{ca,LT} - \dot{Q}_r - \dot{W}_{\text{lg}} \tag{4.10}$$

So, all the equations that are needed to perform the energy balance have been defined. The method is now applied to both engine types. Table 4.2 presents both the available data that have been used (white cells) and the results of the calculations (light shaded cells). Table 4.3 shows in detail the specific fuel energy consumption of the engines considering both types of fuels. The information about the load 85% is calculated by interpolation from the other data. The total specific fuel energy consumption is directly related to the efficiency of the engine that is presented as a function of the load in Figure 4.3. Despite the mechanical power output of the two types of engine is strongly different, they show same specific fuel consumption and efficiency. This is due to the fact that they are built with a different number of cylinders that are equal to each other.

Eq. (4.7) was solved for the electrical losses for the load 100%. For the other loads, Eqs. (4.8) and (4.9) have been used in order to calculate the electrical power and the

electrical losses, respectively. The electrical efficiency of the generator was considered to be equal to 96.49%, which correspond to the design value.

The total energy flow rate associated with the fuels $\dot{H}_f$ has been calculated through Eq. (4.5), and the heat flow rate associated with the exhaust gas through Eq. (4.10).

The values of $\dot{Q}_{lo}$, $\dot{Q}_{jw}$, $\dot{Q}_{ca,HT}$, $\dot{Q}_{ca,LT}$ and $\dot{Q}_r$ for the load 85% have been calculated interpolating the available information and considering that each thermal flow has to be null if the load of the engine is 0%.

Table 4.2 Source data (white background) and results of the calculations (blue background) for the two types of engines.

Load	$\dot{W}_m$	$\dot{W}_e$	$\dot{W}_{lg}$	b_f	$\dot{H}_f$	$\dot{Q}_{lo}$	$\dot{Q}_{jw}$	$\dot{Q}_{ca,HT}$	$\dot{Q}_{ca,LT}$	$\dot{Q}_r$	$\dot{Q}_{eg}$
%	kW	kW	kW	kJ/kWh	kW	kW	kW	kW	kW	kW	kW
Wärtsilä 6L50DF											
100	5700	5500	200	7780	12318	510	710	840	500	160	3898
90	5130	4950	180	7830	11158	490	660	700	430	170	3578
85	4845	4675	170	7896	10627	486	641	610	396	174	3475
75	4275	4125	150	8090	9607	480	610	430	330	180	3302
50	2850	2750	100	8720	6903	430	520	180	190	180	2553
Wärtsilä 12V50DF											
100	11400	11000	400	7780	24637	1020	1420	1680	1000	320	7797
90	10260	9900	360	7830	22316	980	1320	1400	860	340	7156
85	9690	9350	340	7896	21253	971	1283	1221	791	348	6949
75	8550	8250	300	8090	19214	960	1220	860	660	360	6604
50	5700	5500	200	8720	13807	860	1040	360	380	360	5107

Table 4.3 Specific fuel energy consumption of the engines, total b_f, gas fuel b_{fg}, pilot fuel b_{fl}. Data for *Wärtsilä 6L50DF* and *Wärtsilä 12V50DF* engines.

Load	%	100	90	85	75	50
b_f	kJ/kWh	7780	7830	7896	8090	8720
b_{fg}	kJ/kWh	7740	7780	7843	8030	8610
b_{fl}	g/kWh	1.0	1.2	1.3	1.5	2.5

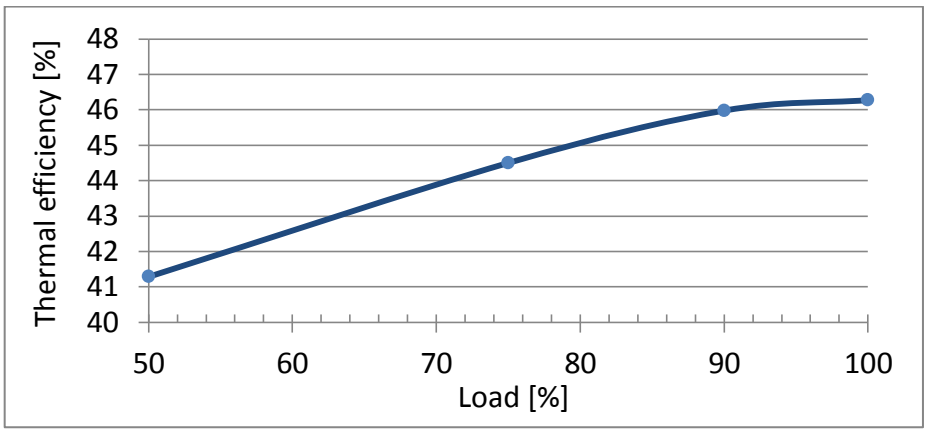

Figure 4.3 Thermal efficiency of the engine-generator set, models *Wärtsilä 6L50DF* and *Wärtsilä 12V50DF.*

Figure 4.4 shows the Sankey diagram for the Wärtsilä 12V50DF engine which provides a better understanding of the energy conversion process of the fuels. Figure 4.5 shows various heat flows that are dissipated by the engine-generator set Wärtsilä 12V50DF engine as a function of load.

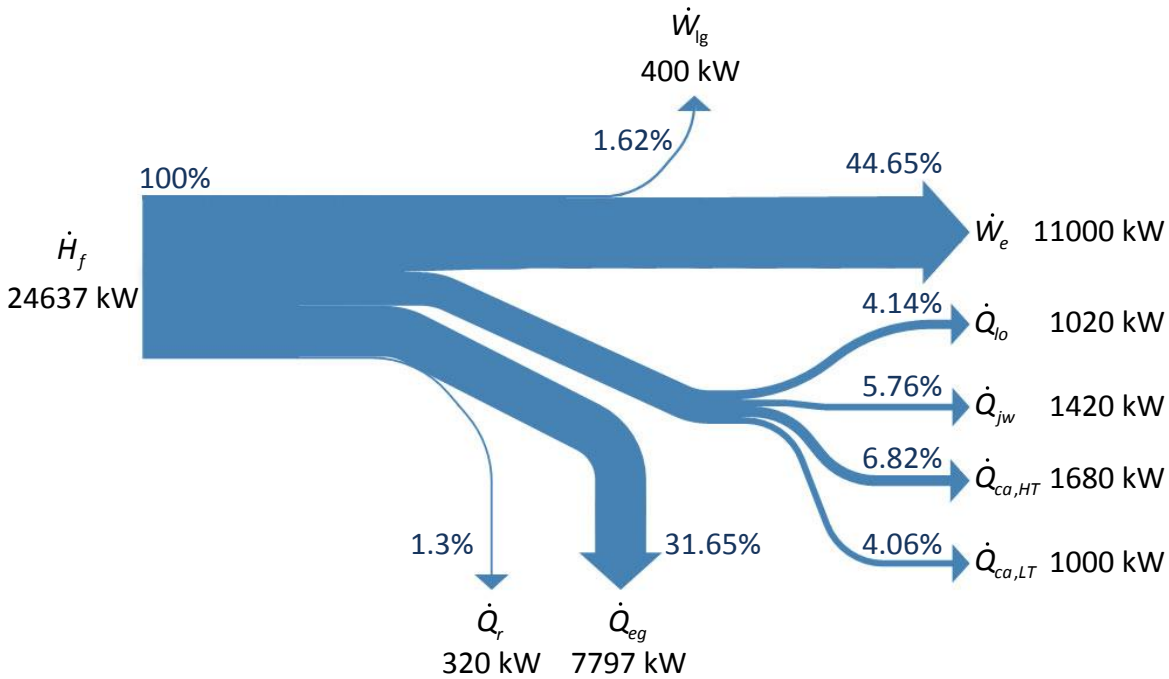

Figure 4.4 Sankey diagram for the Wärtsilä 12V50DF engine, load 100%.

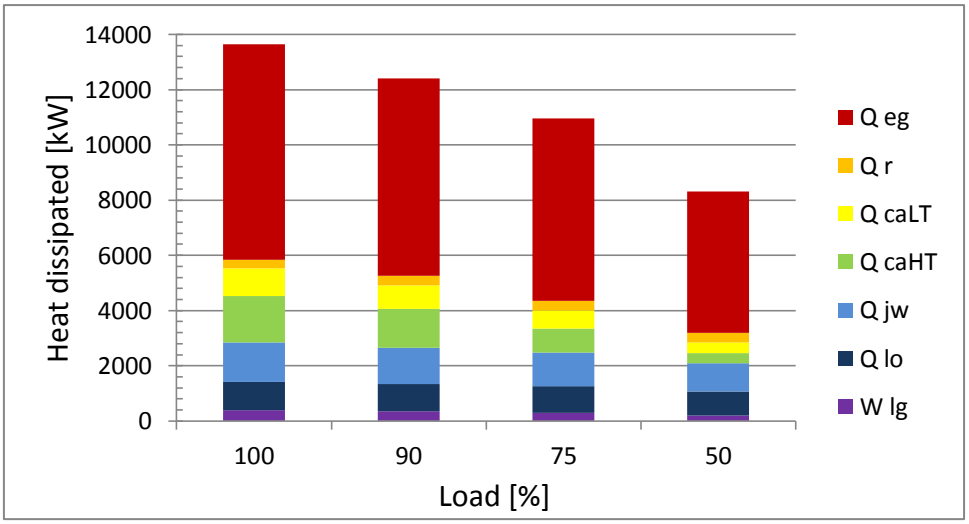

Figure 4.5 Heat flows dissipated as a function of the load for *Wärtsilä 12V50DF*.

4.2.2. Quality of Rejected Heat

In the previous sub-section, the energy balance of the engines have been performed and the heat flow rates that are dissipated through the cooling systems and heat associated with the exhaust gas have been identified. The study of the integration of a recovery system requires to know the quality (in terms of temperature) of the available heat. The aim of this sub-section is to provide this information.

All main engines that compose the generating power plant of the present ship have a similar cooling system that rejects heat at certain temperature levels to the cooling water provided by the “central cooler”. This last component is a system mainly composed of heat exchangers which in turns dissipate heat to seawater.

In particular, the cooling system of each engine is composed of the low temperature circuit (LT) and of the high temperature one (HT) as shown in Figure 4.6. In these circuits, the cooling flows (water) coming from the central cooler pass through various components and absorb heat, which increases their temperature.

The figure shows that the cooling flow in the HT circuit passes through the cylinder jackets and heads thus being heated from state *w1* to state *w2*. Then, it passes through the first stage of the charge air cooler (cooler *AC1* in the figure). A control valve after this cooler keeps the temperature of the HT water flow (T_{w3}) at an appropriate level, re-circulating a certain quantity of water. An additional valve is installed before the engine in order to maintain the temperature T_{w1} approximately constant.

The cooling flow of the LT circuit coming from the central cooler (state *w7*) passes through the second stage of the charge air cooler (cooler *AC2* in the figure) and then absorbs heat from the lubricating oil at the lubricating oil cooler (*LOC)*. A charge air temperature control valve regulates the mass flow rate of the LT cooling water through the second stage of the charge air cooler (partly bypassing the cooler), in order to set the

temperature of the air at state *a4*. Note that LT water flow comes directly from the central cooler so that its temperature depends on the operation of this component also in response to the climate conditions.

A tank of the lubricating oil is located just below the engine. From this, the oil is pumped into the lubricating oil cooler (*LOC)* where it is cooled down by transferring heat to the LT cooling flow, it passes through the engine and the turbocharger (*T/C)* and comes back to the tank. A temperature control valve is installed after the lubricating oil cooler to keep oil temperature constant at the engine inlet.

The arrangement shown in Figure 4.6 is valid for the two types of engines. The figure shows that the heat associated with the exhaust gas after the turbine of the T/C (state *eg2*) can be exploited by an exhaust gas boiler (*EGB*) (Section 4.4). Also, a water flow can be derived from the cooling flow of the HT cooling circuit to feed a Fresh water generator (FWG) which produces desalinated water (Section 4.3).

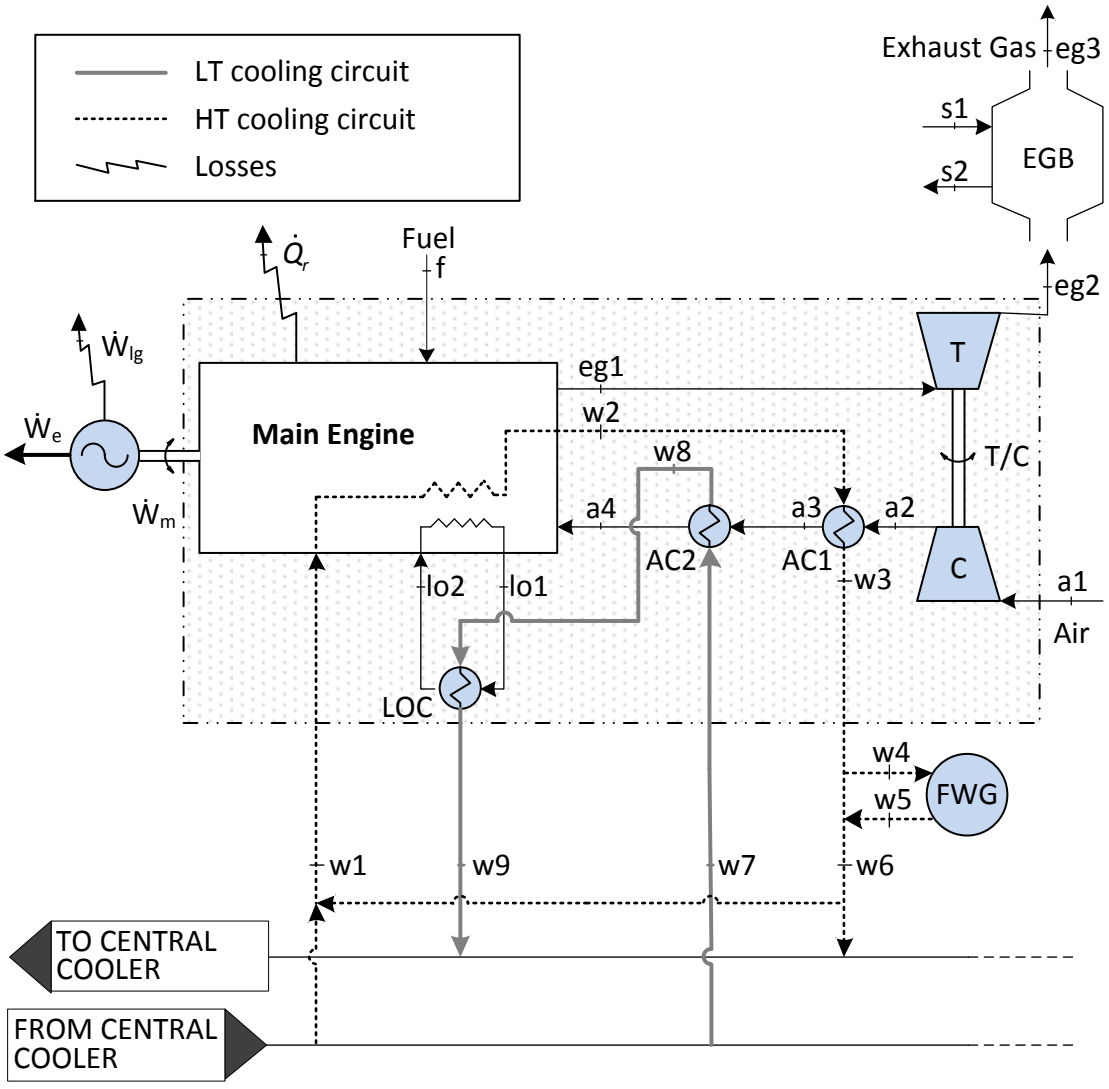

Figure 4.6 Arrangement of Main Engine and cooling circuits.

In the previous sub-section the energy balance of the two types of engines was performed by defining the value of the various heat flows that are rejected to the cooling water, lubricating oil and exhaust gas. Referring to Figure 4.6, these flows can be defined also through the thermodynamic quantities such as temperatures and enthalpies.

Equation (4.11) defines the jacket water heat flow rate $\dot{Q}_{jw}$ that is the heat rejected by cylinder jackets and heads to the HT circuit cooling flow and Eq. (4.12) gives the heat flow rate rejected by the charge air flow at the first stage of the charge air cooler $\dot{Q}_{ca,HT}$. This last quantity can also be defined by considering the cooling process of the air at the same component, Eq. (4.13).

$$\dot{Q}_{jw} = \dot{m}_{w1} \cdot (h_{w2} - h_{w1}) \tag{4.11}$$

$$\dot{Q}_{ca,HT} = \dot{m}_{w1} \cdot (h_{w3} - h_{w2}) \tag{4.12}$$

$$\dot{Q}_{ca,HT} = \dot{m}_{a} \cdot (h_{a2} - h_{a3}) \tag{4.13}$$

The total heat flow rate that is transferred to the cooling flow of the HT circuit is:

$$\dot{Q}_{HT} = \dot{Q}_{jw} + \dot{Q}_{ca,HT} = \dot{m}_{w1} \cdot (h_{w3} - h_{w1}) \tag{4.14}$$

As mentioned above, a fresh water generator (FWG) can be installed after the engine and operates receiving heat by the hot water of the HT circuit. The heat absorbed in this case is defined by Eq. (4.15) or Eq. (4.16). The remaining heat available for an additional recovery system $\dot{Q}_{HT,Available}$ is defined by Eq. (4.17).

$$\dot{Q}_{FWG} = \dot{m}_{FWG} \cdot q_{FWG} \tag{4.15}$$

$$\dot{Q}_{FWG} = \dot{m}_{4} \cdot (h_{w4} - h_{w5}) \tag{4.16}$$

$$\dot{Q}_{HT,Available} = \dot{Q}_{HT} - \dot{Q}_{FWG} = \dot{m}_{w1} \cdot (h_{w6} - h_{w1}) \tag{4.17}$$

The heat absorbed by the low temperature circuit is defined by the following equations where $\dot{Q}_{ca,LT}$ and $\dot{Q}_{lo}$ are related to the second stage of the air cooler and to the lubricating oil cooler, respectively.

$$\dot{Q}_{ca,LT} = \dot{m}_{w7} \cdot (h_{w8} - h_{w7}) \tag{4.18}$$

$$\dot{Q}_{lo} = \dot{m}_{w7} \cdot (h_{w9} - h_{w8}) \tag{4.19}$$

$$\dot{Q}_{LT} = \dot{Q}_{ca,LT} + \dot{Q}_{lo} = \dot{m}_{w7} \cdot (h_{w9} - h_{w7}) \tag{4.20}$$

The quantities $\dot{Q}_{ca,LT}$ and $\dot{Q}_{lo}$ are defined also by Eqs. (4.21) and (4.22) that consider fluids on the other side of the respective heat exchangers.

$$\dot{Q}_{ca,LT} = \dot{m}_a \cdot (h_{a3} - h_{a4}) \tag{4.21}$$

$$\dot{Q}_{lo} = \dot{m}_{lo} \cdot (h_{lo2} - h_{lo1}) \approx \dot{m}_{lo} \cdot c_{p,lo} \cdot (T_{lo2} - T_{lo1}) \tag{4.22}$$

Useful heat of the exhaust gas boiler:

$$\dot{Q}_{EGB} = \dot{m}_s \cdot (h_{s2} - h_{s1}) \tag{4.23}$$

or

$$\dot{Q}_{EGB} = \eta_{EGB} \cdot \dot{m}_{eg} \cdot c_{p,eg} \cdot (T_{eg2} - T_{eg3}) \tag{4.24}$$

Equation (4.25) allows the mass flow rate of the air to be calculated when the mass flow rate of the exhaust gas and fuels are known:

$$\dot{m}_a = \dot{m}_{eg} - \dot{m}_{fg} - \dot{m}_{fl} \tag{4.25}$$

Table 4.4 presents the information that has been collected about various states (white cells). The values of the parameters T_{w1}, T_{w3}, T_{w7}, T_{a4}, T_{eg2}, T_{lo2}, $\dot{m}_{eg2}$, p_{bar} and p_{a2} are known only for some of the considered engine loads. The missing values (light shaded cells) have been calculated by interpolation. As regards the *Wärtsilä 12V50DF* engine, the values of the temperatures T_{w1} and T_{w7} found on the available documents and related to the loads 85% and 50%, respectively, have not been accepted as valid values. Substitute values have been calculated by interpolating through the data of the other loads and they are presented in the table in light shaded cells.

The equations that have been defined up to now allow the calculation of the missing values for the operating parameters to be performed.

For each cooling circuit, the properties of the “water” have been calculated using the NIST Refprop database [Lemmon et al. (2007)] and assuming that the pressures p_{w1} and p_{w7} remain constant through the various components. Analogous hypothesis has been considered for the air flow: it is considered that the given value for the pressure p_{a2}

does not change before state *a4*. The properties of the air have been evaluated by considering a relative humidity of 30%, in accordance with ISO conditions.

With regard to the HT cooling circuit, Eq. (4.14) can be solved for the mass flow rate of the water to give:

$$\dot{m}_{w1} = \frac{\dot{Q}_{jw} + \dot{Q}_{ca,HT}}{(h_{w3} - h_{w1})} \tag{4.26}$$

while the temperature T_{w2} can be calculated knowing the pressure of the water in the HT circuit and the specific enthalpy h_{w2} that is obtained by solving Eq. (4.11):

$$h_{w2} = h_{w1} + \frac{\dot{Q}_{jw}}{\dot{m}_{w1}} \tag{4.27}$$

As regard to the LT circuit, a control valve is installed after the central cooler and maintains the temperature of the water before each engine T_{w7} close to the set-point of 35°C, partly bypassing the central cooler. No information is provided about the rate ($\dot{m}_{w7}$) and the outlet temperature (T_{w9}) of the LT circuit cooling flow. It is known that the nominal value of the temperature T_{w8} is equal to 45°C [Wärtsilä (2012)]. This value is taken as representative of the engine load 100% allowing the calculation of the values of various parameters at the same load: Eq. (4.18) can be solved in order to estimate the mass flow rate $\dot{m}_{w7}$, Eq. (4.28); Eq. (4.19) is solved for the specific enthalpy of the cooling flow (water) at LT circuit outlet h_{w9}, Eq. (4.29):

$$\dot{m}_{w7} = \frac{\dot{Q}_{ca,LT}}{(h_{w8} - h_{w7})} \tag{4.28}$$

$$h_{w9} = h_{w8} + \frac{\dot{Q}_{lo}}{\dot{m}_{w7}} \tag{4.29}$$

The mass flow rate $\dot{m}_{w7}$ calculated for the load 100% is considered valid also for the other loads. This assumption is considered reasonable because of the fact that pumps are engine driven [“Machinery operating manual”].

For all loads except 100%, the specific enthalpy h_{w8} is calculated solving Eq. (4.18). The specific enthalpy of the water at state *w9* that is given by Eq. (4.29) allows the temperature T_{w9} to be calculated.

As regards the lubricating oil system, available information is the oil temperature T_{lo2} at engine inlet for various loads and the outlet temperature T_{lo1} for the load 100%.

Considering a constant value for the specific heat capacity of the oil $c_{p,lo}$ equal to 1.88 kJ/(kg·K) ["Energy and steam balance of the ship"], the mass flow rate of the oil $\dot{m}_{lo}$ is calculated by solving Eq. (4.22) for the load 100%:

$$\dot{m}_{lo} \approx \frac{\dot{Q}_{lo}}{c_{p,lo} \cdot (T_{lo2} - T_{lo1})} \tag{4.30}$$

This value is considered valid also for the other loads because the pump is engine driven. The temperature T_{lo1} is then calculated for all the loads but 100% solving Eq. (4.22), Eq. (4.31):

$$T_{lo1} \approx T_{lo2} + \frac{\dot{Q}_{lo}}{m_{lo} \cdot c_{p,lo}} \tag{4.31}$$

States *a2*, *a3* and *a4* need to be characterized by the mass flow rate of the air and the temperature. The mass flow rate can be calculated using Eq. (4.25) which require to know the mass flow rates of the two fuels that are given by Eqs. (4.32) and (4.33):

$$\dot{m}_{fg}\left[\frac{\text{kg}}{\text{s}}\right] = b_{fg}\left[\frac{\text{kJ}}{\text{kWh}}\right] \cdot \dot{W}_m \text{ kW} \cdot \frac{\text{h}}{3600\text{s}} \cdot \frac{1}{H_{u,fg}} \tag{4.32}$$

$$\dot{m}_{fl}\left[\frac{\text{kg}}{\text{s}}\right] = b_{fl}\left[\frac{g}{\text{kWh}}\right] \cdot \dot{W}_m \text{ kW} \cdot \frac{\text{h}}{3600\text{s}} \cdot \frac{\text{kg}}{1000\text{g}} \tag{4.33}$$

where

- $\dot{m}_{fg}$ mass flow rate of the fuel gas,
- $\dot{m}_{fl}$ mass flow rate of the pilot fuel (liquid),
- b_{fg} specific fuel gas energy consumption (Table 4.3),
- b_{fl} specific pilot fuel energy consumption (Table 4.3),
- $H_{u,fg}$ lower heating value of the fuel gas assumed to be 49000 kJ/kg.

Equation (4.21) can be solved for the specific enthalpy h_{a3}, Eq. (4.34). Equation (4.13) is solved for the specific enthalpy h_{a2}, Eq. (4.35).

$$h_{a3} = h_{a4} + \frac{\dot{Q}_{ca,LT}}{\dot{m}_a} \tag{4.34}$$

$$h_{a2} = h_{a3} + \frac{\dot{Q}_{ca,HT}}{\dot{m}_a} \tag{4.35}$$

The temperatures T_{a3} and T_{a4} are calculated by knowing the specific enthalpy of the related state and the value of pressure p_{a2}.

Table 4.4 Summary of the operating parameters, source data (white cells) and results of the calculations (light shaded cells) for the two types of engines.

		Wärtsilä 6L50DF					*Wärtsilä 12V50DF*				
Par.	Unit	100	90	85	75	50	100	90	85	75	50
T_{w1}	°C	74	74.6	75	76	78	76	76.4	76.6	77	78
T_{w2}	°C	79.4	78.3	78.6	79.5	81.0	80.1	79.8	79.9	80.5	81.0
T_{w3}	°C	83	82.2	82	82	82	85	83.3	83	83	82
T_{w7}	°C	36	36	36	38	38	36	36	36	36	36
T_{w8}	°C	45	43.7	43.1	43.9	41.4	45	43.7	43.1	41.9	39.4
T_{w9}	°C	54.2	52.6	51.9	52.6	49.7	54.2	52.6	51.9	50.6	47.2
T_{a2}	°C	187.0	177.6	170.5	151.9	113.1	183.3	176.8	169.6	151.9	113.1
T_{a3}	°C	97.8	95.2	94.1	91.1	79.3	96.3	94.9	93.7	91.1	79.6
T_{a4}	°C	44	44.6	45	46	50	45	44.2	44	45	51
T_{eg2}	°C	390	397	409.7	441	438	390	397	409.7	441	438
T_{lo1}	°C	76	75.4	75.3	75.1	73.6	76	75.4	75.3	75.1	73.6
T_{lo2}	°C	61	61	61	61	61	61	61	61	61	61
$\dot{m}_{lo}$	kg/s	18.1	18.1	18.1	18.1	18.1	36.2	36.2	36.2	36.2	36.2
$\dot{m}_{w1}$	kg/s	31.5	42.7	42.6	41.3	41.7	82.1	93.9	93.2	82.6	83.4
$\dot{m}_{w7}$	kg/s	13.3	13.3	13.3	13.3	13.3	26.6	26.6	26.6	26.6	26.6
$\dot{m}_a$	kg/s	9.15	8.27	7.78	6.9	5.26	18.3	16.64	15.67	13.81	10.52
$\dot{m}_{eg2}$	kg/s	9.4	8.5	8.0	7.1	5.4	18.8	17.1	16.1	14.2	10.8
p_{bar}	bar	1.028	1.028	1.028	1.030	1.031	1.015	1.015	1.015	1.016	1.016
p_{a2}	bar-g	2.4	2.14	2	1.7	1	2.3	2.16	2	1.6	0.9
p_{w1}	bar	3.15	3.15	3.15	3.15	3.15	3.15	3.15	3.15	3.15	3.15
p_{w7}	bar	3.15	3.15	3.15	3.15	3.15	3.15	3.15	3.15	3.15	3.15

Figure 4.7 shows the arrangement of the Wärtsilä 12V50DF Main Engine and cooling circuits presented in Figure 4.6, together with the values of temperature and mass flow rate at various states. This information is referred to the load of 100%.

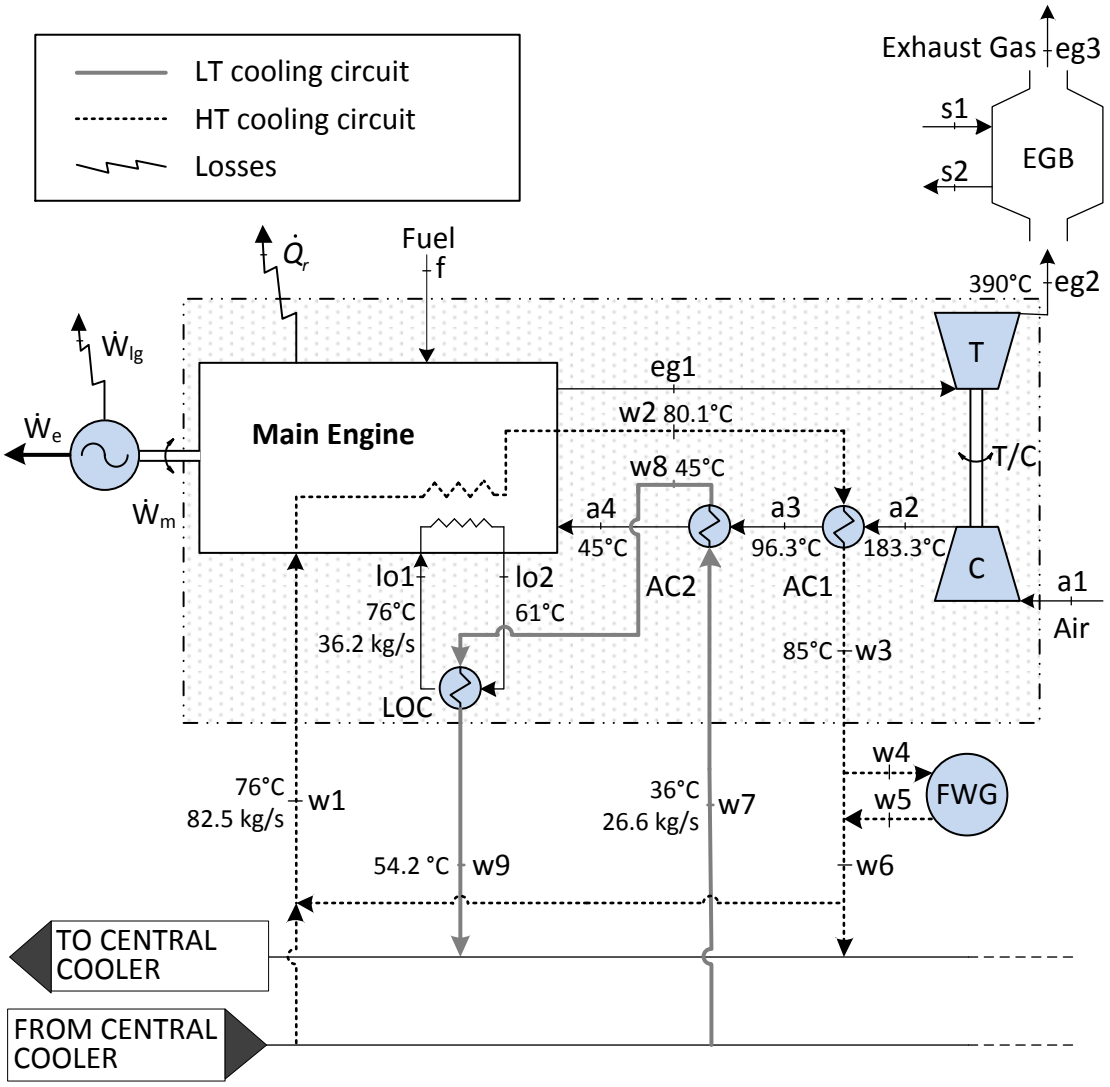

Figure 4.7 Arrangement of Wärtsilä 12V50DF Main Engine and cooling circuits; load 100%.

4.3 Fresh Water Generators

Fresh water (desalinated water) needs of the present ship are supplied by two different Alfa Laval generators. In particular, a JWP-26-C100 and a HWL 20-35 FWG are installed on board. Basically, they are driven by the hot water of the engines cooling systems but the HWL 20-35 unit is equipped with an additional heating unit driven by steam. The use of steam instead of water allows the generation of fresh water to be performed even when the engines are not running.

Thermal flow rates that are needed for fresh water production have to be taken into consideration in order to quantify the effective heat available to be exploited by the recovery system studied in this work. According to Figure 4.6, the fresh water generators (FWGs) are fed by the water of HT engine cooling circuits. Due to flexibility reasons, the

FWGs are not connected to a particular engine: the feeding flow is taken after the water collected from the various HT cooling systems is mixed at circuits outlet.

As regards the JWP-26-C100 unit, the heat absorbed can be expressed by the following two equations copied here for convenience from Sub-section 4.2.2:

$$\dot{Q}_{FWG} = \dot{m}_{FWG} \cdot q_{FWG} \tag{4.15}$$

$$\dot{Q}_{FWG} = \dot{m}_4 \cdot (h_{w4} - h_{w5}) \tag{4.16}$$

where

$\dot{m}_{FWG}$ mass flow rate of fresh water to be generated,

q_{FWG} specific heat consumption of the FWG,

$(h_{w4} - h_{w5})$ difference of specific enthalpy of the feeding water (inlet and outlet conditions, respectively),

$\dot{m}_4$ mass flow rate of the feeding water.

The operation of the FWG model HWL 20-35 is defined by Eq. (4.15) and a modified expression of Eq. (4.16) that considers the additional heat provided by the steam $\dot{Q}_{steam}$, Eq. (4.36):

$$\dot{Q}_{FWG} = \dot{m}_4 \cdot (h_{w4} - h_{w5}) + \dot{Q}_{steam} \tag{4.36}$$

Table 4.5 reports the main characteristic of the fresh water generators taken from the manuals of the manufacturer. The design inlet temperature of the feeding water is

Table 4.5 Main characteristics of the fresh water generators [Alfa Laval Desalt A/S (a); Alfa Laval Desalt A/S, (b)].

Model JWP-26-C100		
Generator capacity	m^3/24h	30
Inlet temperature of the feeding water (range)	°C	55÷95
Inlet temperature of the feeding water (design)	°C	91
Outlet temperature of the feeding water	°C	73
Heat absorbed	kW	891.7
Model HWL 20-35		
Generator capacity	m^3/24h	30
Maximum steam flow	kg/h	1425
Pressure of steam	bar	5÷7

reported for the JWP-26-C100 model. Note that the actual temperature can vary in the range presented in the table.

The provided information indicates that only the FWG model JWP-26-C100 is kept in operation. The other unit usually does not operate and it will not be taken into consideration in the present work.

As regards the JWP-26-C100 generator, there is no need to use Eq. (4.15) to calculate the heat absorbed at the design condition because this value is provided by the manual and it is reported in Table 4.5. Equation (4.16) can then be solved for the mass flow rate of the feeding water $\dot{m}_{w4}$ to give:

$$\dot{m}_{w4} = \frac{\dot{Q}_{FWG}}{h_{w4} - h_{w5}} = \frac{891.7\text{kW}}{381.43\frac{\text{kJ}}{\text{kg}} - 305.87\frac{\text{kJ}}{\text{kg}}} = 11.80\frac{\text{kg}}{\text{s}}$$

where the specific enthalpy difference is calculated by considering the values of the temperature reported in Table 4.5 with the assumption of constant pressure from the inlet to the outlet condition of the feeding water flow. In this way, according to the specifications of the engines, the pressure of the state *w4* and *w5* is equal to 3.15 bar. The thermodynamic properties of the water are calculated using the NIST Refprop database [Lemmon et al. (2007)].

If the inlet-outlet temperature difference of the feeding water is different from the design value, a bypass valve is used to adjust the water flow $\dot{m}_{w4}$. Equation (4.37) can be used to calculate the mass flow rate:

$$\dot{m}_{w4} = \frac{K \cdot \dot{V}_d}{\Delta T} \tag{4.37}$$

where

$\dot{m}_{w4}$ mass flow rate of the feeding water [kg/s],

K proportionality constant to be considered equal to $7.08\frac{\text{kg}}{\text{s}} \cdot \frac{24\text{h}}{\text{m}^3} \cdot °\text{C}$ (as determined from the manual of the FWG),

$\dot{V}_d$ capacity of the fresh water generator [m^3/24h],

ΔT inlet-outlet difference of temperature of the feeding water [°C].

Note that Eq. (4.37) considers that the heat absorbed by the FWG is constant and equal to design value even in off-design conditions. The mass flow rate of the feeding water is in fact adjusted in order to fix its value.

4.4 Boilers for Steam Production

The equipment of the ship for steam production is composed of four “Alfa Laval” generators. Two exhaust gas economizers are coupled with two different engines: one with a Wärtsilä 12V50DF engine and the other one with a Wärtsilä 6L50DF unit. Two auxiliary boilers produce additional steam in case of high demand or low availability of heat from the exhaust gas. Table 4.6 presents the available information taken from the “Heat and steam balance” of the ship.

Table 4.6 Steam generating plant.

	Unit	Auxiliary Boiler	Exhaust gas economizer
No. of sets	-	2	2
Evaporation pressure	bar	7	7
Capacity	kg/h	6500	2500

4.5 Conclusions

The main equipment that composes the integrated energy system of the ship has been presented in the current chapter. The electric power generation plant has been described in details: the operation of the engine-generator sets has been defined by an energy balance that has allowed the thermal flow rates rejected to the cooling systems to be defined for various loads. Mass flow rates and temperatures of the flows which are involved in the removal of heat from the engines have been calculated for various loads.

The actual arrangement of the engine-generator sets cooling systems has been presented in order to understand how waste heat is collected. This step allows to individuate the way in which it is possible to integrate the ORC based recovery system in the ship energy system.

The existing equipment for fresh water (desalinated water) and steam generation have been presented. The operation of the fresh water generator which is practically used has been defined both in design and off-design conditions.

5 ENERGY DEMANDS OF THE SHIP

5.1 Introduction

Each ship has its own peculiarities and specific energy needs related to the purpose of the vessel. Mechanical or electrical power is requested for propulsion and to drive auxiliary systems. In addition, electrical power is requested to cover other needs (i.e., demands of the hotel), and fresh water and steam have to be provided as well.

The aim of this chapter is to characterize the current ship by its energy demands, which are needed to evaluate the integration of a Rankine cycle into the "ship energy system" in order to obtain a better exploitation of the primary energy of the fuel.

5.2 Power Demands of the Vessel

Power demands of a vessel are different in each phase of a trip and generally are a function of its service speed V_s. Propulsion represents the most important power need of a ship and, depending on the case, it can be satisfied directly by the mechanical power generated by the main engine plant or indirectly after conversion to electric energy. In this last case, electrical needs of the vessel can be expressed by:

$$\dot{W}_e(V_s) = \dot{W}_{e,p}(V_s) + \dot{W}_{e,ep}(V_s) \tag{5.1}$$

where $\dot{W}_{e,p}(V_s)$ is the electrical power demand for propulsion (usually proportional to the cube of the service speed) and $\dot{W}_{e,ep}(V_s)$ represents the requirements of the additional electric loads (i.e., the electric loads except of propulsion).

Dimopoulos and Frangopoulos (2008) presented the power demands of an LNG vessel of 150000 m^3 in typical operating phases, considering certain values for the service speed in the range of 17÷25 kn. Based on their work and with regards to the laden voyage, Eqs. (5.2) and (5.3) define the electrical needs for propulsion and for the additional electric loads, respectively:

$$\dot{W}_{e,p} = 83.3333 \cdot V_s^3 - 4375.0000 \cdot V_s^2 + 80216.6667 \cdot V_s - 491125.0000 \tag{5.2}$$

$$\dot{W}_{e,ep} = 6.2500 \cdot V_s^3 - 356.2500 \cdot V_s^2 + 6843.7500 \cdot V_s - 42793.7500 \tag{5.3}$$

where the unit of the electrical power and service speed are kW and kn, respectively. These equations are considered applicable in the range 17÷23 kn. Similar equations are proposed for the ballast voyage, Eqs. (5.4) and (5.5):

$$\dot{W}_{e,p} = 79.1667 \cdot V_s^3 - 4156.2500 \cdot V_s^2 + 76205.8333 \cdot V_s - 467518.7500 \tag{5.4}$$

$$\dot{W}_{e,ep} = 5.6250 \cdot V_s^3 - 320.6250 \cdot V_s^2 + 6159.3750 \cdot V_s - 38514.3750 \tag{5.5}$$

The needs expressed through these equations include also the energy losses that take place after the generator sets and before the final uses. In other words, the values represent the electrical power that the generation plant has to make available for the referred purpose.

Equations (5.6) and (5.7) are based on the definition of Eq. (5.1) and express the total electric power demand of the vessel in the laden and ballast voyage, respectively:

$$\dot{W}_{e,laden} = 89.5833 \cdot V_s^3 - 4731.2500 \cdot V_s^2 + 87060.4167 \cdot V_s - 534918.7500 \tag{5.6}$$

$$\dot{W}_{e,ballast} = 84.7917 \cdot V_s^3 - 4476.8750 \cdot V_s^2 + 82365.2083 \cdot V_s - 506033.125 \tag{5.7}$$

The equations defined up to here are evaluated for various service speed values and the results are reported in Table 5.1 and in Table 5.2 for the laden and ballast voyage, respectively. Results are then presented in Figure 5.1 and Figure 5.2. The first one shows the electrical power demand for propulsion and the second one presents the electrical needs of the ship except of propulsion.

Table 5.1 Electrical power demands in the laden voyage.

V_s	$\dot{W}_{e,p}$	$\dot{W}_{e,ep}$	$\dot{W}_{e,laden}$
kn	kW	kW	kW
17	16600	1300	17900
18	20275	1419	21694
19	24200	1500	25700
20	28875	1581	30456
21	34800	1700	36500
22	42475	1894	44368
23	52400	2200	54600

Table 5.2 Demand of electrical power in the ballast voyage.

V_s	$\dot{W}_{e,p}$	$\dot{W}_{e,ep}$	$\dot{W}_{e,ballast}$
kn	kW	kW	kW
17	15770	1170	16940
18	19261	1277	20538
19	22990	1350	24340
20	27432	1423	28855
21	33060	1530	34590
22	40352	1704	42056
23	49780	1980	51760

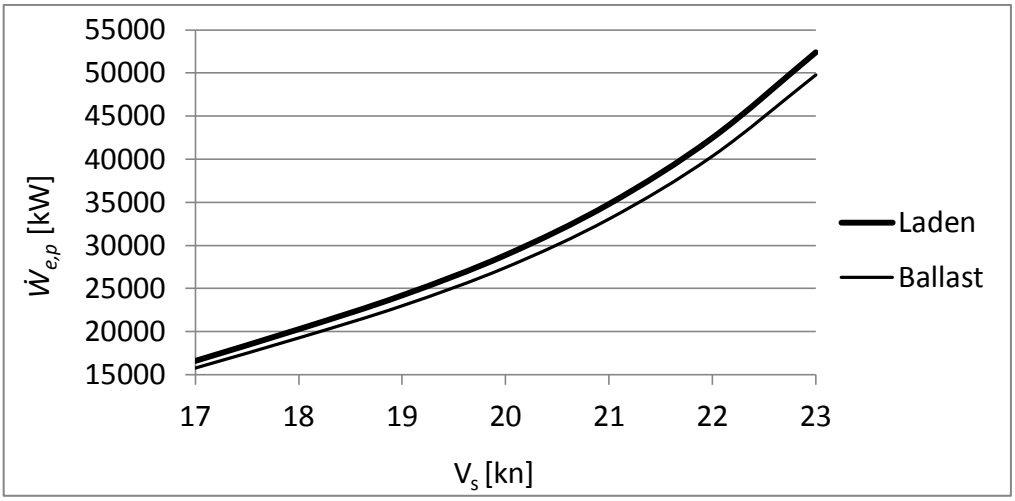

Figure 5.1 Electrical power required for the propulsion as a function of the service speed V_s in laden and ballast voyage.

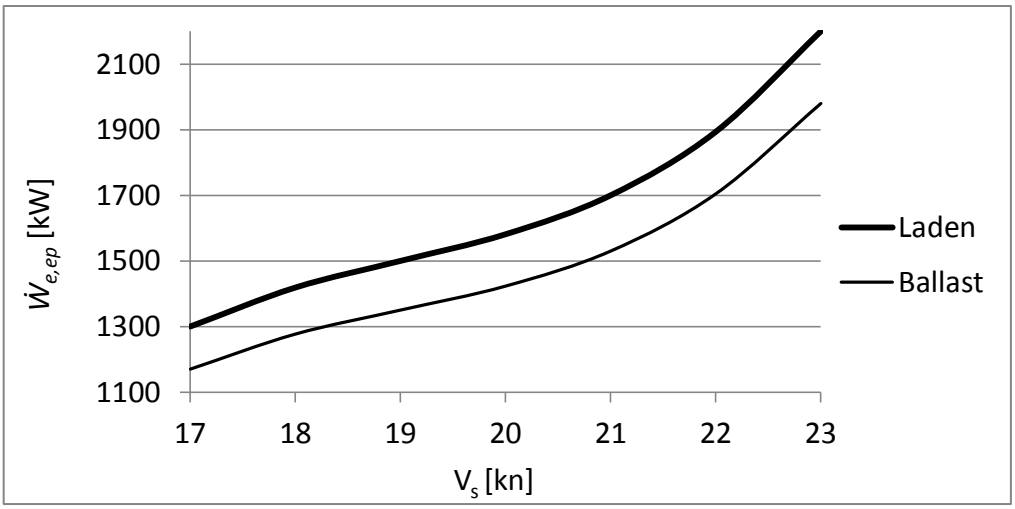

Figure 5.2 Electrical power required by the systems except of propulsion, as a function of the service speed of the vessel V_s, laden and ballast voyage.

Equations (5.6) and (5.7) can be used to calculate the maximum service speed of the vessel in both the laden and the ballast voyage. Considering the maximum electrical power that can be made available by the generation plant when all the diesel generators are in operation at the condition of 100% load (equal to 33000 kW, as defined in Section 4.2), these values are:

$V_{s,laden}$ = 20.45 kn

$V_{s,ballast}$ = 20.75 kn

The same results are shown graphically in Figure 5.3. The plotted curves are the total demand of electrical power in laden and ballast voyage and the horizontal line represents the maximum power.

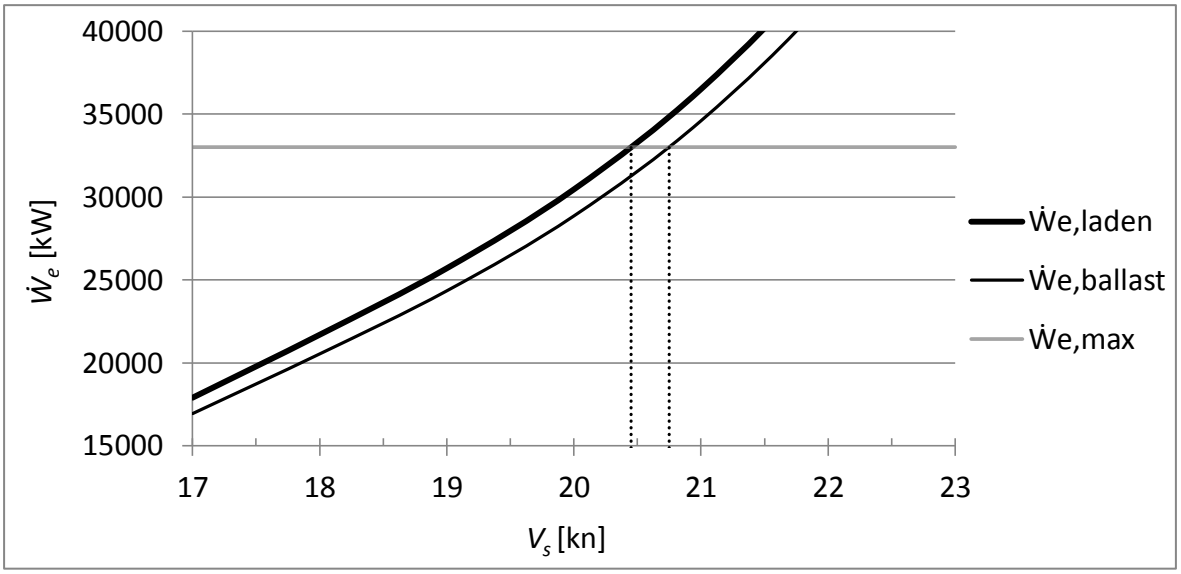

Figure 5.3 Total electrical power required as a function of the service speed of the vessel V_s, laden and ballast voyage.

As stated before, the equations presented in the current section are valid in the range of 17÷23 kn for the service speed. There is the need to overcome this limitation searching for a criterion that allows the electrical power needs for lower values of the service speed to be calculated.

It is well known that the power needed for propulsion basically depends on the cube of the service speed of the vessel V_s^3 with a constant of proportionality a:

$$\dot{W}_{e,p} = a \cdot V_s^3 \tag{5.8}$$

It is assumed that this equation can be used to describe the power needed for propulsion of the current vessel. The value of the constant of proportionality is calculated for each voyage, if the power required at the speed of 20 kn is considered and Eq. (5.8) is solved:

$$a_{laden} = \frac{\dot{W}_{e,p}}{V_s^3} = \frac{28875\text{kW}}{(20\text{kn})^3} = 3.6094 \frac{\text{kW}}{\text{kn}^3}$$

$$a_{ballast} = \frac{\dot{W}_{e,p}}{V_s^3} = \frac{27432\text{kW}}{(20\text{kn})^3} = 3.429 \frac{\text{kW}}{\text{kn}^3}$$

The so defined equations for the calculation of the electrical needs for propulsion are considered valid in all the range of speed in which the current ship is operated:

$$\dot{W}_{e,p,laden} = 3.6094 \cdot V_s^3 \tag{5.9}$$

$$\dot{W}_{e,p,ballast} = 3.429 \cdot V_s^3 \tag{5.10}$$

whereas Eqs. (5.3) and (5.5) give the additional electric loads for laden and ballast voyage in case of service speed over 17 kn. These loads are considered constant and equal to the values calculated for 17 kn for the lower speeds. This is based on the assumption that below a certain value of the service speed, the power required by systems other than propulsion does not decrease. Table 5.3 summarises the electrical needs of the ship for various values of service speed in the laden and ballast voyage.

Table 5.3 Electrical needs of the ship, laden (left) and ballast (right) voyage.

V_s	$\dot{W}_{e,p}$	$\dot{W}_{e,ep}$	$\dot{W}_{e,laden}$
kn	kW	kW	kW
8	1848	1300	3148
10	3609	1300	4909
12	6237	1300	7537
14	9904	1300	11204
16	14784	1300	16084
18	21050	1419	22469
20	28875	1581	30456

V_s	$\dot{W}_{e,p}$	$\dot{W}_{e,ep}$	$\dot{W}_{e,ballast}$
kn	kW	kW	kW
8	1756	1170	2926
10	3429	1170	4599
12	5925	1170	7095
14	9409	1170	10579
16	14045	1170	15215
18	19998	1277	21275
20	27432	1423	28855

5.3 Operating Profile of the vessel and of the engines

The operating profile of a vessel is a document which describes numerically how the vessel is operated during the year. The operating profile of the present LNG carrier considers three operating modes: “laden voyage”, “ballast voyage” and “staying in port”. The data define a typical year of operation as an average of 3.75 years. Figure 5.4 presents the percentage of the time and the number of hours of the operation in each mode. Note that the “staying in port” mode represents a significant phase of the vessel operation (25% of the time). In this case, the output of the electric power generating plant is usually low because of the absence of the demand associated with propulsion. Only an engine-generator set is usually kept into operation and the resulting low waste heat availability leads to not consider this operating mode in the present study.

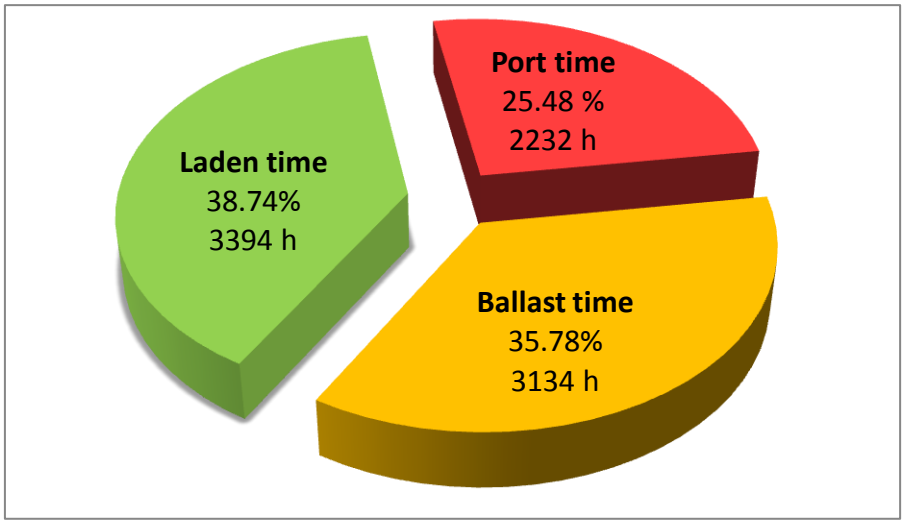

Figure 5.4 Operating modes of the current ship.

The vessel speed distribution profile is provided for laden and ballast modes. The overall range of the service speed (from 0 kn to 21 kn) is divided into 21 intervals of 1 kn, and for each of them, the number of hours is given as a percentage of total time in the mode; the number of hours of each interval is attributed to its average speed. The profile is presented in Figure 5.5 where values for the service speed below 6 kn are not considered. The two percentages that are reported for each interval are referred to the laden and ballast modes, respectively.

Note that most of the time the speed of the vessel is lower than the maximum value. Thus, the vessel sails in “slow steaming” mode: a lower service speed leads to a significant reduction in power for propulsion reducing at the same time the fuel consumption.

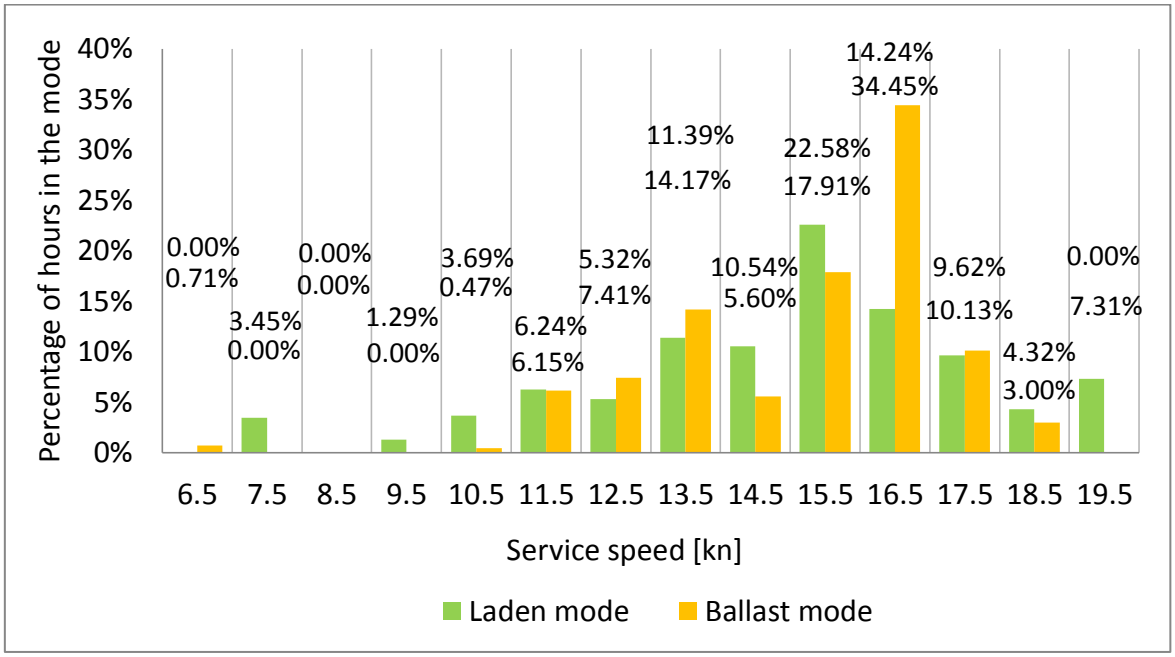

Figure 5.5 Distribution profile of the vessel speed at laden and ballast voyage. The percentages are referred to the hours in laden and ballast modes, respectively.

The method presented in Section 5.2 allows the various values of speed reported in Figure 5.5 to be correlated to the electrical power that has to be made available. However, this calculation does not dictate how the electrical power is produced: the same value can be obtained through the operation of different combination of engine – generator sets. At the same time the load at which each of them is operated could be different introducing a complication in the control logic.

The present work makes two assumptions in order to overcome the missing information: the electrical power is generated by the lowest possible number of engine-generator sets trying to operate them at a load that is closed to the maximum efficiency; the second assumption considers that the total electric load is distributed to the operating generators in proportion to their nominal power.

Table 5.4 shows the electrical power that has to be generated, in case of laden voyage, for the values of speed considered by the profile of Figure 5.5. For each condition, the engines that are kept in operation are presented and the corresponding power production is reported in accordance with the two aforementioned assumptions. The load of the engines is reported as well. Table 5.5 provides similar information relating to the case of ballast voyage. Each operating condition (row) reported in the two tables is identified univocally by the number reported in the column “No.”.

Table 5.4 Operating profile of the engines, laden voyage.

No.	Average speed	Hours	Hours	W_e	12V50DF No.1	6L50DF No. 2	6L50DF No. 3	12V50DF No.4	Load
-	kn	%	-	kW	kW	kW	kW	kW	%
1	7.5	3.5	117.1	2823	0	0	2823	0	51
2	8.5	0.0	0.0	3517	-	-	-	-	-
3	9.5	1.3	43.8	4395	0	0	4395	0	80
4	10.5	3.7	125.2	5478	0	0	5478	0	100
5	11.5	6.2	211.8	6789	0	0	0	6789	62
6	12.5	5.3	180.6	8350	0	0	0	8350	76
7	13.5	11.4	386.6	10180	0	0	0	10180	93
8	14.5	10.5	357.7	12304	0	0	4101	8202	75
9	15.5	22.6	766.4	14741	0	0	4914	9827	89
10	16.5	14.2	483.3	17514	0	4378	4378	8757	80
11	17.5	9.6	326.5	20711	0	5178	5178	10355	94
12	18.5	4.3	146.6	24315	9726	0	4863	9726	88
13	19.5	7.3	248.1	28302	9434	4717	4717	9434	86

Table 5.5 Operating profile of the engines, ballast voyage.

No.	Average speed	Hours	Hours	W_e	12V50DF No.1	6L50DF No. 2	6L50DF No. 3	12V50DF No.4	Load
-	kn	%	-	kW	kW	kW	kW	kW	%
14	6.5	0.7	22.3	2112	0	0	2112	0	38
15	7.5	0.0	0.0	2617	-	-	-	-	-
16	8.5	0.0	0.0	3276	-	-	-	-	-
17	9.5	0.0	0.0	4110	-	-	-	-	-
18	10.5	0.5	14.7	5139	0	0	5139	0	93
19	11.5	6.2	192.8	6385	0	0	0	6385	58
20	12.5	7.4	232.3	7867	0	0	0	7867	72
21	13.5	14.2	444.1	9607	0	0	0	9607	87
22	14.5	5.6	175.5	11624	0	0	3875	7749	70
23	15.5	17.9	561.4	13939	0	0	4646	9293	84
24	16.5	34.5	1079.8	16573	8287	0	0	8287	75
25	17.5	10.1	317.5	19607	9804	0	0	9804	89
26	18.5	3.0	94.0	23027	9211	0	4605	9211	84

Figure 5.6 shows the duration curve of the total electric power: each point of the curve defines the time duration (abscissa) during which a certain power (ordinate) is exceeded.

Figure 5.7 presents the same curve for the load of the engine-generator sets. Note that the shape of this curve is affected by the control logic of the engines and in this case is affected by the two assumptions that have been considered. However, this curve has a

practical value: it can be read as a duration curve of the quality (in terms of temperature) of the waste heat. Data considered for the construction of the two curves are taken from Table 5.4 and Table 5.5. Note that while the electrical power generation varies in a wide range of values and most of the time is significantly lower than the maximum value, the load at which the engines are operated is most of the time high and close to maximum efficiency. Figure 5.8 shows the total electric power duration curve (line) that has already been presented in Figure 5.6 together with the information that regards the operating engines. In particular, the dot above each corresponding point on the line gives the load of the working engines if read with the right y-axis. Also, each of these points is associated with a number that identify the corresponding operating condition (No.) reported in Table 5.4 or Table 5.5 and allows to know which engines are working.

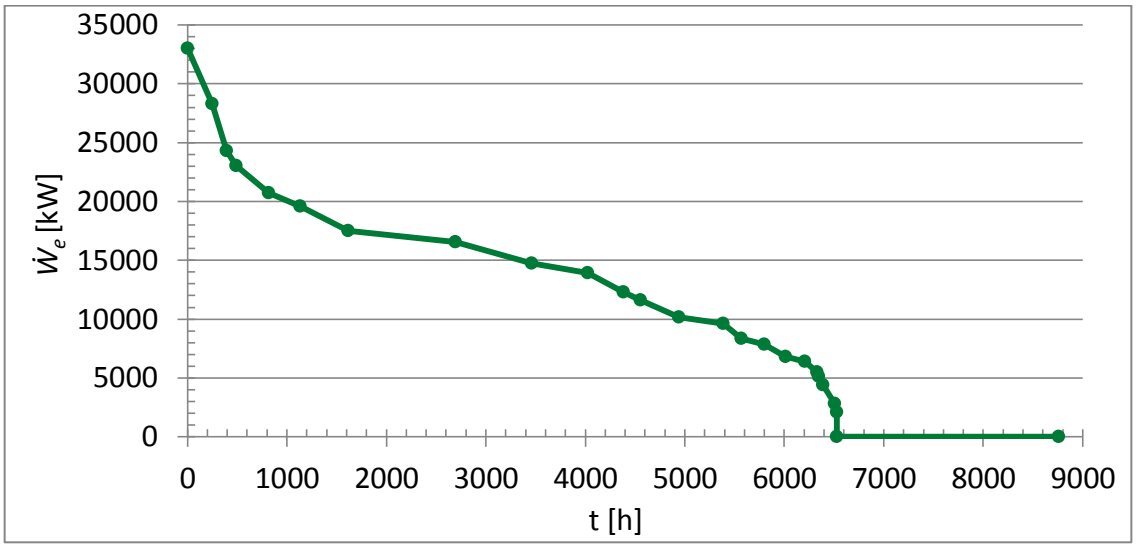

Figure 5.6 Duration curve of the total electric power.

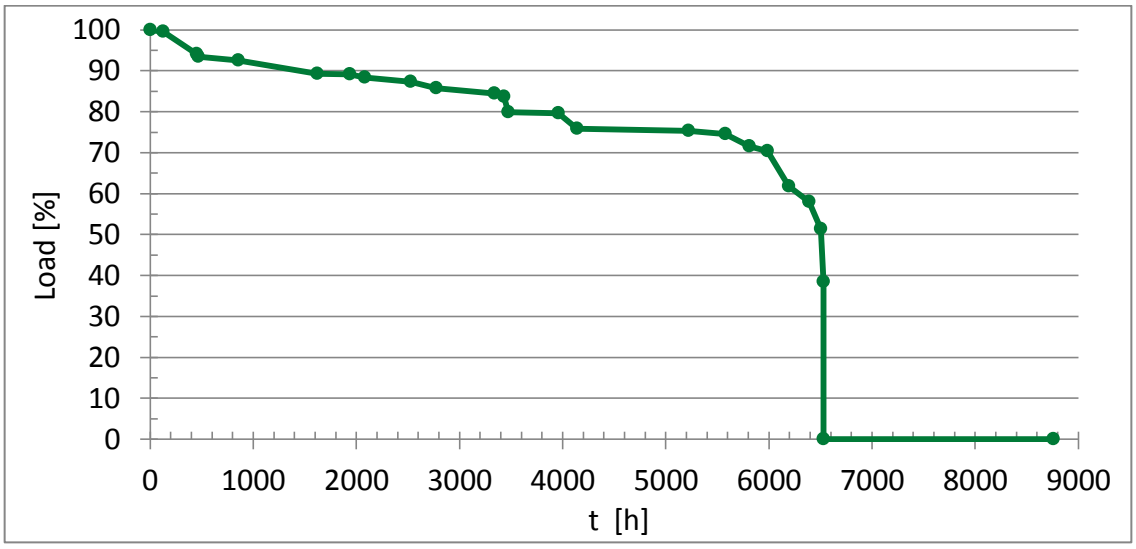

Figure 5.7 Duration curve of the load of the engines.

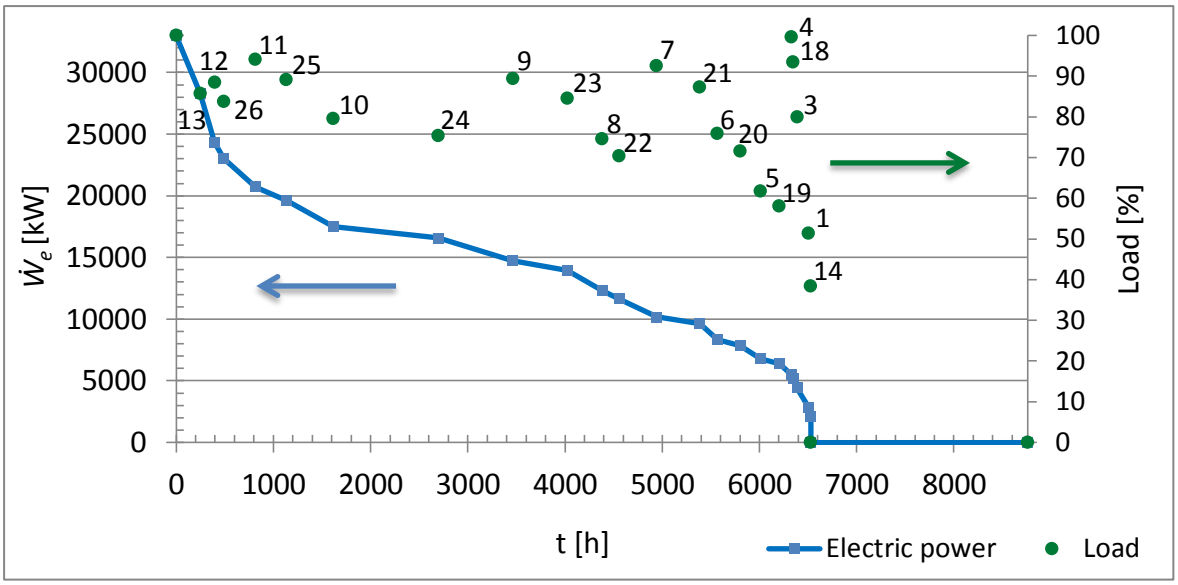

Figure 5.8 Duration curve of the total electric power (line). The dot above each corresponding point on the line represents the load of the working engines (right y-axis). The number associated with each dot identify the operating condition reported in Table 5.4 or in Table 5.5.

5.4 Fresh Water Demand

Fresh water (i.e., desalinated water) has to be produced on board in order to supply the needs of the crew and for other uses. The fresh water generation plant has been described in Section 4.3. Two different units are installed on board.

The available information indicates that the FWG model JWP-26-C100 is kept in continuous operation whereas the other unit does not operate so that it will not be taken into consideration in the present work.

5.5 Steam Demand of the Vessel

Another typical demand of a vessel is represented by low pressure steam to drive auxiliary equipment and for sanitary purposes. As regards the present ship, steam might also be requested to feed the LNG forcing vaporizer. In fact, a certain quantity of LNG evaporates during the maritime transport. This is the so called “natural boil-off gas” that is used to fuel the electric power generating plant. According with the needs of the vessel, if the natural boil-off gas is not sufficient, the forcing vaporizer is used to produce the additional required quantity of fuel by absorbing heat from steam. A significant quantity

of steam is also required in certain phases of the voyage for activities related to the cargo transportation (e.g., loading, unloading).

Steam production is realized by two exhaust gas boilers and two auxiliary boilers as presented in Section 4.4. Steam needs for auxiliary systems and sanitary purposes can be expressed by Eq. (5.11) as a function of the service speed of the vessel V_s [Dimopoulos and Frangopoulos (2008)].This equation is valid for both the laden and the ballast voyage and it is applied in Table 5.6 to provide examples at various service speeds.

$$\dot{m}_{steam} = 0.075 \cdot V_s - 0.775 \tag{5.11}$$

Table 5.6 Steam requirements for auxiliary systems and sanitary purposes.

V_s	$\dot{m}_{steam}$
kn	kg/s
17	0.50
18	0.58
19	0.65
20	0.73
21	0.80
22	0.88
23	0.95

A temperature of 60°C and a pressure of 1.5 bar can be assumed for the water flow that feeds the steam generators whereas saturated steam is produced at a pressure of 8 bar.

5.6 Conclusions

The electrical power demand has been defined as a function of the service speed of the vessel in case of laden and ballast voyage. Both the needs for propulsion and for other uses have been considered according to the related literature. This information combined with the annual speed distribution profile of the vessel (number or percentage of the operating hours as a function of the service speed) has allowed the electrical power demand to be defined as a function of the time (number or percentage of hours in the year). The annual duration curve of the electrical power has been determined and presented in graphical form. Criteria has been introduced in order to assume which engine-generator sets operate for each value of the service speed that was considered by the speed distribution profile. The load of the engine-generator sets has been calculated as well for each operating condition of the vessel. The duration curve of the engines load

has been presented and can be read as a duration curve of the quality of the engines waste heat. The operation of the fresh water generators have been presented and the demand of steam has been defined as a function of the service speed.

6 PERFORMANCE OF VARIOUS ORC CONFIGURATIONS OPERATING WITH DIFFERENT WORKING FLUIDS

6.1 Introduction

The aim of the chapter is to compare the performance of various organic Rankine cycles when they are operated with different fluids. Both simple cycles and more complex configurations are investigated taking into account the solutions found in literature. An operating point for the equipment that compose the ship energy system is selected and the waste heat available to be exploited is defined. Three configurations of the engines cooling systems collecting this heat are investigated: they are the actual configuration and two other arrangements which enable higher temperature heat extraction.

For each combination cooling systems-ORC cycle, the optimum thermal matching that maximizes the net power output of the total system and the optimum operating characteristics are found by applying the Heatsep method. The hot and cold composite curves are built to check the overall heat transfer feasibility and pinch point limitations through Pinch Analysis rules.

6.2 Heatsep Method

The Heatsep method allows the synthesis/design optimization of a complex energy system by optimizing the heat transfer interactions within the whole system. The main problem is divided into two sub-problems. The concept of the energy system is first defined by considering the components that perform the “basic” thermodynamic transformations (e.g., pumps, turbines, condensers). Links between these components are “cut” from the thermal point of view only, so that heat can be transferred through an unspecified heat exchanger network (HEN) represented by a black-box. The thermal interactions within the black-box are then determined as results of the design optimization problem which considers the overall system.

The second sub-problem regards the definition of the heat exchanger network inside the black-box which allows the optimum thermal interactions (found by solving the first sub-problem) to be realized.

Figure 6.1 shows three ORC basic configurations built according with the Heatsep method. Thermal links between different components are cut and the various hot and

cold streams are enclosed within a black box. Figure 6.1a and Figure 6.1b propose a simple ORC and a regenerative ORC, respectively, whereas Figure 6.1c shows a more complex basic configuration which is represented by a two-stage ORC. These ORC cycles are studied in the present work and discussed deeply in the next sections. Note that not all thermal links between basic components are cut in the figureFigure 6.1. In fact, the choice of the cuts to be investigated can be made to avoid over-complex and too expensive heat exchanger networks.

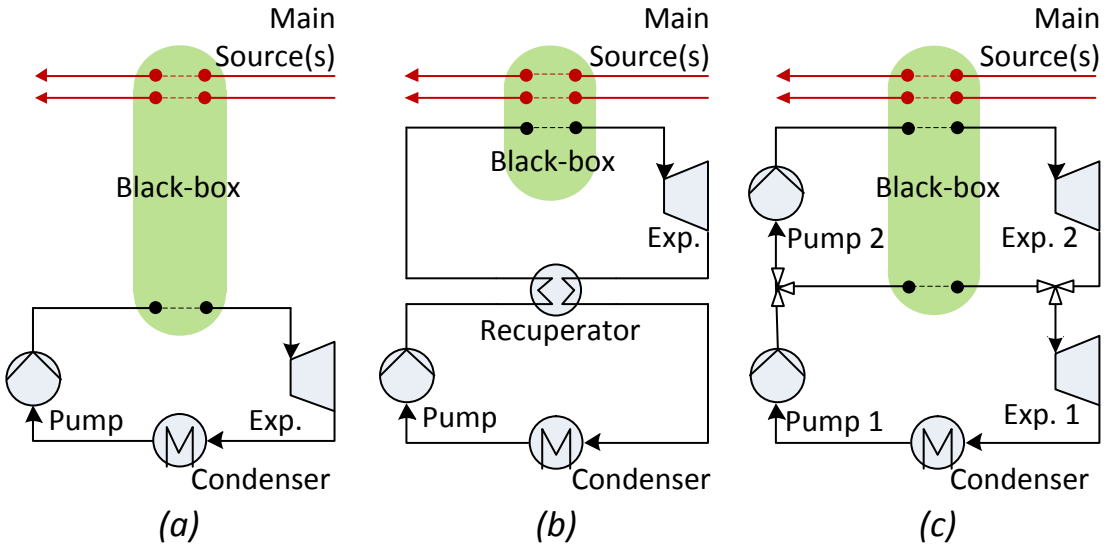

Figure 6.1 ORC basic configurations presented in accordance with the Heatsep method: a) simple cycle, b) regenerative cycle, c) two-stage cycle.

6.3 Pinch Analysis and Composite Curves

Pinch Analysis is a methodology developed to optimize the design of complex heat exchanger networks (HENs) [Linnhoff et al. (1994)]. Considering a system composed by hot streams that have to be cooled down and cold streams that have to be heated, the method looks for their best matching that maximizes the heat that is transferred internally. The higher is the integration between hot and cold streams, the higher is the energy efficiency of the system because the thermal flows provided externally are lower. This is shown in Figure 6.2 for a hot and a cold stream: if no heat is transferred internally (left) a certain thermal flow has to be provided by an external “hot utility” (HU) and a certain quantity of heat has to be rejected to a “cold utility” (CU). The integration between the hot and cold stream (right) reduces the interactions with the external utilities.

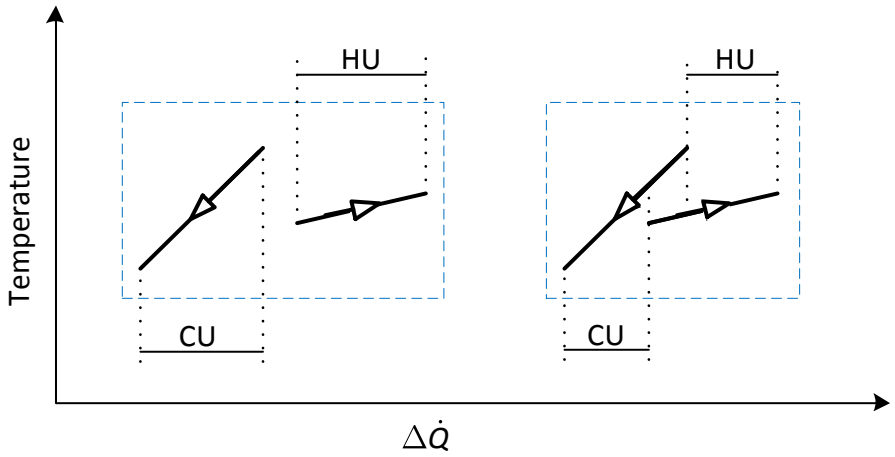

Figure 6.2 Matching between a hot and a cold stream.

One of the tools provided by Pinch Analysis is the composite curve (CC) that represents the heating or the cooling process of the cold or the hot streams separately. With reference to the example of Figure 6.3, the heat capacity of the streams that appear in each temperature interval is added and multiplied by the magnitude of this interval. The quantity so calculated is the heat flow rate that is transferred in the considered range of temperature. The CC is built by adding the contribution of all intervals, as shown on the right hand-side in Figure 6.3.

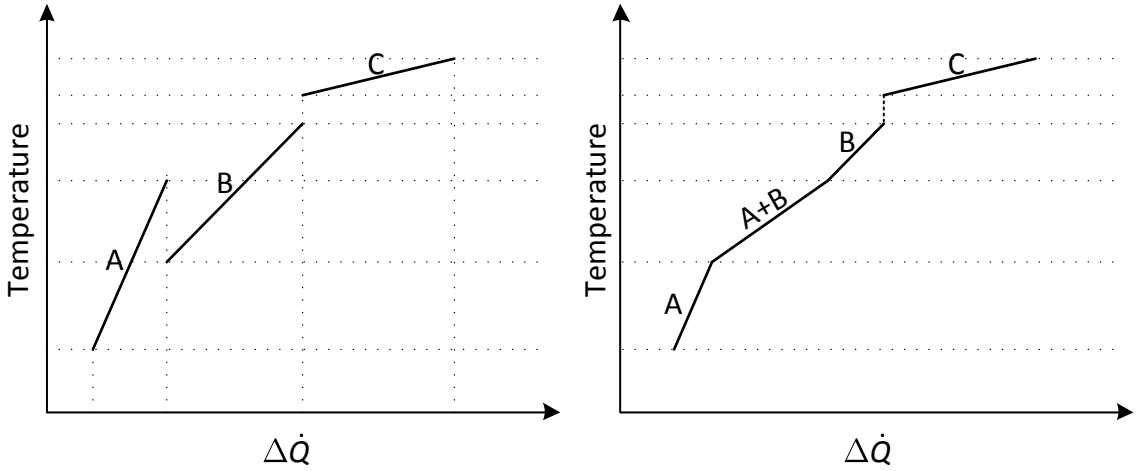

Figure 6.3 Calculation of the CC. Considered streams (left) and CC (right).

The composite curve can be interpreted as the heat exchange curve of a variable heat capacity stream. Generally, two CCs are calculated: the so called “hot composite curve” (HCC) and “cold composite curve” (CCC), which include hot and cold streams, respectively.

Figure 6.4 presents as example the matching between a HCC and a CCC in the $T/\dot{Q}$ diagram. The quantity ΔT_{pp} is the difference of temperature at the minimum distance between HCC and CCC (pp: pinch point). In the proposed diagram, the CCs can be moved horizontally because the abscissa is a difference. This means that the value of ΔT_{pp} can change. The horizontal projection of the overlapping portion of the curves is the thermal flow rate that is transferred internally. This quantity is maximized when ΔT_{pp} is equal to the minimum difference of temperature that is allowed.

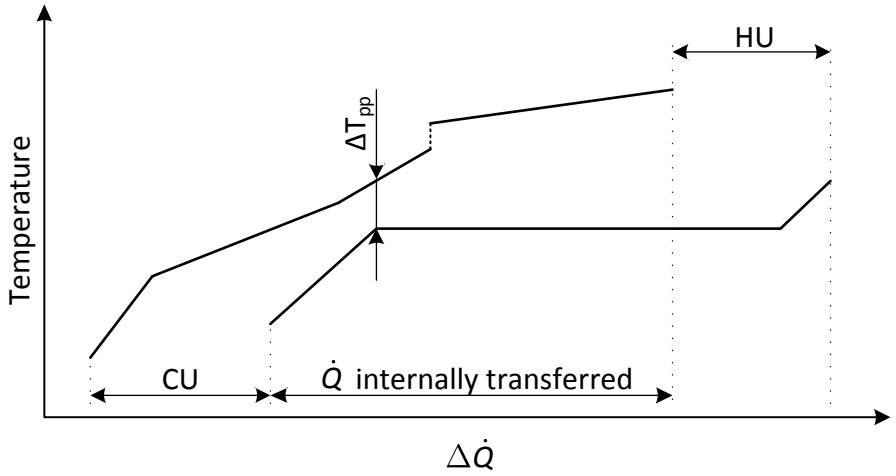

Figure 6.4 Example of the matching between HCC and CCC.

In the present work, the HCCs are built taking into account the thermal flows available from the engines cooling systems whereas the CCCs depend on the cold streams of the ORCs. The optimum match between HCCs and CCCs determines the heat sources that are used by the ORC among those available.

6.4 Operating Point of the Energy Systems of the Vessel

An operating point for the energy systems of the vessel has to be selected to allow a first estimation of the performance of the organic Rankine cycle. This is important also to understand which is the best way to collect heat from the engines and which configuration for the ORC system is more suitable.

Considering the current vessel, the selection of a certain value for the electrical power that has to be generated is not sufficient to define the heat flows that are exploitable by a recovery system. This is because the electric power generating plant is composed of four engine-generator sets, and usually not all of them are kept in operation except in the case of high power demand. Thus, the electrical power that is required can

be made available through different engines. An additional complication is due to the load of the working engines that might not be the same for all of them.

In order to overcome these complications, the operating profile of the vessel and the engines (Section 5.3) has to be considered. The profile defines the control strategy of the engines: the selection of a value for the electrical power to be generated allows the engines that are in operation and the related load to be known.

The operating point that has been selected for the calculations is presented in Table 6.1. Three engines are in operation while the engine No.2 is turned off. The load of the working engines is equal to 85%. The choice takes into consideration the observations on the speed distribution profile of the vessel that have been presented in Section 5.3.

Table 6.1 Operating point for the engines.

$\dot{W}_e$	12V50DF No.1	6L50DF No. 2	6L50DF No. 3	12V50DF No.4	Load
kW	kW	kW	kW	kW	%
23375	9350	0	4675	9350	85

The choice allows the calculation of the thermal flows that are rejected to the engines cooling systems and the heat associated with the exhaust gas (Section 4.2). The quality of the heat (in terms of temperature) that is possible to exploit coupling an ORC system with the cooling systems depends on their configuration and it will be discussed in details in the next section.

The needs of the fresh water generator (FWG) have to be satisfied at the selected operating point of the engines. These needs have also to be considered in order to calculate the effective heat availability that is exploitable by the ORC. Because the FWG is normally fed by the hot water of the HT cooling circuits of the engines, the operating point of this unit is defined in the next section.

6.5 Configurations for the Cooling Systems of the Engines

The aim of this section is to present the configurations that will be considered for the engines cooling systems. For each of them, the available heat is characterized in quantity and quality (temperature).

The first case considers the actual arrangement without introducing any modifications whereas the second and the third cases enable higher temperature heat extraction for the ORC by modifying the heat exchanger network (HEN). For each case, the method that is followed for the calculations of the heat availability is explained first.

The results are collected and presented in table form and transferred into the graphical representation provided by the composite curve CC. The operation of the fresh water generator will be considered the same in all the case so the results of the calculations that are performed subsequently will be comparable.

6.5.1. First case: current configuration of the cooling systems

In this case, the ORC system absorbs heat from the cooling flows (i.e., water flows) of the engines cooling circuits and no modification in the layout of the cooling systems is introduced. Figure 6.5 presents this first cooling system configuration showing the coupling with the ORC system and the FWG. Two thermal sources are available from each engine-generator set that is considered as operating in accordance with the choice of the operating point made in Section 6.4. The ORC system absorbs heat from the water flows of the HT and LT circuits at the point *HE1* and *HE2*, respectively. *HE1* and *HE2* are defined as positions where heat can be transferred. The effective heat exchanger network (HEN) that allows the match between ORC and cooling systems is not designed yet.

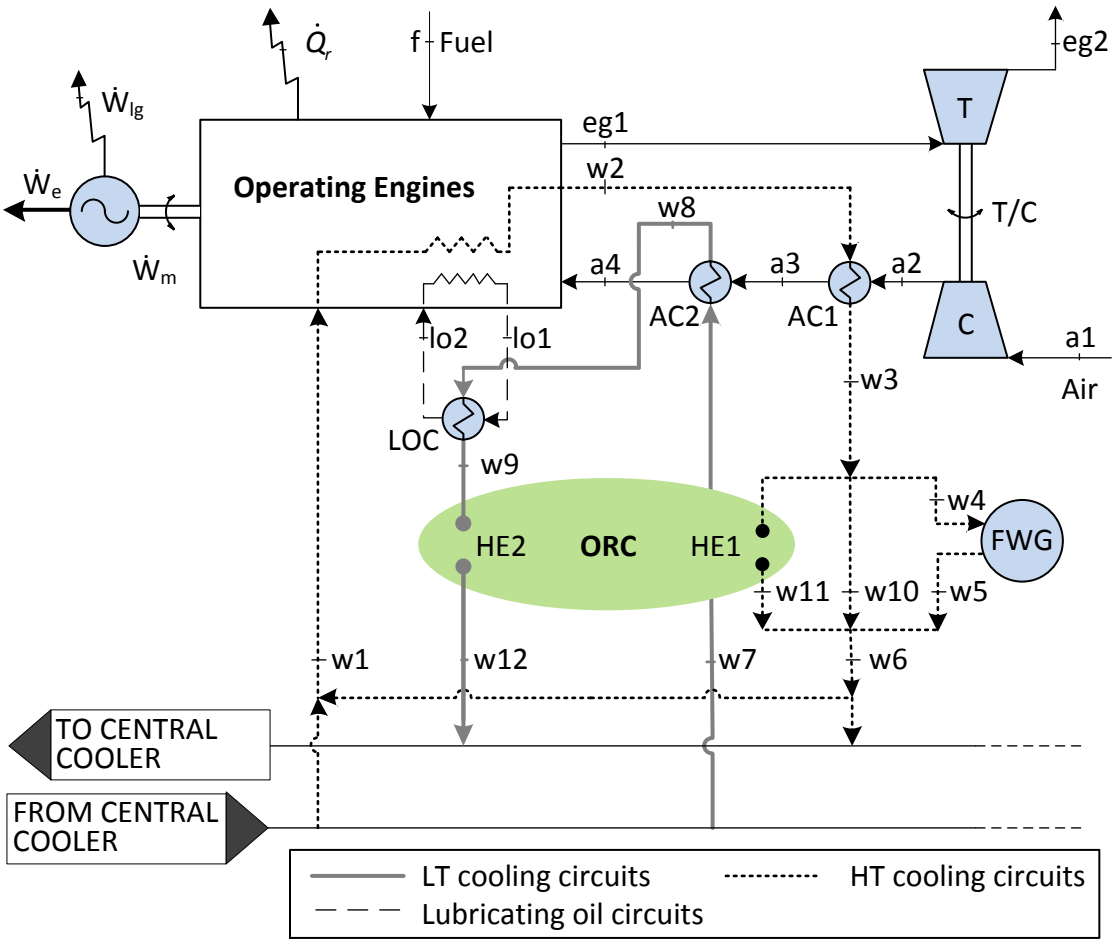

Figure 6.5 Configuration of the cooling systems and coupling with the ORC, first case.

The figure is similar to the one presented in Sub-section 4.2.2 with the difference that the points where the ORC is coupled with the existing plant are shown here and various states in the HT and LT circuits are introduced. It is important to note that the figure is representative of the operation of three engines according to the selected operating point. The values of the parameters that characterize the various states have to be calculated taking into account this aspect. Energy and mass balances are defined for this purpose hereunder. The parameters related to engine model Wärtsilä 6L50DF are indicated with the subscript "A" and those for the Wärtsilä 12V50DF type with the subscript "B".

With regard to the HT circuit, the value of the temperature T_{w3} can be calculated considering that at this state the flows coming from the operating engines are mixed into an unique flow. The energy balance expressed by Eq. (6.1) can be solved for the specific enthalpy of the water h_{w3}, Eq. (6.2). This information combined with the pressure of the water at the same state allows the calculation of the temperature T_{w3} to be performed. The sub-subscripts indicate the model of engine.

$$\dot{m}_{w1,A} \cdot h_{w3,A} + 2 \cdot \dot{m}_{w1,B} \cdot h_{w3,B} = (\dot{m}_{w1,A} + 2 \cdot \dot{m}_{w1,B}) \cdot h_{w3} \tag{6.1}$$

$$h_{w3} = \frac{\dot{m}_{w1,A} \cdot h_{w3,A} + 2 \cdot \dot{m}_{w1,B} \cdot h_{w3,B}}{\dot{m}_{w1,A} + 2 \cdot \dot{m}_{w1,B}} \tag{6.2}$$

The same procedure is followed in order to calculate the temperature T_{w1}. Eqs. (6.1) and (6.2) are used and the specific enthalpy h_{w3} is replaced by the parameter h_{w1}.

The mass balance gives the flow rate of the water collected at the outlet of the HT circuits of the engines:

$$\dot{m}_{w1} = \dot{m}_{w1,A} + 2 \cdot \dot{m}_{w1,B} \tag{6.3}$$

The fresh water generator (Section 4.3) is fed by the water coming from the outlet of the HT cooling circuits. Equation (4.37) gives the mass flow rate $\dot{m}_{w4}$ when the FWG is operated in off-design conditions and it is reported here for convenience:

$$\dot{m}_{w4} = \frac{K \cdot \dot{V}_d}{\Delta T} \tag{4.37}$$

As mentioned before, this equation considers that the heat absorbed by the FWG is constant and equal to the design value. The quantity ΔT is the inlet-outlet temperature difference of the feeding water (T_{w4} - T_{w5}). Figure 6.5 shows that the inlet temperature

T_{w4} is equal to T_{w3}. The value of the outlet temperature T_{w5} is assumed to be equal to that obtained in the design conditions.

Figure 6.5 shows that the HT cooling flow ($\dot{m}_{w1}$) is split into three flows after state *w3*. The outlet temperature of the water flow that feeds the FWG (T_{w5}) is lower than T_{w1} as a consequence of the value assumed for this parameter. This is allowed if the temperature T_{w6} is equal to or higher than T_{w1}. The flow $\dot{m}_{w10}$ is by-passed and mixed after FWG and ORC in order to respect this constraint. Heat associated with the flow $\dot{m}_{w11}$ is available for the OR system.

The ORC is assumed to be integrated in complete parallel with the FWG as shown in the figure. In case of maximum exploitation of the heat associated with the water flow coming from the HT circuits, the temperature T_{w6} is equal to T_{w1}. The flow $\dot{m}_{w11}$ is as high as possible so that the temperature T_{w11} is equal to T_{w1}. The low temperature of the flow $\dot{m}_{w4}$ after FWG is balanced by the higher temperature of the flow $\dot{m}_{w10}$ by mixing before state *w6.* Note that if the temperature T_{w11} is lower than T_{w1}, the ORC would absorb heat at a lower mean temperature and the flow $\dot{m}_{w10}$ would be increased (by reducing $\dot{m}_{w11}$) leading to higher exergy losses. The operating condition is expressed by the energy balance of Eq. (6.4), that can be solved for the mass flow rate $\dot{m}_{w10}$, Eq. (6.5).

$$\dot{m}_{w10} \cdot h_{w3} + \dot{m}_{w4} \cdot h_{w5} = (\dot{m}_{w10} + \dot{m}_{w4}) \cdot h_{w1} \tag{6.4}$$

$$\dot{m}_{w10} = \dot{m}_{w4} \cdot \frac{h_{w1} - h_{w5}}{h_{w3} - h_{w1}} \tag{6.5}$$

The maximum amount of heat that can be absorbed from the high temperature circuits of the cooling systems is given by Eq. (6.6). This equation is based on Eqs. (4.17) and (4.14) and assumes that more engines are in operation.

$$\dot{Q}_{HT,Available} = (\dot{Q}_{jw} + \dot{Q}_{ca,HT})_A + 2 \cdot (\dot{Q}_{jw} + \dot{Q}_{ca,HT})_B - \dot{Q}_{FWG} \tag{6.6}$$

This value does not depend on the of temperature of the water flow at FWG outlet (T_{w5}); the thermal flow $\dot{Q}_{FWG}$ has been considered constant according to the hypothesis of Eq. (4.37). If the actual value of this temperature is different than the one that has been assumed, the mass flow rate of the feeding water $\dot{m}_{w4}$ changes in accordance with Eq. (4.37) and $\dot{m}_{w10}$ changes in accordance with Eq. (6.5). However, note that the sum of $\dot{m}_{w4}$ and $\dot{m}_{w10}$ does not change and both the quantity and the quality of the heat available for the ORC remain the same.

The mass flow rate of the HT water flow available for the ORC is given by the mass balance:

$$\dot{m}_{w11} = \dot{m}_{w1} - \dot{m}_{w10} - \dot{m}_{w4} \tag{6.7}$$

Considering now the water flows coming from the LT cooling circuits, heat can be absorbed after their mixing at the state *w9*. The energy balance expressed by Eq. (6.8) can be solved for the specific enthalpy of the water h_{w9}, Eq. (6.9).

$$\dot{m}_{w7,A} \cdot h_{w9,A} + 2 \cdot \dot{m}_{w7,B} \cdot h_{w9,B} = (\dot{m}_{w7,A} + 2 \cdot \dot{m}_{w7,B}) \cdot h_{w9} \tag{6.8}$$

$$h_{w9} = \frac{\dot{m}_{w7,A} \cdot h_{w9,A} + 2 \cdot \dot{m}_{w7,B} \cdot h_{w9,B}}{\dot{m}_{w7,A} + 2 \cdot \dot{m}_{w7,B}} \tag{6.9}$$

The value of temperature T_{w9} can be calculated knowing the specific enthalpy h_{w9} and the pressure of the water. The mass balance gives the mass flow rate:

$$\dot{m}_{w7} = \dot{m}_{w7,A} + 2 \cdot \dot{m}_{w7,B} \tag{6.10}$$

The same procedure can be followed in order to calculate the value of the temperature T_{w7}. The energy balance of Eq. (6.8) has to be considered for the state *w7*. The maximum amount of the heat that can be absorbed is defined by Eq. (6.11). This equation adapts Eq. (4.20) to the particular case under study:

$$\dot{Q}_{LT,Available} = (\dot{Q}_{ca,LT} + \dot{Q}_{lo})_A + (\dot{Q}_{ca,LT} + \dot{Q}_{lo})_B \tag{6.11}$$

The maximum exploitation of the heat from the low temperature circuits is realized if the total flow $\dot{m}_{w7}$ is cooled down to the temperature T_{w7}.

The method that has been explained so far has been applied considering the data that are provided by Section 4.2. Table 6.2 reports the results of the calculations. The thermodynamic properties of water have been calculated using the NIST Refprop database [Lemmon et al. (2007)]. Table 6.3 presents the data that have been used to build the hot composite curve of this configuration, which is presented in Figure 6.6. In the same figure, the thermal sources of each portion of the curve are indicated.

Table 6.2 Calculation of various parameters, first configuration.

Parameter	Unit	Value
T_{w3}	°C	82.8
T_{w1}	°C	76.3
T_{w7}	°C	36.0
T_{w9}	°C	51.9
$\dot{m}_{w4}$	Kg/s	21.67
$\dot{m}_{w1}$	Kg/s	229.0
$\dot{m}_{w10}$	Kg/s	10.97
$\dot{m}_{w11}$	Kg/s	196.36
$\dot{m}_{w7}$	Kg/s	66.5
$\dot{Q}_{HT,Available}$	kW	5367.3
$\dot{Q}_{LT,Available}$	kW	4406

Table 6.3 Data used for the construction of the hot composite curve, first configuration.

Source	$\dot{Q}$	T_{max}	T_{min}	pressure
-	kW	°C	°C	bar
HT circuits	5367	82.8	76.3	3.15
LT circuits	4406	51.9	36	3.15

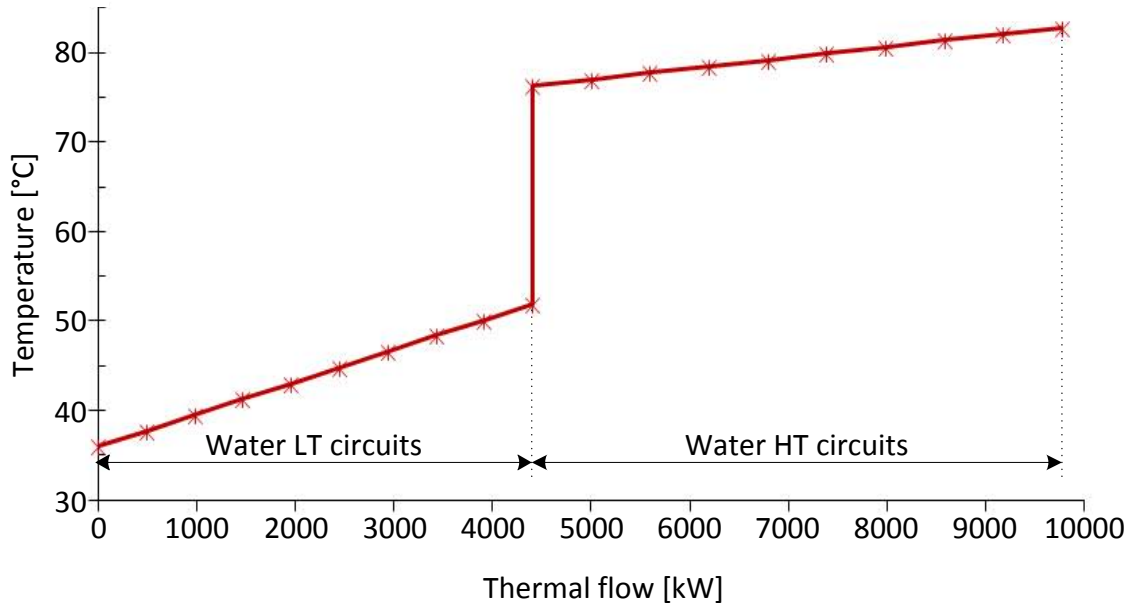

Figure 6.6 Hot composite curve of the available heat, first configuration.

6.5.2. Second case: modification of the LT circuits of the cooling systems

Normally, the water flows of the LT cooling circuits of the engines first collect the heat that is rejected by the air at the LT air coolers and then they pass through the lubricating oil coolers. The previous sub-section indicated that the temperature of the mixture of these water flows at engines outlet (T_{w9}) is equal to 51.9°C. This value is relatively low if compared with the temperature level of the lubricating oil. The outlet temperature from the engine of this medium is approximately 23°C higher than the temperature reached by the water, at the specified conditions (Section 6.4). Based on this observation, this second case investigates the possibility to split the LT cooling circuits into two parts as shown in Figure 6.7. This allows a direct heat transfer between lubricating oil and organic fluid of the ORC system at the point *HE3*. The water flows heated by the charge air in the heat exchanger *AC2* are also considered as thermal sources even if the quality of the heat associated with is low. These flows transfer heat to the ORC system at the point *HE2*. Water flows belonging to the HT circuits represent the third thermal source for the ORC system (*HE1*).

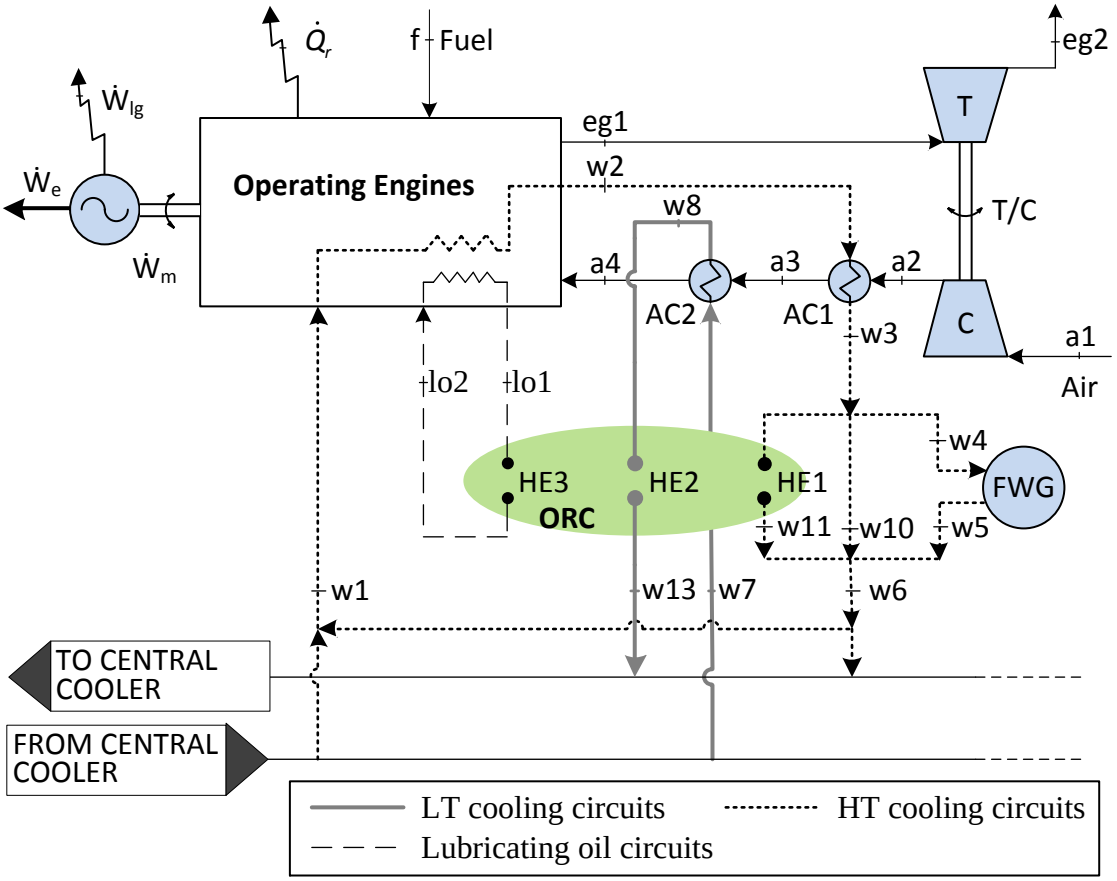

Figure 6.7 Configuration of the cooling system and the heat sources of the ORC, second case.

As regards the HT cooling circuits, no modifications have been introduced, hence the quality and the quantity of the available heat is identical to the first case (Sub-section 6.5.1). With regard to the remaining section of the LT cooling circuits, the energy balance expressed by Eq. (6.12) considers the mixing of the water flows after the air coolers *AC2*. This balance can be solved for the specific enthalpy h_{w8}, Eq. (6.13). The temperature of the state *w8* is determined knowing the specific enthalpy and the pressure of the water.

$$(\dot{m}_{w7,A} \cdot h_{w8,A}) + 2 \cdot \dot{m}_{w7,B} \cdot h_{w8,B} = (\dot{m}_{w7,A} + 2 \cdot \dot{m}_{w7,B}) \cdot h_{w8} \tag{6.12}$$

$$h_{w8} = \frac{\dot{m}_{w7,A} \cdot h_{w8,A} + 2 \cdot \dot{m}_{w7,B} \cdot h_{w8,B}}{\dot{m}_{w7,B} + 2 \cdot \dot{m}_{w7,B}} \tag{6.13}$$

The same method is used to calculate the specific enthalpy of the state *w7* and the temperature T_{w7}. The heat that the ORC system can absorb from these water flows is given by Eq. (6.14) whereas Eq. (6.15) gives the mass flow rate $\dot{m}_{w7}$.

$$\dot{Q}_{LT,available} = \dot{Q}_{ca,LT,A} + 2 \cdot \dot{Q}_{ca,LT,B} \tag{6.14}$$

$$\dot{m}_{w7} = \dot{m}_{w7,A} + 2 \cdot \dot{m}_{w7,B} \tag{6.15}$$

As regards the lubricating oil, there is no need to perform the energy balances and consider the mixing of different flows to calculate the temperatures of states *lo1* and *lo2* because these temperatures are the same in both engines models, as presented in Table 4.4. The heat associated with lubricating oil that is available for the ORC is given by Eq. (6.16) whereas the mass flow rate $\dot{m}_{lo}$ is defined by Eq. (6.17).

$$\dot{Q}_{lo,available} = \dot{Q}_{lo,A} + 2 \cdot \dot{Q}_{lo,B} \tag{6.16}$$

$$\dot{m}_{lo} = \dot{m}_{lo,A} + 2 \cdot \dot{m}_{lo,B} \tag{6.17}$$

The values of the new parameters that have been calculated are reported in Table 6.4. Table 6.5 collects the data that have been used to realize the hot composite curve of Figure 6.8.

Table 6.4 Calculation of various parameters, second configuration.

Parameter	Unit	Value
T_{w7}	°C	36.0
T_{w8}	°C	43.1
T_{lo1}	°C	75.3
T_{lo2}	°C	61
$\dot{m}_{w7}$	Kg/s	66.5
$\dot{m}_{lo}$	Kg/s	90.5
$\dot{Q}_{LT,Available}$	kW	1978
$\dot{Q}_{lo,available}$	kW	2428

Table 6.5 Data used for the construction of the hot composite curve, second configuration.

Source	$\dot{Q}$	T_{max}	T_{min}	pressure
-	kW	°C	°C	bar
HT circuits	5367	82.8	76.3	3.15
LT circuits	1978	43.1	36	3.15
Lubricating oil	2428	75.3	61	-

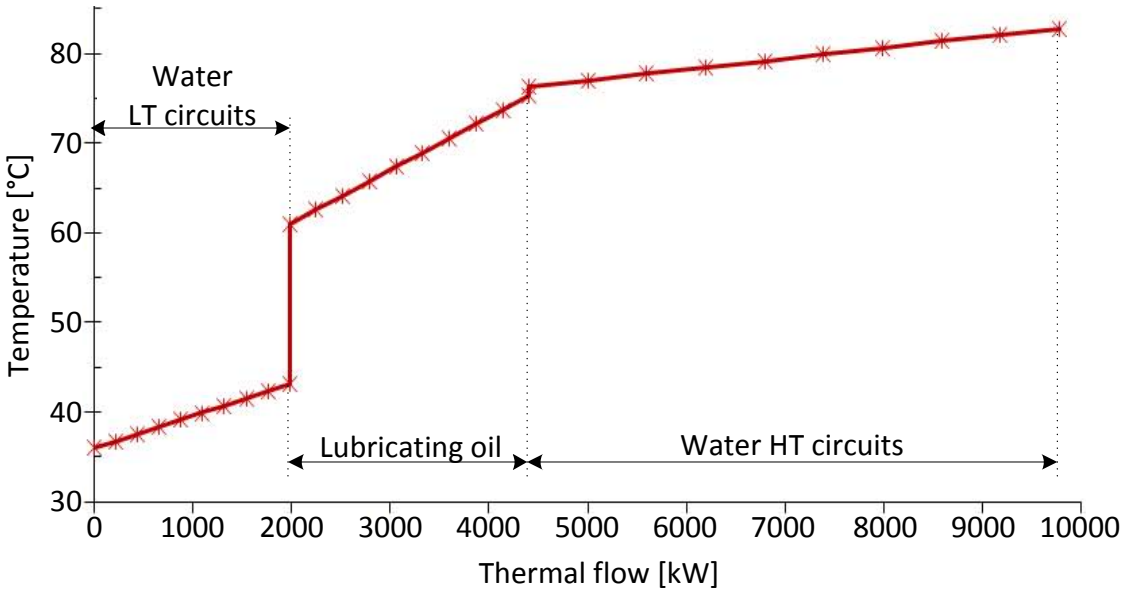

Figure 6.8 Hot composite curve of the available heat, second case.

6.5.3. Third case: new design for the engines cooling systems

This study case considers the possibility of proposing a new design for the engines cooling systems in order to better exploit the quality of the rejected heat. According with this new design presented in Figure 6.9, thermal sources for the ORC are the jacket water, the lubricating oil and the charge air that has to be cooled after the compressor of the T/C. This layout allows the higher heat extraction to be performed. The temperature of the air at the beginning of the cooling (state *a2*) is relatively high so that the removal of the intermediate heat transfer with the HT cooling flows allows the occurring irreversibility to be reduced significantly.

As it is shown in the figure, the water flow resulting from the mixing of the jacket flows is split into three flows: one of them is heated by the air and then feeds the FWG, another one is exploited by the ORC system and the third one is bypassed in order to keep the temperature at the state *w6* at an appropriate value.

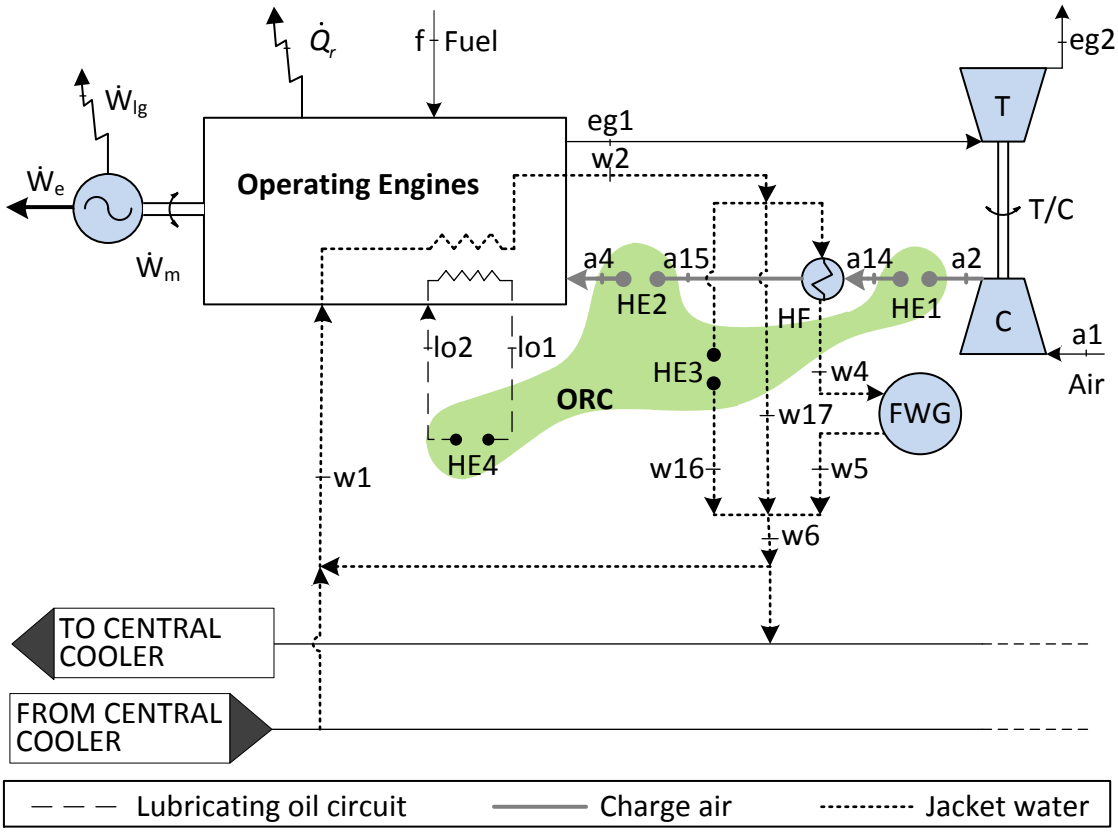

Figure 6.9 Configuration of the cooling system and the heat sources of the ORC, third case.

The value of the temperature at state *w2* comes from the energy balance expressed by Eq. (6.18) that can be solved for the specific enthalpy h_{w2}, Eq. (6.19).

$$\dot{m}_{w1,A} \cdot h_{w2,A} + 2 \cdot \dot{m}_{w1,B} \cdot h_{w2,B} = (\dot{m}_{w1,A} + 2 \cdot \dot{m}_{w1,B}) \cdot h_{w2} \tag{6.18}$$

$$h_{w2} = \frac{\dot{m}_{w1,A} \cdot h_{w2,A} + 2 \cdot \dot{m}_{w1,B} \cdot h_{w2,B}}{\dot{m}_{w1,A} + 2 \cdot \dot{m}_{w1,B}} \tag{6.19}$$

The temperature T_{w2} depends on the specific enthalpy and pressure of the water flow at the same state. Analogous equations are used in order to perform the calculation of the temperature T_{w1}. The unit that heats the water flow before the FWG sets the temperature T_{w4} in order to be equal to the value considered in the previous cooling systems cases. This allows an objective comparison between the various configurations thanks to the fact that the operating conditions of the FWG are the same. The values of the parameters $\dot{m}_{w4}$ and T_{w5} are equal to those considered for the other configurations.

The flow $\dot{m}_{w17}$ has the same function as $\dot{m}_{w10}$ in the previous configurations. Here it is presented with a new label because the equation from which it is calculated is based on a different energy balance.

Like the previous cases, the maximum exploitation of the heat associated with the water flow is obtained when the temperature T_{w6} is equal to T_{w1}. The flow $\dot{m}_{w16}$ is considered to be as high as possible so the temperature T_{w16} is equal to T_{w1}. The low temperature of $\dot{m}_{w4}$ after FWG is balanced by the higher temperature of the flow $\dot{m}_{w17}$ by mixing. The energy balance of Eq. (6.20) is solved for the mass flow rate $\dot{m}_{w17}$, Eq. (6.21).

$$\dot{m}_{w17} \cdot h_{w2} + \dot{m}_{w4} \cdot h_{w5} = (\dot{m}_{w17} + \dot{m}_{w4}) \cdot h_{w1} \tag{6.20}$$

$$\dot{m}_{w17} = \dot{m}_{w4} \cdot \frac{h_{w1} - h_{w5}}{h_{w2} - h_{w1}} \tag{6.21}$$

The maximum amount of heat that can be absorbed from the flow $\dot{m}_{w16}$ is given by Eq. (6.22). The last term of the equation is the heat required by the FWG that is absorbed from the jacket water, Eq. (6.23). Equation (6.24) gives the mass flow rate of the hot water that can be exploited by the OR system.

$$\dot{Q}_{jw,available} = \dot{Q}_{jw,A} + 2 \cdot \dot{Q}_{jw,B} - \dot{Q}_{FWG,jw} \tag{6.22}$$

$$\dot{Q}_{FWG,jw} = \dot{Q}_{FWG} - \dot{m}_{w4} \cdot (h_{w4} - h_{w2}) \tag{6.23}$$

$$\dot{m}_{w16} = \dot{m}_{w1,A} + 2 \cdot \dot{m}_{w1,B} - \dot{m}_{w4} - \dot{m}_{w17} \tag{6.24}$$

As stated previously, heat can be transferred directly between the lubricating oil and the ORC. The maximum thermal flow rate and the temperatures at which it is available are the same as in the cases analysed in the two previous sub-sections.

Finally, the heat flow associated with the air can be calculated by Eq. (6.25). The temperatures T_{a2} and T_{a4} have to be calculated considering that the various flows are mixed. The energy balances at the respective states and the pressure have been calculated.

$$\dot{Q}_{ca} = (\dot{Q}_{ca,HT} + \dot{Q}_{ca,LT})_A + (\dot{Q}_{ca,HT} + \dot{Q}_{ca,LT})_B \tag{6.25}$$

The effective heat availability for the ORC system is lower than the quantity given by Eq. (6.25) because a certain part is exploited by the heat exchanger that increases the temperature of the water for the FWG. The position of this unit in the cooling process of the air is not decided in the present sub-section. The related flow is introduced in the simulation procedure as a cold water stream to be heated between the states *w2* and *w4*. The thermal flow rate is given by Eq. (6.26).

$$\dot{Q}_{FWG,air} = \dot{m}_{w4} \cdot (h_{w4} - h_{w2}) \tag{6.26}$$

The results of the new calculations are reported in Table 6.6. Table 6.7 presents the data that have been used to build the composite curves in Figure 6.10.

Table 6.6 Calculation of various parameters, third configuration.

Parameter	Unit	Value
T_{a2}	°C	169.75
T_{a4}	°C	44.15
T_{w2}	°C	79.66
$\dot{m}_{w16}$	kg/s	186.05
$\dot{m}_{w17}$	kg/s	21.29
$\dot{m}_a$	kg/s	39.12
$\dot{Q}_{jw,available}$	kW	2602.3
$\dot{Q}_{ca}$	kW	5030
$\dot{Q}_{FWG,air}$	kW	287

Table 6.7 Data used for the construction of the composite curves, third configuration.

Source	$\dot{Q}$	T_{max}	T_{min}	pressure
-	kW	°C	°C	bar
Jacket water	2602	79.66	76.3	3.15
Lubricating oil	2428	75.3	61	-
Charge air	5030	169.75	44.15	3.02
$\dot{Q}_{FWG,air}$	287	82.8	79.66	3.15

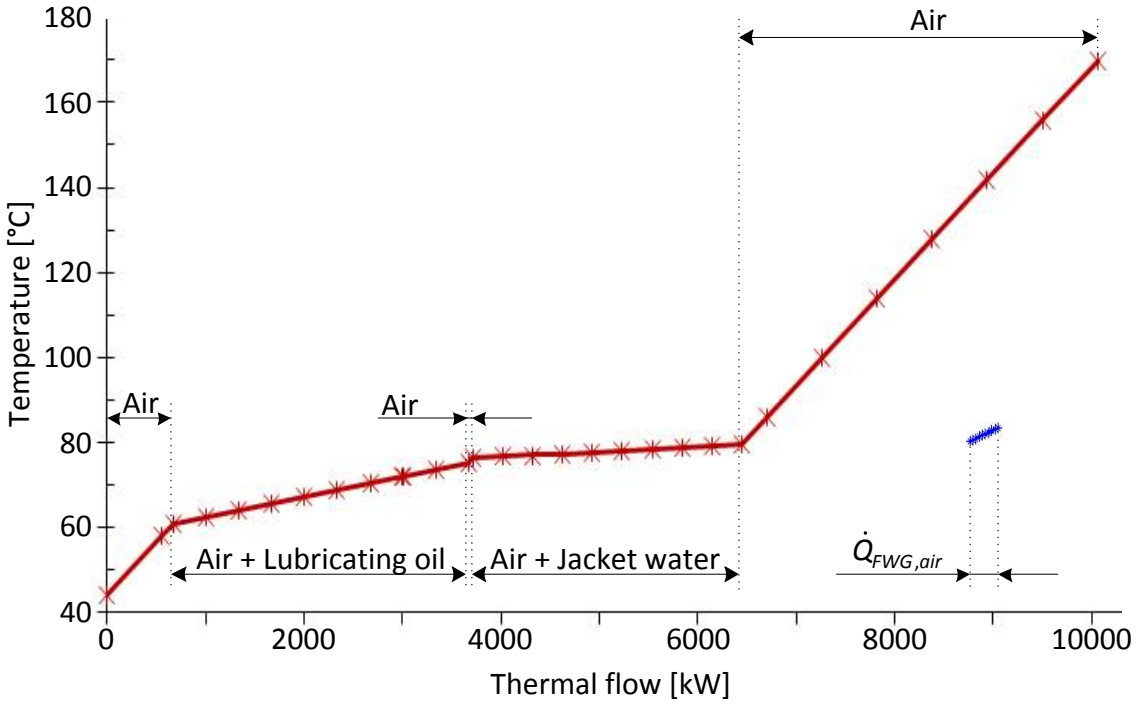

Figure 6.10 Hot composite curve of the available heat, third case.

6.6 ORC Configurations and Fluids Selection

Three organic Rankine cycle configurations have been considered: a simple cycle, a regenerative cycle and a two-stage cycle. They are presented in the next three sub-sections together with the definition of the thermodynamic models. These models have been implemented in MATLAB-Simulink environment whereas the simulation procedure is written in MATLAB code. The properties of the organic fluid are evaluated through the NIST Refrprop database [Lemmon et al. (2007)]. The simulation procedure applied to the three configurations presents some differences related to the peculiarities of each cycle.

These aspects are presented in details in the next sub-sections. Basically, some values are assigned to the independent variables that are assumed as constant parameters (i.e., the performance of the components, HCC) and to the decision variables (independent variables that are free to vary). The simulation of the cycle calculates the values of other intensive variables. If the solution is feasible, the extensive variables are evaluated.

A common aspect is represented by the assumptions that have been considered in the definition of the thermodynamic models:

(1) The cycle is operated at steady state conditions,
(2) Pressure losses and heat rejection in the components and the pipes are neglected.

Six substances are investigated to be used as working fluid of the ORC cycle. They have been selected from those suggested in literature for low temperature heat recovery and presented in Table 2.8. They are characterized by low flammability and toxicity and they are oxone-friendly. They are R-134a, R-125, R-236fa, R-245ca, R-245fa, R-227ea. Main thermodynamic and environmental properties are reported in Table 6.8 for convenience from Table 2.8.

Table 6.8 Main thermodynamic and environmental properties of the considered fluids.

Fluid	T_c	p_c	ODP	GWP_{100}	ASHRAE Safety group
-	°C	bar	-	-	-
R-134a	101.06	40.593	0	1300	A1
R-125	66.2	36.177	0	3400	A1
R-236fa	124.92	32.0	0	9400	A1
R-245ca	174.42	39.25	0	640	A1
R-245fa	154.01	36.51	0	950	B1
R-227ea	101.75	29.28	0	3500	A1

6.6.1. Simple ORC

This is the case of a single pressure level, organic Rankine cycle, where the plant configuration is composed of four components, as shown in Figure 6.11. The developed model manages both subcritical and supercritical ORCs. The “evaporator” indicated in the figure represents the component where the working fluid is heated, independently from the kind of cycle that is realized (I.e., subcritical or supercritical). Figure 6.12 shows the qualitative T-s diagram of the cycle for both the subcritical and supercritical case.

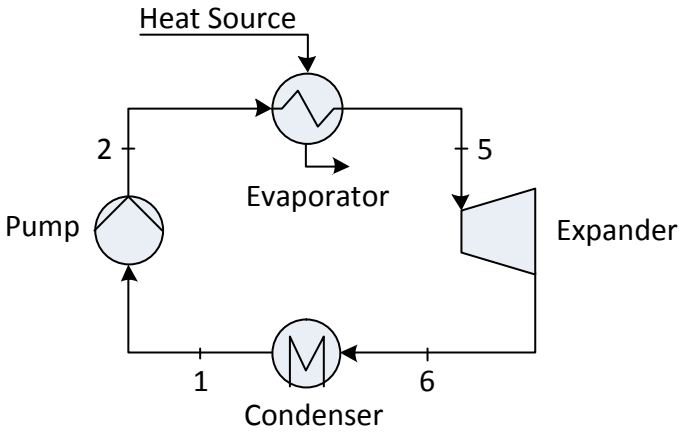

Figure 6.11 Arrangement of the simple organic Rankine cycle.

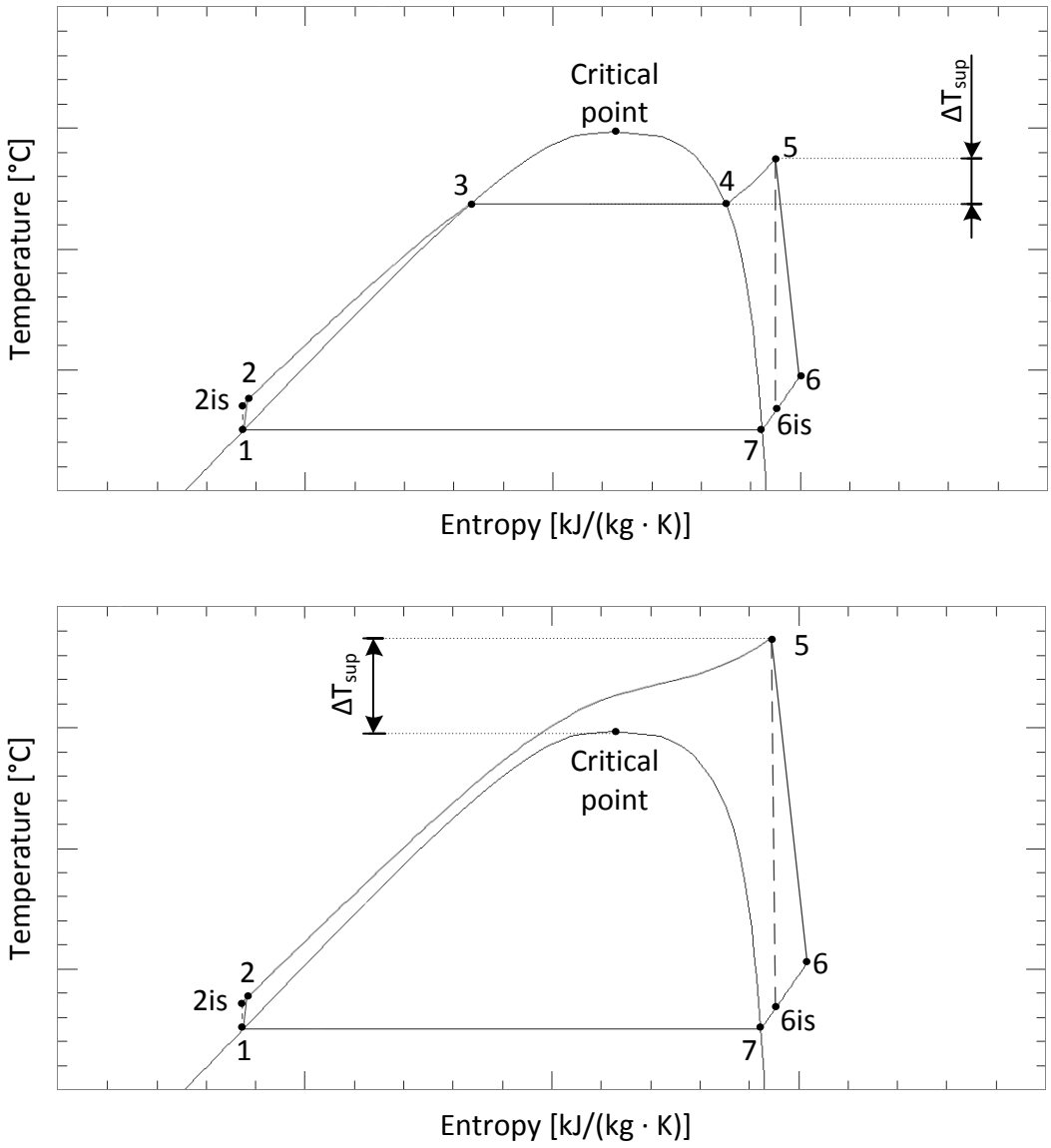

Figure 6.12 Qualitative T-s diagrams of the simple ORC, subcritical and supercritical cycle.

The equations that compose the thermodynamic model are now presented. The pressure of the working fluid in the liquid state is first increased in the pump through a non-isentropic process (state *1* to *2*). The specific work input to the pump is defined by Eq. (6.27). The isentropic efficiency of the pump gives a relation between inlet and outlet conditions, Eq. (6.28).

$$w_{pump} = (h_2 - h_1) \cdot \frac{1}{\eta_{me,pump}} \tag{6.27}$$

$$\eta_{is,pump} = \frac{h_{2,is} - h_1}{h_2 - h_1} \tag{6.28}$$

where

h specific enthalpy of the working fluid in the subscripted state,

$\eta_{me,pump}$ mechanical and electrical efficiency of the pump.

The state *1* is on the saturated liquid curve at the condensation pressure. In the following process, the specific heat that is absorbed by the working fluid is defined by Eq. (6.29) where h_5 and h are the specific enthalpies at the outlet and inlet conditions of the evaporator, respectively:

$$q_{absorbed} = h_5 - h_2 \tag{6.29}$$

The specific power of the expander is given by Eq. (6.30) in a non-isentropic process. The isentropic efficiency is expressed by Eq. (6.31).

$$w_{\exp} = (h_5 - h_6) \cdot \eta_{me,\exp} \tag{6.30}$$

$$\eta_{is,\exp} = \frac{h_5 - h_6}{h_5 - h_{6,is}} \tag{6.31}$$

where

h specific enthalpy of the working fluid in the subscripted state,

$\eta_{me,exp}$ mechanical and electrical efficiency of the expander.

The specific heat rejected from the working fluid in the condenser is defined by Eq. (6.32). In other words, the cooling and condensation processes start immediately after

the expander. Equation (6.33) gives the specific net power that is the desired output of the cycle.

$$q_{con} = h_6 - h_1 \tag{6.32}$$

$$w_{net} = w_{\exp} - w_{pump} \tag{6.33}$$

The thermal efficiency of the cycle is defined as:

$$\eta_{th} = \frac{w_{net}}{q_{absorbed}} \tag{6.34}$$

The extensive parameters are then calculated multiplying the specific quantities by the mass flow rate of the working fluid to give:

$$\dot{W}_{pump} = \dot{m}_{wf} \cdot w_{pump} \tag{6.35}$$

$$\dot{W}_{\exp} = \dot{m}_{wf} \cdot w_{\exp} \tag{6.36}$$

$$\dot{W}_{net} = \dot{m}_{wf} \cdot w_{net} \tag{6.37}$$

$$\dot{Q}_{absorbed} = \dot{m}_{wf} \cdot q_{absorbed} \tag{6.38}$$

$$\dot{Q}_{con} = \dot{m}_{wf} \cdot q_{con} \tag{6.39}$$

6.6.1.1. *Simulation procedure*

The simulation procedure considers two decision variables (independent variables that are free to vary) that are the evaporation pressure of the working fluid p_{ev} [bar] and the degree of superheating ΔT_{sup} that is measured in terms of temperature [°C]. For subcritical cycles, this last quantity has to be considered as the temperature difference between the state *5* and the saturated vapour at the evaporation pressure. In case of supercritical cycles, the degree of superheating is measured from the temperature of the critical point.

The independent variables that are considered as constant parameters are the performance of the pump and the expander (isentropic efficiency, mechanical and

electrical efficiency), the condensation temperature, the “hot composite curve” (HCC) and the pinch point temperature difference ΔT_{pp}. The hot composite curve is considered as a constant parameter because it collects in a combined form the information related to various hot streams (thermal flow and temperature) that are traditionally considered as constant parameters. If the third engines cooling systems configuration is considered, the information (in terms of temperatures and heat flow rate) related to the heating process of the water flow at the point “*HE4*” (Figure 6.9, Sub-section 6.5.3) is considered as an additional independent variable fixed at constant value. This water flow feeds the FWG and has to be taken into consideration for the construction of the “cold composite curve” (CCC) as an additional cold stream.

Table 6.9 presents the constant values assumed for various independent variables. The isentropic efficiency of the pump is considered to be lower than the turbine one whereas the value for the mechanical and electrical efficiency is the same for the two components. The value for the condensation temperature (T_{con}) is set to be equal to 30°C. This is representative of the case of direct rejection of heat from organic fluid to seawater at ISO conditions (the temperature of the seawater is 25°C). ΔT_{pp} is the minimum allowed temperature difference between HCC and CCC.

Table 6.9 Values of various independent variables considered as constant parameters.

Parameter	Unit	Value
$\eta_{is,pump}$	-	0.7
$\eta_{is,exp}$	-	0.85
$\eta_{me,pumo}$, $\eta_{me,exp}$	-	0.9
T_{con}	°C	30
ΔT_{pp}	°C	10

Dependent variables are the thermodynamic properties of the working fluid in various states, the information related to the heating process of the working fluid (in terms of temperatures and heat flow) that is used for the construction of the CCC, the CCC, the mass flow rate $\dot{m}_{wf}$, the heat that is exchanged at various components, the work of the expander and the pump, and two parameters that have been defined in Sub-section 3.8.2: size factor *SF* and volumetric expansion ratio *VR*.

The various steps of the simulation procedure are presented in the diagram of Figure 6.13. First of all, the information that regards the hot streams available from the engine cooling systems configuration that is considered is read from a spreadsheet (.xlsx file). The total heat associated with each stream is divided into nine intervals and the intermediate temperatures are calculated. The HCC is built applying the method

explained in Section 6.3. The independent variables that are considered as constant parameters are fixed and the values for the decision variables are selected. Then, the simulation of the cycle allows the calculation of the values of intensive variables and specific ones to be performed. The thermodynamic properties of the working fluid in the various states are given by the NIST Refprop database [Lemmon et al. (2007)].

Subsequently, the CCC is built considering the heating process of the working fluid that takes place from pump outlet (state *2*) to turbine inlet (state *5*) for a guess value of mass flow rate (0.5 kg/s) and the needs of the FWG if the third arrangement for the

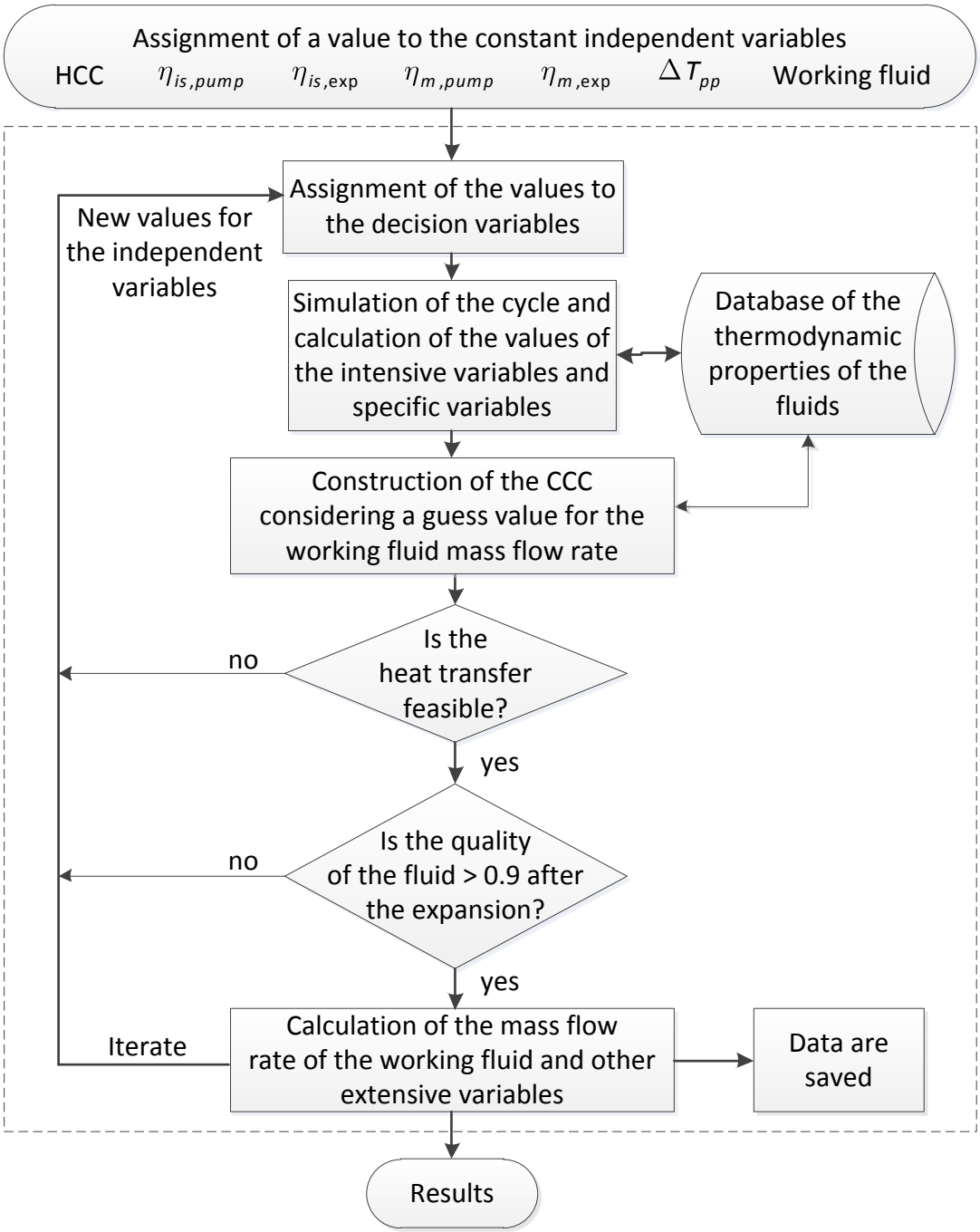

Figure 6.13 Simulation procedure for the simple ORC.

engines cooling systems is studied. The heat required by each cold stream is split into 20 intervals so that the CCC is discretized with 21 points in the case of the first two cooling systems configurations and 42 points for the third one. The additional points required in this last case takes into consideration the heating of the water flow that feeds the FWG. The temperature of each point is calculated using the external database and then they are connected by linear segments to plot the heating profile.

The thermodynamic feasibility of the heat transfer is checked by measuring the vertical distance between HCC and CCC in several points. In particular, the composite curves are first positioned in the $T/\dot{Q}$ diagram so that their points of maximum temperature have the same abscissa. Then, the curves are redrawn considering all the points through which the heat was discretized in the previous ones. The check is performed for each of these points. The quality of the fluid at state *6* (after expander) is calculated as well and it has to be higher than 0.9.

If feasibility of the heat transfer and minimum quality of the fluid after turbine are satisfied, the actual value of the mass flow rate is calculated. This is the quantity that minimizes the vertical distance between HCC and CCC (respecting ΔT_{pp}). The calculation is performed by first identifying a guess range in which the actual mass flow rate of the working fluid is included. Then, the MATLAB function *fmincon* is used in order to find the maximum allowed value.

6.6.1.2. *Simulation and optimization*

The simulation procedure can be managed by a script that varies the values of the decision variables in predefined ranges. The results of the calculations are collected and presented in a graphical form to allow the identification of the optimal and sub-optimal regions. A second script uses the simulation procedure in order to solve the optimization problem of a multivariable function with non-linear constraints (quality of the fluid at expander outlet and feasibility of the thermal exchange). The objective is the maximization of the net power of the system $\dot{W}_{net}$ with respect to $\underset{\sim}{x}$:

$$\max_{\underset{\sim}{x}} \ \dot{W}_{net}(\underset{\sim}{x}) \tag{6.40}$$

$$\underset{\sim}{x} = (p_{ev}, \Delta T_{\text{sup}}) \tag{6.41}$$

The MATLAB function that has been used to solve the optimization problem is the *fmincon* function. The results obtained from the first script have been taken into consideration to set the ranges of the decision variables of the second script.

6.6.1.3. *Evaluation of the simple ORC applied to the first cooling systems configuration*

The optimization problem is solved with respect to the first engines cooling systems configuration (Sub-section 6.5.1). No modifications are introduced in the actual arrangement of the HT and LT cooling circuits. The objective function is the maximum of the net power. The optimal design operating characteristics of the system are reported in Table 6.10 for the selected fluids.

Table 6.10 Optimized operating characteristics for the simple ORC, first cooling systems configuration.

Fluid	—	R-134a	R-125	R-236fa	R-245ca	R-245fa	R-227ea
p_{ev}	bar	20.132	35.197	9.327	4.054	5.695	14.288
p_{con}	bar	7.702	15.685	3.210	1.217	1.778	5.284
T_{con}	°C	30.0	30.0	30.0	30.0	30.0	30.0
ΔT_{sup}	°C	5.0	8.0	0.0	0.0	0.0	0.0
T_5	°C	72.8	72.8	67.8	67.4	67.5	68.2
T_6	°C	34.1	34.8	41.3	40.9	39.2	41.0
χ	—	1.02	1.05	1.07	1.05	1.05	1.09
sub/sup	—	sub	sub	sub	sub	sub	sub
w_{exp}	kJ/kg	14.968	8.923	12.395	17.153	16.133	9.547
w_{pump}	kJ/kg	1.658	2.651	0.722	0.328	0.469	1.044
w_{net}	kJ/kg	13.310	6.273	11.672	16.825	15.664	8.503
$q_{absorbed}$	kJ/kg	192.525	117.742	166.239	227.523	213.729	128.443
q_{con}	kJ/kg	177.385	110.212	153.118	208.760	196.226	118.775
$\dot{m}_{wf}$	kg/s	30.388	51.517	35.450	25.372	27.109	44.699
$\dot{W}_{net}$	kW	404.5	323.1	413.8	426.9	424.6	397.1
η_{th}	%	6.91	5.33	7.02	7.39	7.33	6.62
η_t	%	4.14	3.31	4.23	4.37	4.34	4.06
Φ	%	59.9	62.1	60.3	59.1	59.3	61.4
VR	—	2.801	2.657	3.136	3.323	3.234	3.153
SF	m	0.433	3.881	0.656	0.906	0.777	0.578
$\dot{Q}_{absorbed}$	kW	5850.4	6065.5	5893.2	5772.7	5749.0	5998.1
$\dot{Q}_{con}$	kW	5390.4	5677.6	5428.0	5296.6	5319.5	5546.6

The net power output that is possible to achieve is around 425 kW. All the cycles are subcritical due to the low temperature of the available heat. Fluids R-134a and R-125 are superheated, while the other fluids are expanded from saturated vapour conditions. This validates the findings of research on the inappropriateness of superheating "dry" fluids. Generally speaking, thermal efficiency of the cycles η_{th} is low and leads to absorb a large amount of heat that is mostly rejected at the condenser. Temperature at expander inlet T_5 is around 70°C for all the cycles. Fluids R-125 and R-134a maximize this temperature so that its value is equal to the maximum one allowed by pinch limitations.

The total heat recovery efficiency η_t is in the range 3.30 ÷ 4.40% in all cases; the minimum value is obtained by the fluid R-125 and the higher by R-245ca. The heat recovery factor ϕ is equal to approximately 60% in all the cases so that it is not possible to exploit all the available heat. Temperatures at expander outlet T_6 are higher than the condensation temperature which means that all fluids are superheated. However, note that the temperatures are not high enough to allow a regenerator to be added.

Fluid R-245ca and R-245fa provide the maximum net power output at the expense of the highest values for the parameters *VR* and *SF* that are indicative of high volumes required by the system. In addition, it is noted that their operating pressures are the lowest, which makes them suitable in light of safety concerns.

Further considerations are reported here considering R-245ca as working fluid, which leads to the highest net power. Figure 6.14 presents the thermal matching between the HCC and various CCCs that are obtained by considering a different evaporation pressure each. These CCCs are obtained considering that the fluid is saturated at expander inlet. For relative low values of the evaporation pressure, the pinch point is located at the beginning of the evaporation (state *3* of the simple cycle). For instance, if the evaporation pressure is equal to 1.5 bar, the pinch point is at the so called position "A". If the evaporation pressure is increased up to a certain value close to 2 bar, the pinch point moves progressively from "*A*" to "*B*". For further increases up to a value equal to approximately 4 bar, the position of the pinch point does not change. Then, the additional pinch point called "*C*" is activated and it moves to the right if the evaporation pressure increases again. Figure 6.15 gives the net power output of the cycle operating with R-245ca as a function of the evaporation pressure with ΔT_{sup} as a parameter.

As regards the optimized cycles that have been found, the thermal matching between HCC and CCC of the fluids R-134a and R-125 shows two pinch points: the first one is located at state *5* of the cycle whereas the second one is along the preheating curve, after the pump and before the beginning of the evaporation. Two pinch points are obtained also with the other fluids: the first one is found to be on the preheating curve while the second one is at the beginning of vaporization.

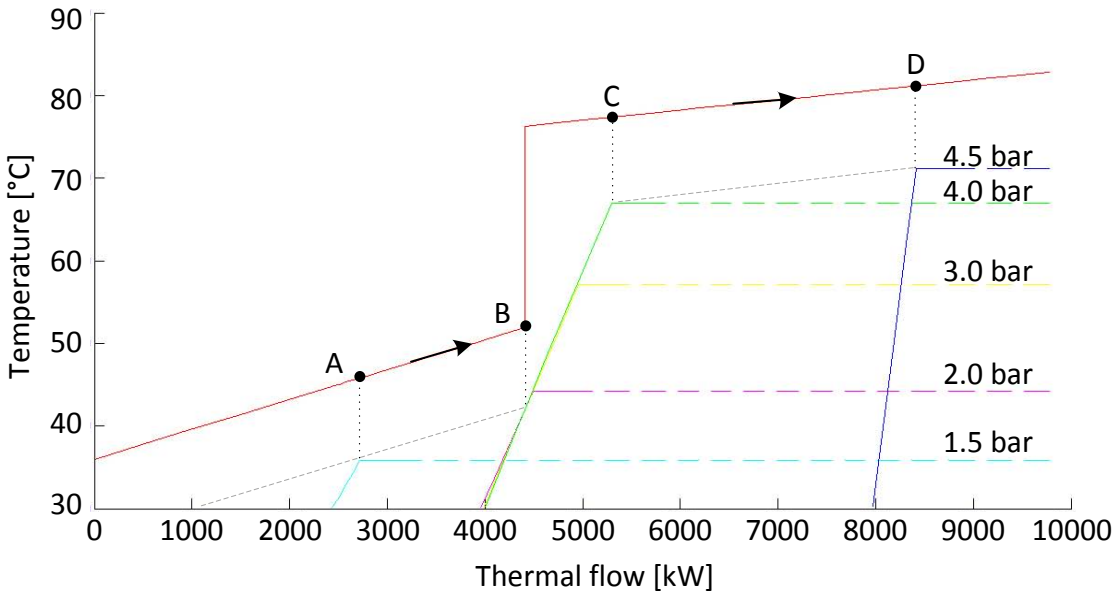

Figure 6.14 Thermal matching HCC and CCC, first configuration, fluid R-245ca saturated.

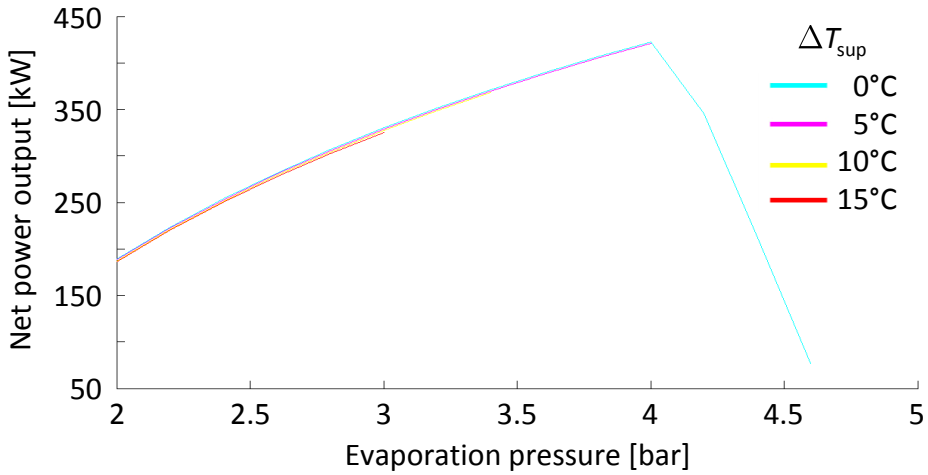

Figure 6.15 Net power output of the simple ORC as a function of the evaporation pressure with ΔT_{sup} as a parameter; fluid R-245ca.

With reference to Figure 6.15, the increase of evaporation pressure leads to the increase of the thermal efficiency of the cycle η_{th} and the specific power output of the expander w_{exp}. The net power output increases with the evaporation pressure up to a maximum value reached at approximately 4 bar. Further increases in pressure lead to a strong reduction of the generated power. The mass flow rate of the working fluid decreases with the increase of the evaporation pressure; this effect is particularly strong when a pinch point is located among the low slope portions of the HCC. Analogous behaviour has been noted with all considered fluids.

The ratio of the volumetric flow rate VR is directly proportional to the evaporation pressure while the size factor SF decreases with the increase of the evaporation pressure with a trend that is similar to that found for the mass flow rate of the working fluid.

6.6.1.4. *Evaluation of the simple ORC applied to the second configuration of the cooling systems*

The optimization problem has been solved for the simple cycle coupled with the second cooling systems configuration and the results are shown in Table 6.11. LT circuits are modified so that heat is exchanged directly between lubricating oil and working fluid.

Table 6.11 Optimized operating characteristics for the simple ORC; second cooling systems configuration.

Fluid	—	R-134a	R-125	R-236fa	R-245ca	R-245fa	R-227ea
p_{ev}	bar	19.510	35.195	9.002	3.683	5.525	13.752
p_{con}	bar	7.702	15.685	3.210	1.217	1.778	5.284
T_{con}	°C	30.0	30.0	30.0	30.0	30.0	30.0
ΔT_{sup}	°C	0.0	8.0	0.0	0.0	0.0	0.0
T_5	°C	66.4	72.8	66.4	64.0	66.4	66.6
T_6	°C	30.0	34.8	40.9	39.9	38.9	40.7
χ	—	0.99	1.05	1.07	1.05	1.05	1.09
sub/sup	—	sub	sub	sub	sub	sub	sub
w_{exp}	kJ/kg	13.887	8.923	11.980	15.729	15.699	9.193
w_{pump}	kJ/kg	1.575	2.651	0.684	0.285	0.449	0.982
w_{net}	kJ/kg	12.312	6.273	11.296	15.444	15.250	8.211
$q_{absorbed}$	kJ/kg	184.948	117.746	165.458	224.940	212.976	127.778
q_{con}	kJ/kg	170.936	110.217	152.763	207.719	195.937	118.448
$\dot{m}_{wf}$	kg/s	40.722	66.670	45.100	31.369	32.603	62.511
$\dot{W}_{net}$	kW	501.4	418.2	509.4	484.5	497.2	512.4
η_{th}	%	6.66	5.33	6.83	6.87	7.16	6.43
η_t	%	5.13	4.28	5.21	4.96	5.09	5.24
Φ	%	77.1	80.32	76.4	72.2	71.0	81.6
VR	—	2.747	2.657	3.012	3.012	3.133	3.004
SF	m	0.502	0.442	0.745	1.027	0.858	0.674
$\dot{Q}_{absorbed}$	kW	7531.5	7850.1	7462.1	7056.2	6943.7	7974.7
$\dot{Q}_{con}$	kW	6960.9	7348.2	6887.6	6516.0	6388.1	7392.4

The results reported in the table are compared with those obtained with the first cooling systems configuration (Paragraph 6.6.1.3). All the fluids provide a higher net power compared to the first configuration. The evaporation pressures are generally lower whereas only R-125 shows approximately the same value as in the previous configuration. A lower evaporation pressure leads to lower thermal efficiency η_{th} and lower specific net power output w_{net} of the system.

Net power output of the cycle is given by the product of the working fluid mass flow rate with the specific net power output, according to Eq. (6.37). The increase in net power that has been noted for all the fluids is due to two reasons: first of all, the second engines cooling systems configuration allows a certain amount of heat to be exploited at higher temperature than in the first configuration. Thus, the net power output increases thanks to the increase of the working fluid mass flow rate which can occur without violating the pinch point constraints. The second reason is related to the evaporation process: the decrease in evaporation pressure leads to lower specific net power output; the lower evaporation temperature allows the working fluid mass flow rate to be increased because the CCC moves to a lower temperature level and its length can be higher according to the pinch point constraint. The net power is higher if the decrease of the specific net power output is overcompensated by the increase of the working fluid mass flow rate.

Fluids R-236fa and R-227ea show the maximum power generation whereas R-125 gives the lower output (418 kW) and it is operated at a high evaporation pressure than in the previous cooling systems configuration.

Per cent increases in power and mass flow rate with respect to the previous cooling systems configuration are presented in Table 6.12. Note that the percentage of increase in mass flow rate is higher than that in net power output because of the aforementioned reduction in specific net power.

All the fluids show a higher value for the heat recovery factor ϕ than the previous configuration. The values for this parameter are approximately in the range 70% ÷ 80%.

Table 6.12 Increases of the mass flow rate and the net power with respect to the first configuration.

Fluid	—	R-134a	R-125	R-236fa	R-245ca	R-245fa	R-227ea
$\Delta\dot{m}_{wf}$	%	34	29	27	24	20	40
$\Delta\dot{W}_{net}$	%	24	29	23	13	17	29

6.6.1.5. *Evaluation of the simple ORC applied to the third configuration of the cooling systems*

The optimization problem has been solved for the third cooling systems configuration (third case, Sub-section 6.5.3). The optimal design values of the system parameters are reported in Table 6.13 for the selected fluids.

Table 6.13 Optimized operating characteristics for the simple ORC; third cooling systems configuration.

Fluid	—	R-134a	R-125	R-236fa	R-245ca	R-245fa	R-227ea
p_{ev}	bar	19.352	38.723	8.403	3.545	5.019	13.255
p_{con}	bar	7.702	15.685	3.210	1.217	1.778	5.284
T_{con}	°C	30.0	30.0	30.0	30.0	30.0	30.0
ΔT_{sup}	°C	4.1	15.0	0.0	0.0	0.0	0.0
T_5	°C	70.2	81.0	63.7	62.7	62.9	65.0
T_6	°C	33.1	39.5	40.1	39.4	37.9	40.3
χ	—	1.02	1.10	1.06	1.05	1.04	1.09
sub/sup	—	sub	sup	sub	sub	sub	sub
w_{exp}	kJ/kg	14.289	10.402	11.175	15.165	14.329	8.849
w_{pump}	kJ/kg	1.554	3.125	0.613	0.269	0.388	0.924
w_{net}	kJ/kg	12.735	7.277	10.562	14.897	13.941	7.924
$q_{absorbed}$	kJ/kg	190.895	124.026	163.934	223.923	210.611	127.120
q_{con}	kJ/kg	176.417	115.281	152.069	207.315	195.040	118.120
$\dot{m}_{wf}$	kg/s	44.313	78.812	53.857	37.168	39.895	73.805
$\dot{W}_{net}$	kW	564.3	573.5	568.8	553.7	556.2	584.9
η_{th}	%	6.67	5.87	6.44	6.65	6.62	6.23
η_t	%	5.77	5.87	5.82	5.66	5.53	5.92
Φ	%	86.5	1.00	90.32	85.15	86.0	96.0
VR	—	2.683	2.923	2.786	2.897	2.836	2.869
SF	m	0.528	0.472	0.827	1.127	0.969	0.739
$\dot{Q}_{absorbed}$	kW	8459.1	9774.7	8828.9	8322.7	8402.3	9382.1
$\dot{Q}_{con}$	kW	7817.5	9085.5	8189.9	7705.4	7781.1	8717.9

As presented in Sub-section 6.5.3, the third cooling systems configuration makes available the engines waste heat at a higher temperature level. Theoretically, this should lead to an increase of the thermal efficiency of the ORC obtained by operating the cycle at

a higher pressure and temperature at expander inlet. The enthalpy drop in the expander is so increased leading to a higher net power output. In fact, the solutions of the optimization problem that have been found show an increase of the generated power if compared with the previous configurations but evaporation pressures and temperatures at expander inlet remain relatively low as well as the thermal efficiency in most of the cases. This means that the obtained cycles do not exploit properly the quality of the available heat; Paragraph 6.6.3.3 will show that better performances might be obtained with a different cycle.

Fluids R-134a and R-125 are superheated before the expander. The superheating temperature difference (ΔT_{sup}) is equal to the maximum allowed value in the case of R-125. All the fluids but R-125 are operated at a lower evaporation pressure compared to the second configuration; the evaporation pressure of fluid R-125 is increased so that the cycle is supercritical. Heat that is absorbed by the fluids is higher than in the previous configurations and it is equal to the maximum available quantity in the case of R-125. Indeed, the heat recovery factor ϕ for this fluid is equal to 100% whereas the other mediums show higher values than the previous configurations.

Percentage increases in power and mass flow rate in comparison with the previous configuration are presented in Table 6.14. It can be observed that only fluid R-125 provides a wide increase in the net power output without requiring a significant increase of the mass flow rate. In absolute terms, the best fluid for the power generation is R-227ea. However, the difference with the other fluids is not significant and in the worst case (fluid R-245ca) does not exceed 6%.

Table 6.14 Increases of the mass flow rate and the net power respect the second configuration.

Fluid	—	R-134a	R-125	R-236fa	R-245ca	R-245fa	R-227ea
$\Delta\dot{m}_{wf}$	%	9	18	19	18	22	18
$\Delta\dot{W}_{net}$	%	13	37	12	14	12	14

The optimization problem has found the values of the decision variables that allow the maximum of the net power output to be obtained. Other aspects such as dimensions of the system, economical convenience have not been considered so that the solutions that have been found might not be the best if other criteria are selected.

Since now, fluid R-227ea is considered for further observations that might be applied also to the other fluids. The first MATLAB script (Paragraph 6.6.1.2) that has been developed has run in order to study the performance and characteristics of the Rankine cycle at different values of the decision variables. The results are presented here in

graphical form as a function of the evaporation pressure and superheating temperature difference: Figure 6.16 reports the thermal efficiency of the cycle, Figure 6.17 the net power output and Figure 6.18 shows the mass flow rate of the working fluid. Figure 6.19 and Figure 6.20 show the parameters *VR* and *SF*, respectively. The points that compose the curves are those for which the constraints of feasibility of the heat transfer and minimum quality of the fluid at turbine outlet are fulfilled.

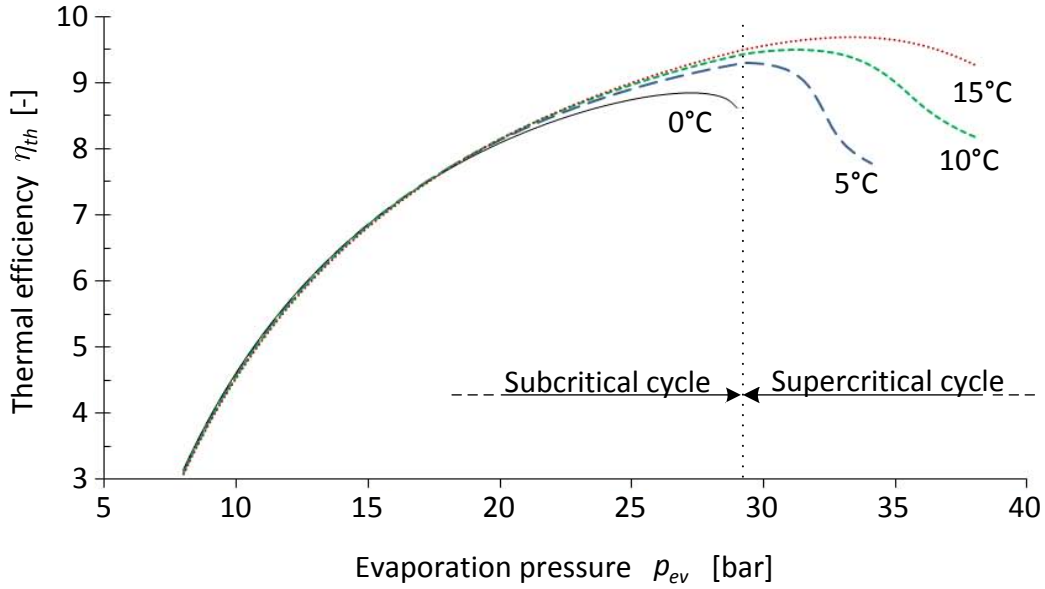

Figure 6.16 Thermal efficiency as a function of the evaporation pressure with the superheating temperature difference (ΔT_{sup}) as parameter; fluid R-227ea.

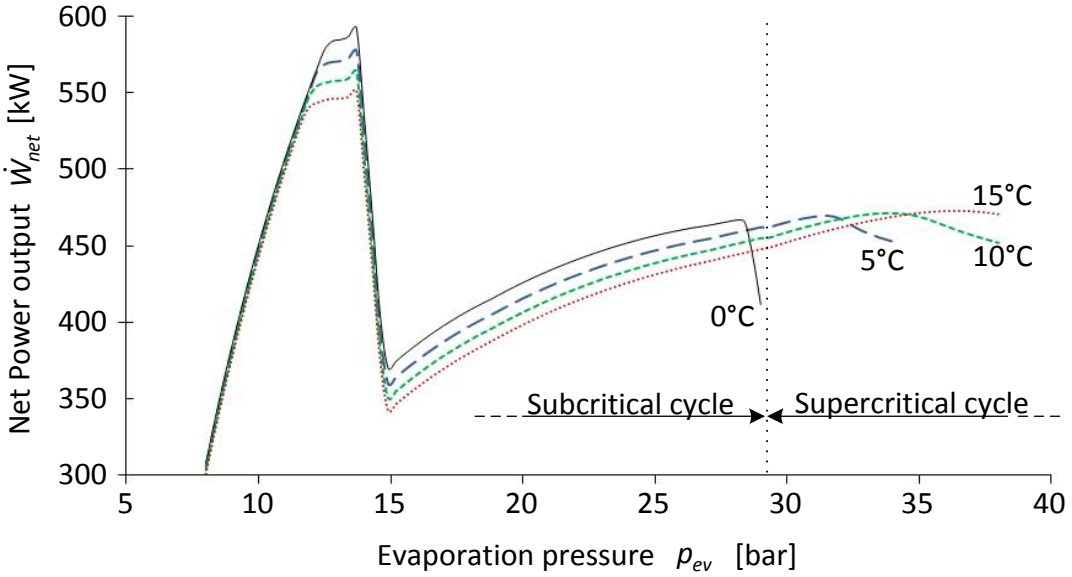

Figure 6.17 Net power output as a function of the evaporation pressure with the superheating temperature difference (ΔT_{sup}) as parameter; fluid R-227ea.

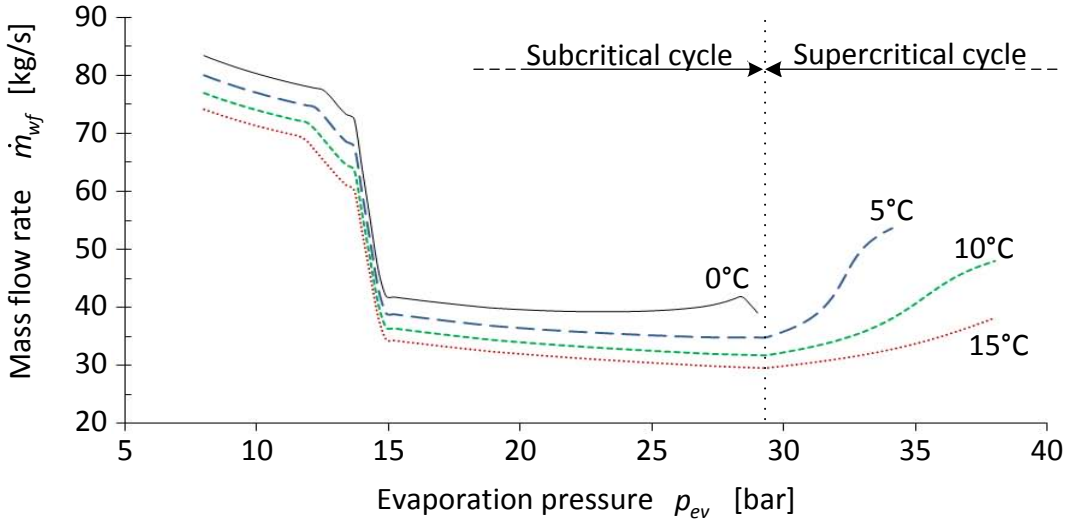

Figure 6.18 Mass flow rate of the working fluid as a function of the evaporation pressure with the superheating temperature difference (ΔT_{sup}) as parameter; fluid R-227ea.

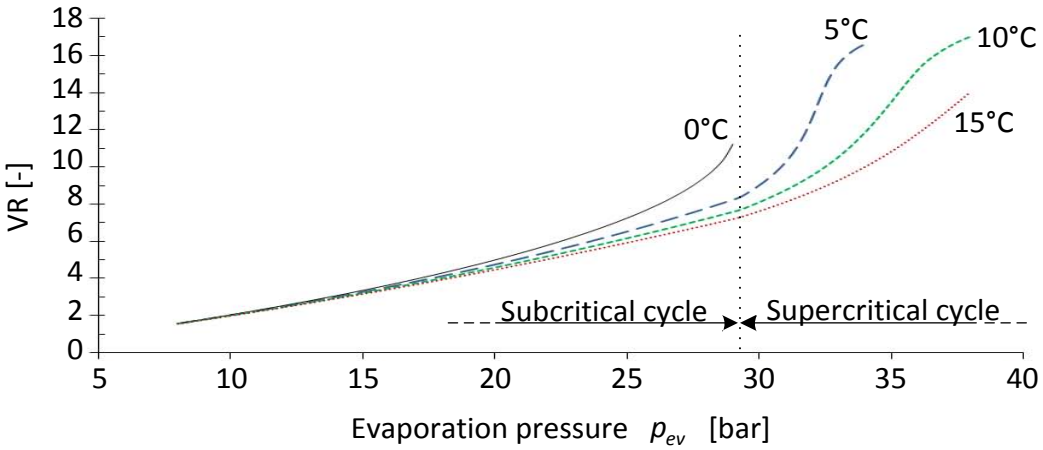

Figure 6.19 Parameter *VR* as a function of the evaporation pressure with the superheating temperature difference (ΔT_{sup}) as parameter; fluid R-227ea.

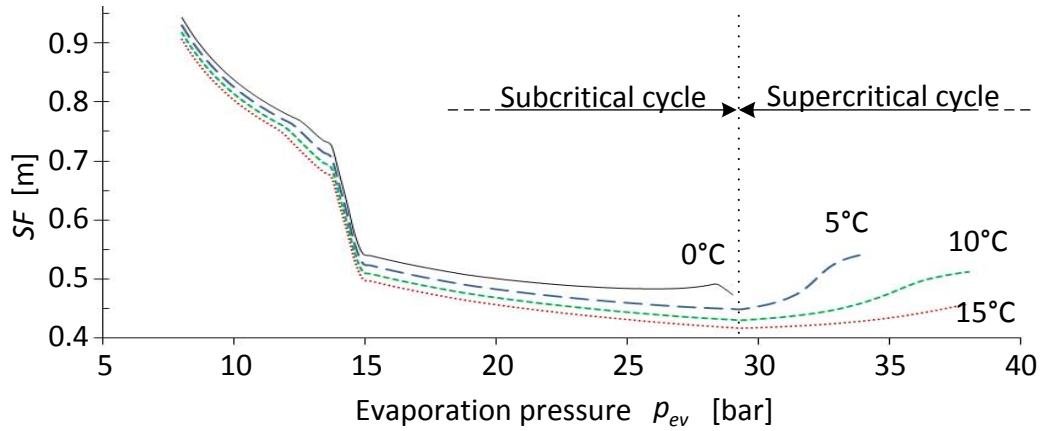

Figure 6.20 *SF* as a function of the evaporation pressure with the superheating temperature difference (ΔT_{sup}) as parameter; fluid R-227ea.

Figure 6.17 shows on the left the area where the maximum of the net power output of the simple ORC operating with R-227ea has been found by the optimizer. This optimum solution is that reported in Table 6.13. The increase in the evaporation pressure from this optimum point (moving to the right in the figure) leads to a strong reduction of the net power output which is basically due to the decrease of the working fluid mass flow rate (Figure 6.18). The behaviour depends on the particular shape of the HCC. The net power output increases again with the evaporation pressure after a value equal to approximately 15 bar. In this case, the increase of the thermal efficiency is stronger than the decrease of the mass flow rate (Figure 6.18), which is then overcompensated. Note that even if the values reached by the thermal efficiency are significantly higher than that of the optimum point, the net power output remains lower because of the low heat recovery factor which indicates that the heat associated with lubricating oil and jacket water is exploited only partially. A local maximum for the net power output is reached at an evaporation pressure of about 36 bar and ΔT_{sup} equal to 15°C, as shown in Figure 6.17. Note that a similar net power is obtained even with a lower evaporation pressure (i.e., in the range 27÷28 bar). In this case the lower maximum pressure might reduce the cost of the system and leads to a lower volumetric expansion ratio (*VR*).

The increase of the superheating temperature difference from the optimum (i.e., saturated vapour conditions) reduces the net power output but the dependence on this parameter is less marked compared to the evaporation pressure.

The analysis of the optimal and sub-optimal regions has pointed out that all fluids but R-125 show the same behaviour that has been presented above for the R-227ea. The maximum net power output values occur in a quite narrow pressure range so that the selection of this condition as design point may lead to operational issues. A more stable operating condition can be achieved at higher evaporation pressures at the expense of a decrease in net power output. The optimization procedure has been applied to find the values of the ORC operating parameters at the local maximum of the net power output; all fluids but R-125 have been considered and the results are presented in Table 6.15.

The values of the evaporation pressure are significantly higher than those found in the case of absolute maximization of the net power output. The cycles operated with the R-134a, R-236fa and R-227ea are here supercritical whereas R-245ca and R-245fa give subcritical cycles. The reduction of the generated power is particularly significant for all the fluids but R-236fa. In this last case the reduction is of 10%. The values of the heat recovery factor (φ) are approximately half than those found in case of absolute maximization of the net power output. Similar reduction is noted for the heat absorbed and the working fluid mass flow rate. Both T_5 (expander inlet) and T_6 (expander outlet) are higher using dry fluids. An increase in the thermal efficiency is found in all the case, the ratios *VR* are significantly higher whereas the values of the size factors *SF* decrease.

Table 6.15 Optimized operating characteristics for the simple ORC, third configuration. Local maximums of the net power at high pressures.

Fluid	—	R-134a	R-236fa	R-245ca	R-245fa	R-227ea
p_{ev}	bar	46.377	39.431	9.489	13.835	36.386
p_{con}	bar	7.702	3.210	1.217	1.778	5.284
T_{con}	°C	30.0	30.0	30.0	30.0	30.0
$\triangle T_{\sup}$	°C	15.0	15.0	0.0	0.0	15.0
T_5	°C	116.1	139.9	101.0	104.1	116.8
T_6	°C	30.0	48.1	51.9	48.6	46.7
χ	—	0.99	1.11	1.11	1.10	1.14
sub/sup	—	sup	sup	sub	sub	sup
$w_{\exp}$	kJ/kg	24.958	26.061	30.117	28.940	16.880
w_{pump}	kJ/kg	5.136	4.260	0.955	1.443	3.589
w_{net}	kJ/kg	19.822	21.800	29.162	27.497	13.291
$q_{absorbed}$	kJ/kg	194.638	184.461	251.960	236.183	139.501
q_{con}	kJ/kg	171.530	159.339	219.356	205.326	123.976
$\dot{m}_{wf}$	kg/s	23.770	24.019	15.682	17.166	35.576
$\dot{W}_{net}$	kW	471.2	523.6	457.3	472.0	472.8
η_{th}	%	10.18	11.82	11.57	11.64	9.53
η_t	%	4.82	5.36	4.68	4.83	4.84
Φ	%	47.33	45.33	40.42	41.48	50.77
VR	—	7.952	22.333	8.210	8.562	12.207
SF	m	0.332	0.455	0.631	0.545	0.444
$\dot{Q}_{absorbed}$	kW	4626.6	4430.6	3951.2	4054.3	4962.8
$\dot{Q}_{con}$	kW	4077.3	3827.2	3439.9	3524.6	4410.5

Figure 6.21 and Figure 6.22 show the HCC and the CCC of the optimized ORC coupled with the third cooling systems configuration and operating with R-227ea. The first one is the subcritical cycle which refers to the maximum power output condition whereas the second one is supercritical cycle and refers to the local maximum achieved at high pressure. The figures show graphically the aforementioned reduction of the absorbed heat (length of the CCC) and the increase of the vapour temperature at expander inlet that has been noted from the first to the second case. The supercritical cycle does not allow the heat associated with the lubricating oil to be exploited.

The heat demand required for the operation of the FWG is overlapped with the ORC heating profile in the case of supercritical cycle whereas it can be clearly distinguished in the case of subcritical cycle.

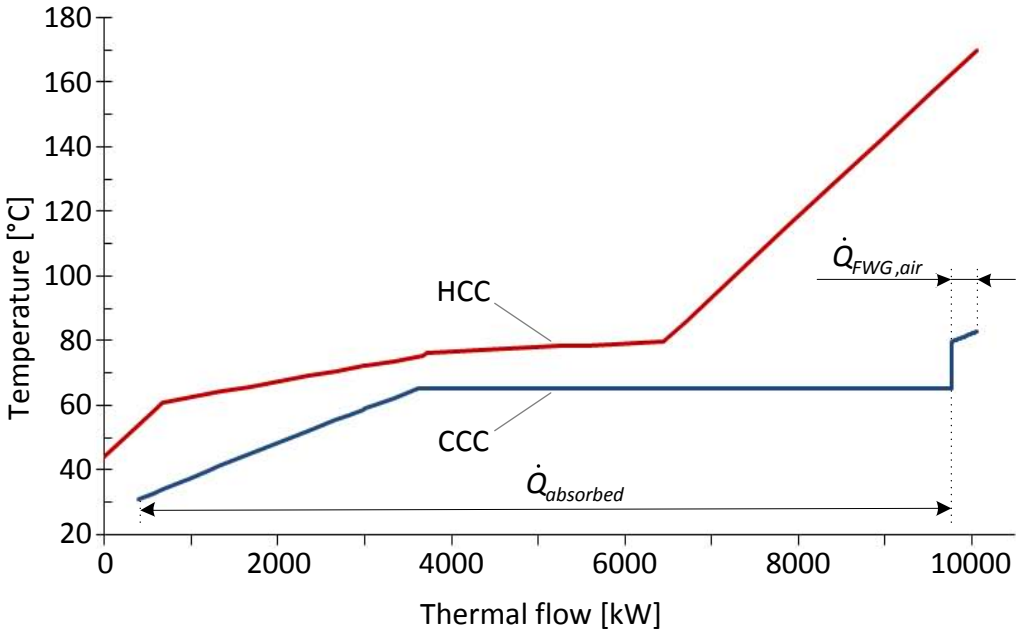

Figure 6.21 HCC and CCC of the simple ORC coupled with the third cooling systems configuration; Fluid R-227ea operated with optimized parameters at the absolute maximum of the net power output.

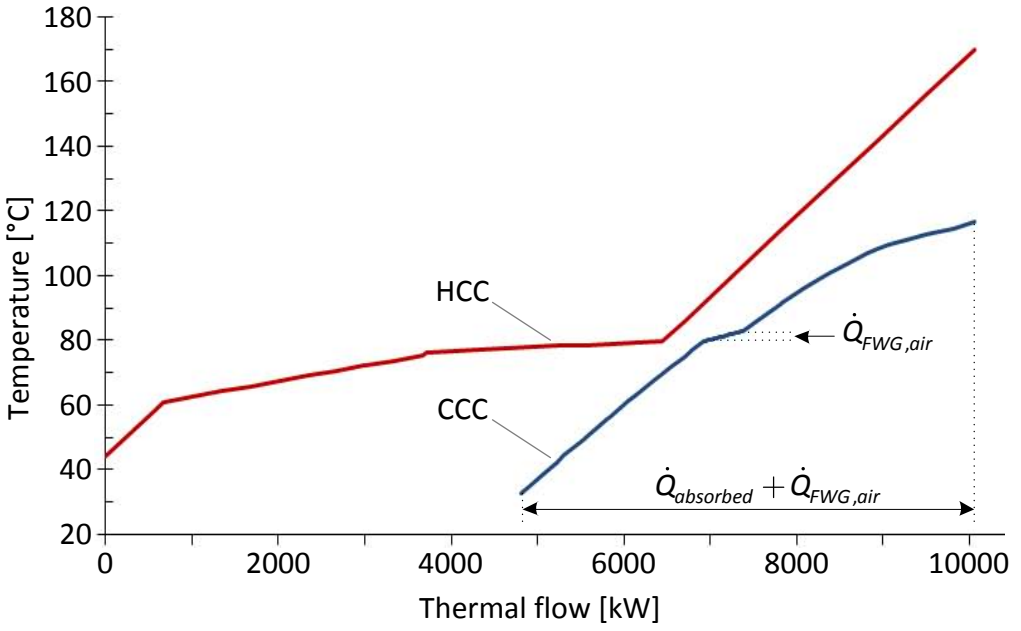

Figure 6.22 HCC and CCC of the simple ORC coupled with the third cooling systems configuration; Fluid R-227ea operated with optimized parameters at the local maximum of the net power output.

6.6.2. Regenerative ORC

The regenerative organic Rankine cycle adds a recuperator to the simple Rankine cycle configuration in order to exploit the heat flow associated with the working fluid after the expansion, if it is superheated. Five components are required as shown in Figure 6.23. Both subcritical and supercritical cycles are considered. Figure 6.24 shows the qualitative *T-s* diagram for a subcritical and supercritical regenerative cycle.

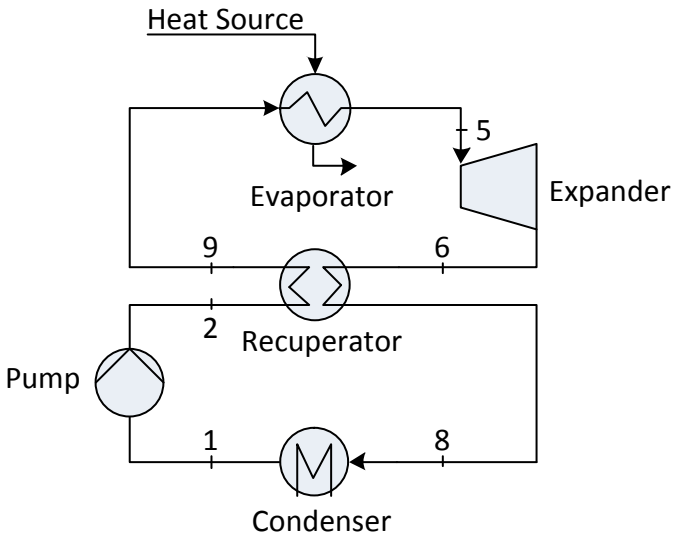

Figure 6.23 Arrangement of the regenerative organic Rankine cycle.

The modelling of the pump and expander is the same as in the previous case. The additional component that is introduced requires a modification in Eqs. (6.29) and (6.32) in order to take into consideration the heat that is transferred internally. The updated equations are Eqs. (6.42) and (6.43), respectively. The first one defines the specific heat that is absorbed at the evaporator and the other gives the heat rejected to the condenser.

$$q_{absorbed} = h_5 - h_9 \tag{6.42}$$

$$q_{con} = h_8 - h_1 \tag{6.43}$$

Heat can be transferred internally only if the working fluid after the expander is sufficiently superheated: the feasibility of the heat transfer should be checked by comparing the profile of the liquid to be heated with that of the vapour, which has to be cooled. Rather than using this method, an "approach difference of temperature" ΔT_{appr} was selected in order to calculate the temperature at state *8.* This state is then identified

by Eqs. (6.44) where ΔT_{appr} is considered to be equal to 15°C and p_{con} is the condensing temperature:

$$\begin{cases} T_8 = T_7 + \Delta T_{appr} \\ p_8 = p_{con} \end{cases} \tag{6.44}$$

If the temperature T_8 is lower than the temperature T_6, the specific heat that is transferred internally is given by Eq. (6.45) and the specific enthalpy of the state *9* is expressed by Eq. (6.46). The value calculated through Eq. (6.45) is then multiplied with the working fluid mass flow rate to give the total heat $\dot{Q}_{reg}$, Eq. (6.47).

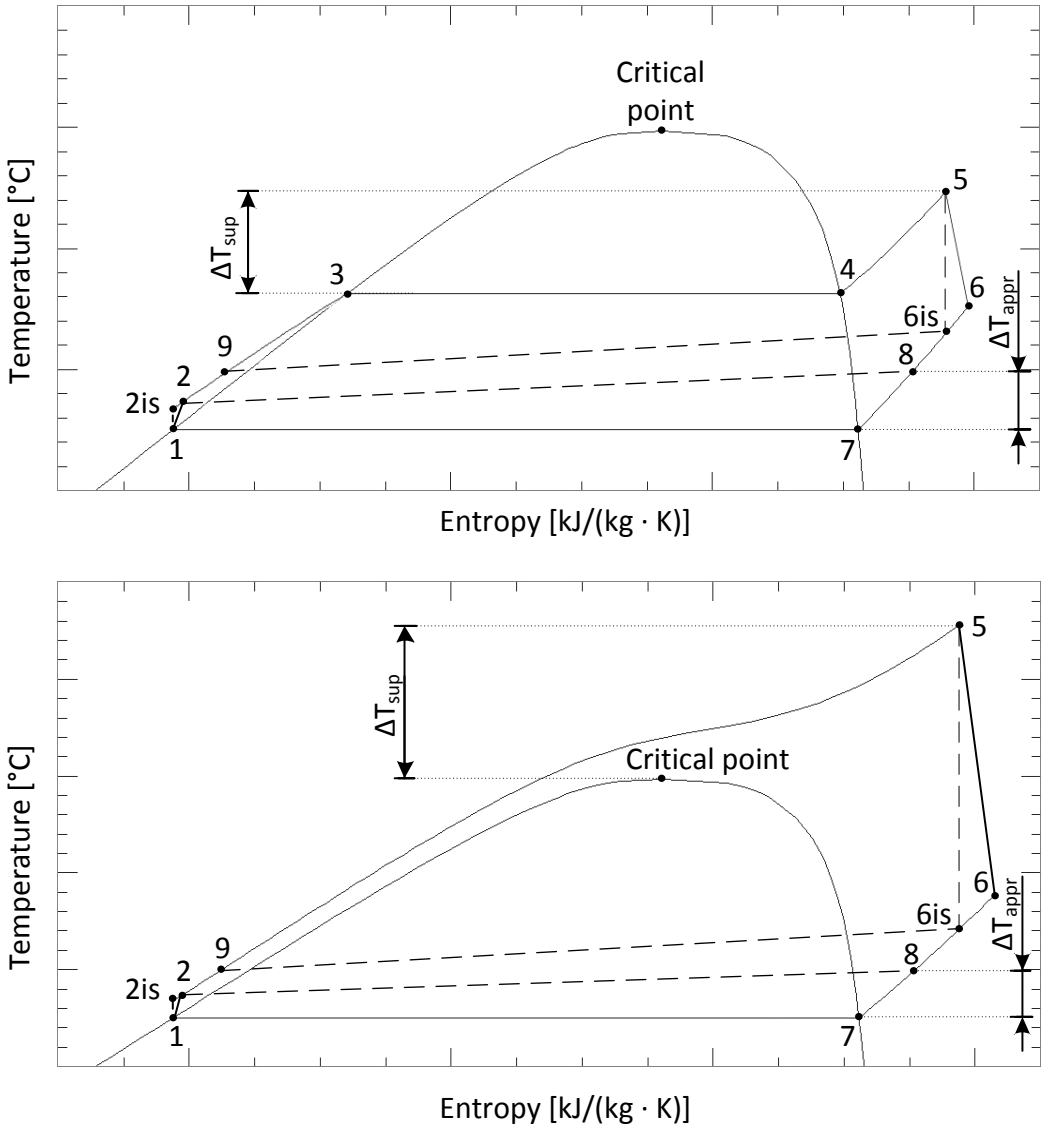

Figure 6.24 Qualitative T-s diagram of the regenerative ORC, subcritical and supercritical.

$$q_{reg} = h_6 - h_8 \tag{6.45}$$

$$h_9 = h_2 + q_{reg} \tag{6.46}$$

$$\dot{Q}_{reg} = \dot{m}_{wf} \cdot q_{reg} \tag{6.47}$$

If the temperature T_8 is higher than the temperature T_6, it is not possible to transfer heat internally: state *8* is considered identical to state *7* and state *9* is considered identical to state *2*.

6.6.2.1. *Simulation procedure and optimization*

Only minor modifications are introduced to the simulation procedure described for the simple ORC in the previous sub-section. An additional independent variable fixed att constant value is the approach temperature difference ΔT_{appr} whereas the additional dependent variables are the heat that is transferred internally and the parameters that characterize states *6* and *8*.

6.6.2.2. *Results*

The regenerative cycle applied to the first and second configurations of the engines cooling systems does not allow to achieve a higher net power output than in the case of simple cycle. It has been noted that only when the evaporation pressure is very low, the regenerative arrangement leads to negligible increases in the net power output which are not sufficient to justify the addition of the recuperator.

With regard to the third cooling systems layout, the regenerative cycle does not allow a higher power output to be obtained because a relevant quantity of heat is available at low temperatures. The use of an internal recuperator leads to the impossibility to exploit this heat and at the same time could increase the cost of the system.

Other studies found in literature such as the work of Di Genova et al. (2013) pointed out the higher power output obtained with the regenerative cycle but in these cases the minimum temperature of the HCC were lower than in the present study.

Figure 6.25 and Figure 6.26 show the heat that is exchanged internally and the temperature of the working fluid at the expander outlet, respectively, for the regenerative cycle coupled with the third cooling systems configuration. R-227ea is considered as working fluid.

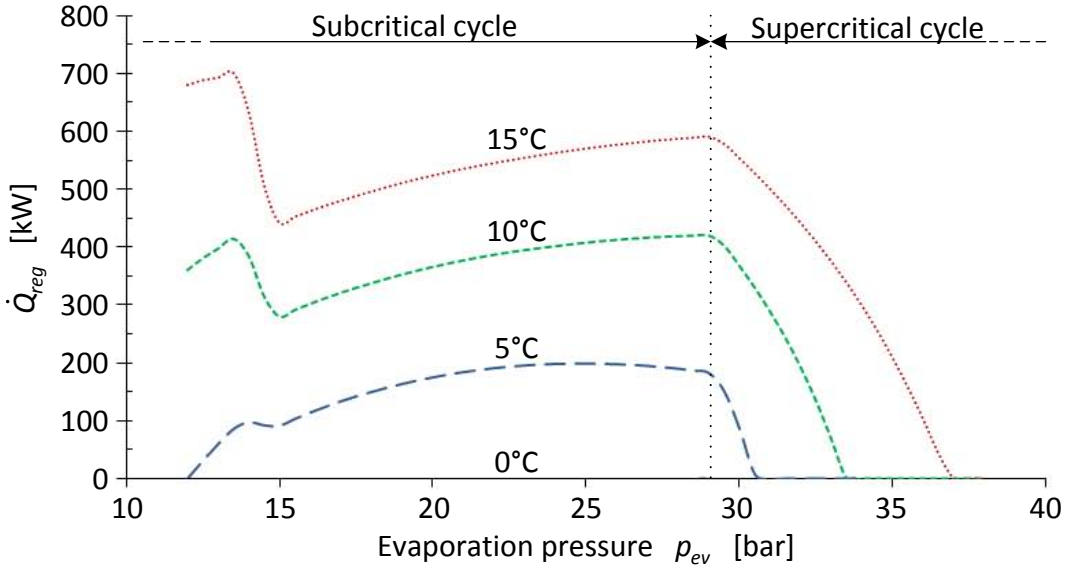

Figure 6.25 Heat transferred internally at the recuperator as a function of the evaporation pressure with the superheating temperature difference ΔT_{sup} as parameter; fluid R-227ea; third cooling systems configuration.

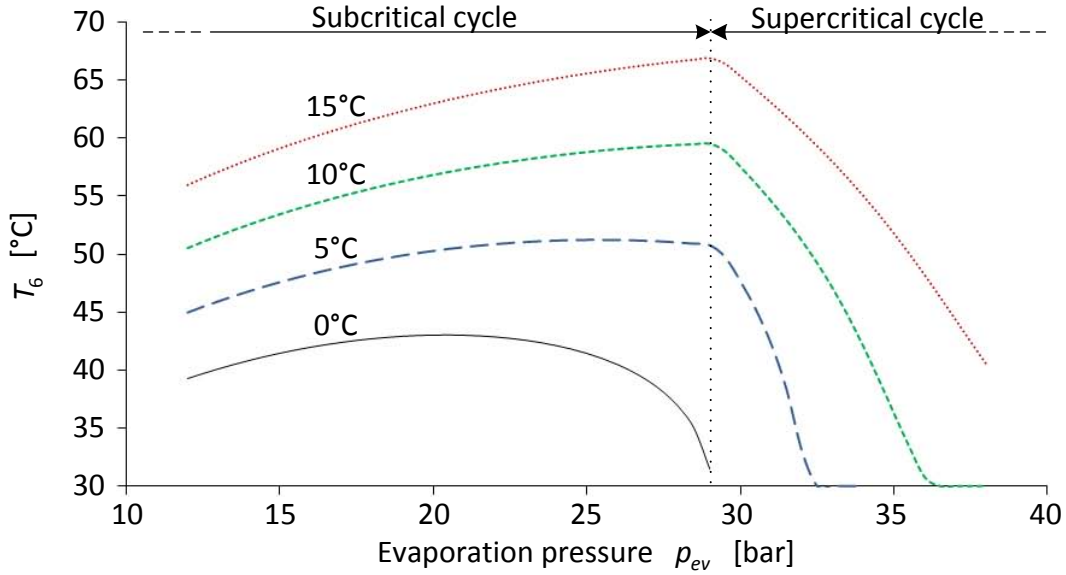

Figure 6.26 Temperature at expander outlet as a function of the evaporation pressure with the superheating temperature difference ΔT_{sup} as parameter; fluid R-227ea; third cooling systems configuration.

6.6.3. Two-stage ORC

This sub-section analyses the effectiveness of a two-stage organic Rankine cycle to exploit the waste heat provided by the engines cooling systems. This cycle has been proposed by Smolen (2011) (Sub-section 3.9.1) to be coupled with a biogas fuelled internal combustion engine. The peculiarity of the cycle is that the evaporation of the working fluid takes place at two different pressure levels. With reference to Figure 6.27, "Pump 1" increases the pressure of the working fluid from condenser outlet up to the lower pressure level. Then, the main flow is split into two flows, $\dot{m}_A$ and $\dot{m}_B$. "Pump 2" increases the pressure of the flow $\dot{m}_B$ to the high pressure level, the evaporation takes place and the vapour expands through the "Expander 2". Instead, $\dot{m}_A$ is directly heated at the "Evaporator 1", it is mixed with the flow $\dot{m}_B$ coming from "Expander 2" outlet and expands through "Expander 1".

The study considers that the organic fluid is operated at subcritical conditions in the low pressure stage while both the subcritical and supercritical cases are investigated for the high pressure stage. Figure 6.28 shows the qualitative *T-s* diagrams of the two-stage cycle for the subcritical and supercritical cycles.

It is considered that the heat provided by the first two engines cooling systems configurationss is not appropriate to be exploited by a two-stage ORC because of the low temperature level of the sources. In fact, no complex cycles exploiting heat at a temperature level lower than 120°C ÷ 150°C have been found in literature. Moreover, the hot composite curves related to the heat provided by the first two cooling systems

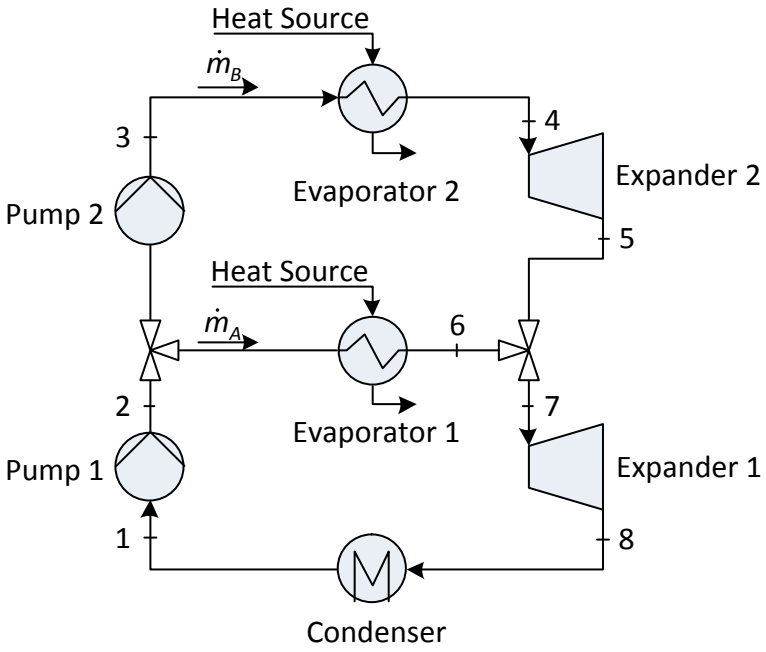

Figure 6.27 Arrangement of the two stage organic Rankine cycle.

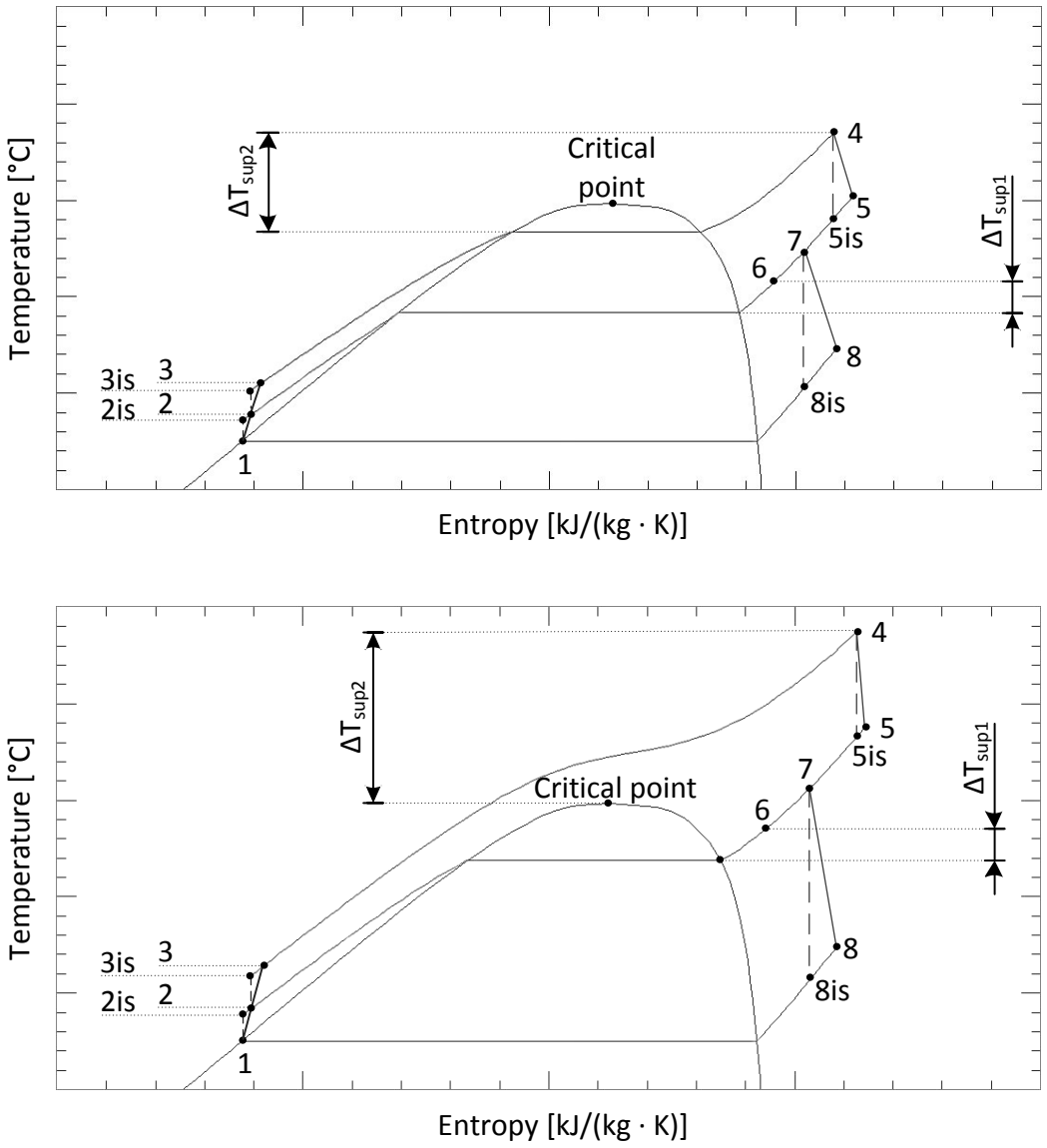

Figure 6.28 Qualitative T-s diagrams of the two stage ORC, subcritical and supercritical cycle.

configurations do not show segments particularly different to each other in terms of temperature or heat flow rate which may suggest the use of a complex ORC (such as a two-stage ORC) to better exploit the available heat. Thus, the two-stage ORC is investigated to be coupled only with the third cooling systems configuration.

The thermodynamic model of the cycle has been defined with respect to the hypotheses presented in Section 6.6. The model is discussed in the following.

According to the modelling of the cycle performed in MATLAB-Simulink environment and for convenience reasons, the specific thermal flow rates absorbed or rejected at the various heat exchangers and the specific power of pumps and expanders are referred to the working fluid mass flow rate in the high pressure level ($\dot{m}_B$). This is made by introducing the parameter defined by Eq. (6.48):

$$\Delta = \frac{\dot{m}_A}{\dot{m}_B} \tag{6.48}$$

"Pump 1" increases the pressure of the total flow of the fluid in a non-isentropic process (from state *1* to state *2*). The specific work input to the pump is given by Eq. (6.49). The isentropic efficiency is defined by Eq. (6.50).

$$w_{pump1} = (1+\Delta)\cdot(h_2 - h_1)\cdot\frac{1}{\eta_{me,pump1}} \tag{6.49}$$

$$\eta_{is,pump1} = \frac{h_{2,is} - h_1}{h_2 - h_1} \tag{6.50}$$

where

h specific enthalpy of the working fluid in the subscripted state,

$\eta_{me,pump1}$ mechanical and electrical efficiency of the pump1.

State *1* is on the saturated liquid curve at the condensation pressure. The pressure of the flow $\dot{m}_B$ is then increased by the "Pump 2". The specific work to the pump and the isentropic efficiency are defined by Eq. (6.51) and Eq. (6.52), respectively.

$$w_{pump2} = (h_3 - h_2)\cdot\frac{1}{\eta_{me,pump2}} \tag{6.51}$$

$$\eta_{is,pump2} = \frac{h_{3,is} - h_2}{h_3 - h_2} \tag{6.52}$$

The two flows $\dot{m}_A$ and $\dot{m}_B$ are then heated at the respective evaporators. Eq. (6.53) and Eq. (6.54) give the specific heat that is absorbed by the high pressure and the low pressure stage, respectively.

$$q_{evaporator2} = h_4 - h_3 \tag{6.53}$$

$$q_{evaporator1} = \Delta\cdot(h_6 - h_2) \tag{6.54}$$

The flow $\dot{m}_B$ passes through the "Expander 2" and it is expanded in a non-isentropic process. The specific power output of the expander is given by Eq. (6.55) whereas Eq. (6.56) defines the isentropic efficiency:

$$w_{\exp 2} = (h_4 - h_5) \cdot \eta_{me,\exp 2} \tag{6.55}$$

$$\eta_{is,\exp 2} = \frac{h_4 - h_5}{h_4 - h_{5,is}} \tag{6.56}$$

where

h specific enthalpy of the working fluid in the subscripted state,

$\eta_{me,exp2}$ mechanical and electrical efficiency of the expander 2.

Subsequently, the flows $\dot{m}_A$ and $\dot{m}_B$ are mixed to give a unique flow. The energy balance of Eq. (6.57) is solved for the specific enthalpy of the state *7*, Eq. (6.58).

$$h_5 + \Delta \cdot h_6 = (1 + \Delta) \cdot h_7 \tag{6.57}$$

$$h_7 = \frac{h_5 + \Delta \cdot h_6}{1 + \Delta} \tag{6.58}$$

This flow passes through the "Expander 1" and undergoes a non-isentropic transformation. Equation (6.59) gives the specific power output of the expander and Eq. (6.60) defines the isentropic efficiency.

$$w_{\exp 1} = (1 + \Delta) \cdot (h_7 - h_8) \cdot \eta_{me,\exp 1} \tag{6.59}$$

$$\eta_{is,\exp 1} = \frac{h_7 - h_8}{h_7 - h_{8,is}} \tag{6.60}$$

Then, the fluid rejects the heat defined by Eq. (6.61) at the condenser. Equation (6.62) gives the specific net power output of the cycle.

$$q_{con} = (1 + \Delta) \cdot (h_8 - h_1) \tag{6.61}$$

$$w_{net} = w_{\exp 1} + w_{\exp 2} - w_{pump1} - w_{pump2} \tag{6.62}$$

The thermal efficiency of the cycle that is defined as:

$$\eta_{th} = \frac{w_{net}}{q_{evaporator1} + q_{evaporator2}} \tag{6.63}$$

The specific parameters (i.e., w_{pump1}, w_{pump2}, w_{exp1}, w_{exp2}, w_{net}, $q_{evaporator1}$, $q_{evaporator2}$, q_{con}) are then multiplied with the mass flow rate $\dot{m}_B$ to give the absolute values of the power or the thermal flow rate that are exchanged.

6.6.3.1. *Simulation procedure*

Five decision variables (independent variables that are free to vary) are considered in the simulation procedure. They are the evaporation pressure and the degree of superheating of the fluid in the two stages (i.e., $p_{ev,1}$, $p_{ev,2}$, $\Delta T_{sup,1}$, $\Delta T_{sup,2}$), and the aforementioned ratio of the mass flow rates in the stages (Δ). Like for the previous cycles, the degrees of superheating are measured in terms of temperature [°C]. With regard to the upper stage, in case of subcritical conditions, $\Delta T_{sup,2}$ is the temperature difference between state *4* and the state characterized by saturated vapour at the evaporation pressure; in case of supercritical conditions, the degree of superheating is measured from the temperature of the critical point. It is considered that the value of the evaporation pressure in the lower stage is lower than the critical one for all the fluids.

The independent variables that are assumed as constant parameters are the performance of pumps and expanders, the condensation temperature, the "hot composite curve" (HCC), the pinch point temperature difference (ΔT_{pp}) and the information (in terms of temperatures and heat flow rate) related to the heating process of the water flow that takes place at the point "*HE4*" of the third engines cooling systems configuration presented in Figure 6.9. As stated previously for the other cycles, the HCC is considered as a constant parameter because it collects in a combined form the information related to various hot steams (heat flow rate and temperatures) that are traditionally considered as constant parameters.

Table 6.16 presents the values assumed for various fixed independent variables. Different values are considered for the isentropic efficiency of pumps and expanders whereas the mechanical and electrical efficiency is equal for all of them. ΔT_{pp} is the minimum allowed temperature difference between HCC and CCC.

Table 6.16 Values of various independent variables assumed as constant parameters.

Parameter	Unit	Value
$\eta_{is,pump1}$, $\eta_{is,pump2}$	-	0.7
$\eta_{is,exp1}$, $\eta_{is,exp2}$	-	0.85
$\eta_{me,pump1}$, $\eta_{me,pump2}$, $\eta_{me,exp1}$, $\eta_{me,exp2}$	-	0.9
T_{con}	°C	30
ΔT_{pp}	°C	10

Dependent variables are the thermodynamic properties of the working fluid in various states, the mass flow rates $\dot{m}_A$ and $\dot{m}_B$, the heat that is exchanged in various components, the work of expanders and pumps, and two parameters that have been defined in Sub-section 3.8.2: size factor (*SF*) and volumetric expansion ratio (*VR*). The CCC is considered as a dependent variable, as well. It is built considering the heating processes of the working fluid at the evaporators and the heating process of the water flow that feeds the FWG.

The various steps of the simulation procedure are similar to those presented for the simple cycle in Figure 6.13 with the difference in the selection of the decision variables, dependent variables, and independent variables that are considered as constant parameters. The CCC is calculated here considering three cold streams instead of two or one of the previous cycles and cooling systems configurations. This means that the curve is here discretized with 63 points (60 intervals).

Like in the previous cases, the solutions that are considered by the MATLAB code are those for which the feasibility of the heat transfer and the minimum quality of the vapour at expanders outlet (minimum equal to 0.9) are fulfilled.

6.6.3.2. *Simulation and optimization*

Like for the previous cycles, two scripts have been built in MATLAB environment. The first one allows the optimal and sub-optimal regions of a defined objective function to be identified. The simulation procedure is iterated for this purpose: the evaporation pressures of the working fluid in the two stages are considered as fixed independent variables instead of decision variables. Their values are selected from appropriate ranges. The values of the other three decision variables are found solving the optimization problem for the given objective function.

The second script solves the optimization problem considering all the five decision variables. The optimized values are found within restricted ranges that are predefined according to the results obtained by the first script. Non-linear constraints that are considered are the quality of the fluid at expander outlet and the feasibility of the heat transfer. The objective is the maximization of the net power of the system $\dot{W}_{net}$ with respect to $\underset{\sim}{x}$:

$$\max_{\underset{\sim}{x}} \ \dot{W}_{net}(\underset{\sim}{x}) \tag{6.64}$$

$$\underset{\sim}{x} = (p_{ev1}, p_{ev2,} \Delta T_{\text{sup1,}} \Delta T_{\text{sup2,}} \Delta) \tag{6.65}$$

6.6.3.3. *Results*

Table 6.17 shows the optimized operating parameters of the two-stage ORC coupled with the third cooling systems configuration. The objective function considered by the optimization problem is the maximum of the net power. The condensation temperature is 30°C. Five fluids have been considered. R-125 has not been considered because of the too low critical temperature which leads to high evaporation pressure values as found for the simple ORC (Paragraphs 6.6.1.3 and 6.6.1.4).

Comparing the results with those obtained for the other cycles (same configuration for the cooling systems) it is noted that the two-stage ORC allows a significant increase in the net power output to be obtained for all the considered fluids. The additional power is approximately in the range of 30 ÷ 40%.

The values of the evaporation pressure of the fluids in the two stages are close to those found in correspondence of the two peaks of the net power output for the simple ORC (Paragraph 6.6.1.5). The high pressure stage is supercritical in the case of fluids R-134a, R-236fa and R-227ea whereas it is subcritical in the cases of R-245ca and R-245fa. R-134, R-236fa and R-227ea require the maximum allowed value for the superheating temperature difference in the high pressure stage ΔT_{sup2}. They are operated in supercritical conditions. R-134a requires also a slight superheating in the low pressure stage. The ratio Δ assumes values always higher than 1. This means that the working fluid mass flow rate in the high pressure stage is lower than that in the low pressure one. All fluids appear superheated after the two expanders. The value of the temperature T_5 (expander outlet of the high pressure stage) for the fluids R-236fa, R-245ca, R-245fa and R-227ea is 10 ÷ 18°C higher than in saturated conditions. The temperature of the fluids at low pressure level expander outlet is relatively low so that a recuperator might not be competitive.

With regard to the net power generated in the two stages, all the fluids show that the higher contribution comes from the low pressure one. The power output of the expander is reduced by the needs of the pump that are relatively low in the low pressure stage. Net power output of the various fluids is in the range 750 ÷ 820 kW. Best fluid for the generation is R-236fa (820.3 kW). However, note that the cycle operating with this fluid is characterized by a high value for the parameter VR_2. Also, the temperature at expander inlet of the high pressure stage is significantly higher than that of the other fluids. Best fluid for the minimization of the size of the turbine according to the parameters *SF* and *VR* is R-134a.

The two-stage ORC allows the complete exploitation of the available heat to be achieved as shown by the high values of the heat recovery factor. In fact, this parameter is equal to approximately 100% with all the considered fluids.

Table 6.17 Optimized operating parameters for the two-stage ORC applied to the third engines cooling systems configuration.

Fluid	—	R-134a	R-236fa	R-245ca	R-245fa	R-227ea
p_4	bar	44.210	37.660	11.997	17.568	34.840
p_6	bar	15.643	7.052	2.887	4.169	11.826
ΔT_{sup2}	°C	15.0	15.0	0.0	0.0	15.0
ΔT_{sup1}	°C	1.7	0.0	0.0	0.0	0.0
Δ	—	1.2382	1.4913	1.9802	1.8607	1.1659
p_{con}	bar	7.702	3.210	1.217	1.778	5.284
T_{con}	°C	30.0	30.0	30.0	30.0	30.0
T_4	°C	116.1	139.9	111.5	115.4	116.8
T_5	°C	61.3	73.0	73.0	70.1	72.0
T_6	°C	58.7	56.9	55.8	56.4	60.2
T_7	°C	59.9	63.3	61.6	61.2	65.6
T_8	°C	32.4	44.9	43.2	41.2	45.2
χ_5	—	1.04	1.13	1.10	1.09	1.14
χ_8	—	1.01	1.09	1.06	1.06	1.13
stage 2	—	sup	sup	sub	sub	sup
stage 1	—	sub	sub	sub	sub	sub
$\dot{W}_{exp1}$	kW	560.5	532.7	512.0	521.2	586.8
$\dot{W}_{exp2}$	kW	332.8	394.9	288.5	304.7	306.8
$\dot{W}_{pump1}$	kW	53.8	25.7	7.9	12.4	55.2
$\dot{W}_{pump2}$	kW	86.0	81.7	14.5	24.4	89.1
$\dot{W}_{net}$	kW	753.1	820.3	778.1	789.0	749.3
$\dot{Q}_{evaporator1}$	kW	5203.5	5414.1	5970.9	5840.9	4893.3
$\dot{Q}_{evaporator2}$	kW	4570.9	4360.3	3571.5	3678.9	4881.4
$\dot{Q}_{con}$	kW	8908.1	8840.4	8673.1	8635.4	8911.7
η_{th}	%	7.71	8.39	8.15	8.29	7.67
η_t	%	7.71	8.39	7.95	8.07	7.67
Φ	%	1.00	1.00	0.97	0.97	1.00
VR_1	—	2.115	2.277	2.347	2.337	2.455
SF_1	m	0.601	0.894	1.254	1.067	0.760
VR_2	—	3.421	8.542	4.573	4.908	4.419
SF_2	m	0.259	0.330	0.426	0.370	0.328
$\dot{m}_A$	kg/s	28.066	33.834	27.317	28.336	39.149
$\dot{m}_B$	kg/s	22.667	22.687	13.795	15.228	33.579

Figure 6.29 presents the matching of HCC and CCC of the optimized two-stage ORC operating with fluid R-236fa.The length of the CCC gives the total heat flow rate that is transferred. The shape of the curve allows to identify the region where the feeding water flow of the FWG is heated (as indicated with an arrow in the figure).

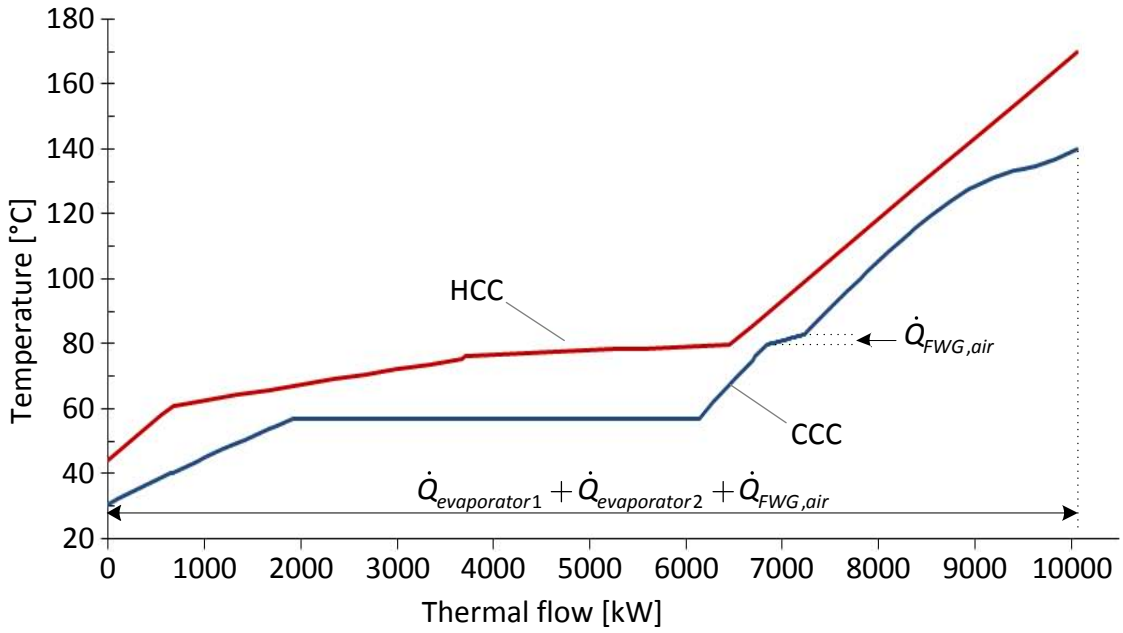

Figure 6.29 HCC and CCC of the optimized two-stage ORC operating with R-236fa; third engines cooling systems configuration.

Figure 6.30 shows the net power generated by the two-stage cycle as a function of the evaporation pressure of the fluid R-236fa in the two stages. The vertices of the grid are the sub-optimal solutions obtained by fixing the evaporation pressures instead of treating them as decision variables so that the optimization problem is solved considering only three decision variables instead of five.

Note that the dependence on the evaporation pressure of the lower stage is stronger than that of the upper stage. Considering for example a constant value for the evaporation pressure in lower stage equal to 7 bar, the decrease of 10 bar of the evaporation pressure of the upper stage from the optimal operating pressure (37.66 bar), leads to a slight decrease in the net power output . In particular, the reduction is about 4%.

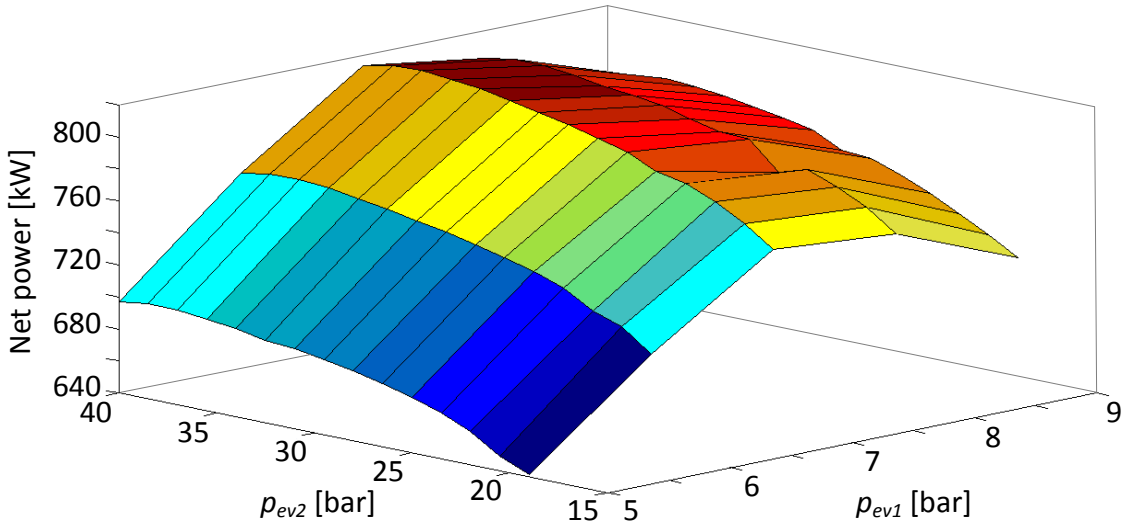

Figure 6.30 Net power output of the two-stage ORC as a function of the evaporation pressure of the fluid in the two stages; fluid R-236fa.

6.7 Design of the Heat Exchanger Network

The Heatsep method has allowed the synthesis/design optimization problem of the ORC system coupled with the main engines of the vessel to be separated into two sub-problems. The optimum thermal interactions within the black-box have been determined in the previous sub-sections for the various ORC cycle concepts that have been considered. The heat cascade is defined by these thermal interactions and is represented through the composite curves. The heat exchanger network (HEN) inside the black-box, which allows the optimum thermal interactions to be realized is here designed. It is considered that heat can be transferred only from higher temperature levels towards lower temperature levels. The use of external hot utilities is not required if the HEN is designed with respect to the "maximum energy recovery" (MER) criteria which leads to avoid heat transfer through the thermal pinch points.

The heat exchanger network has been designed for the simple ORC cycle applied to first and second cooling systems configurations and for the two-stage ORC coupled with the third configuration. With respect to these first two cases, the design of the HEN is easy because of the shape of the HCC and the presence of an unique cold stream that has to be heated. In particular, hot streams can be clearly distinguished on the HCC and there is no overlap between the two temperature levels (or three in case of second cooling systems configuration) as already shown in Figure 6.6 and Figure 6.8. The cold stream is represented by the ORC working fluid that has to be heated from pump outlet to expander inlet. R-245ca and R-227ea have been found to be the best choices for simple cycle coupled with the first two cooling systems configurations, respectively. Related HENs are here designed by considering the optimized operating characteristics presented

in Sub-section 6.6.1. Figure 6.31 shows the arrangement of simple ORC cycle coupled with the first cooling systems configuration. The HEN that realize the coupling is composed with two heat exchangers that are called *H1* and *H2* in the figure. The working fluid first collects the heat provided by the cooling flows belonging to the LT circuits (*H2*) and then absorbs heat from the HT circuits cooling flows (*H1*). Table 6.18 shows the thermal flow rates absorbed at the respective heat exchangers. Heat available from this cooling systems configuration has been presented in Sub-section 6.5.1 whereas the total heat required by the ORC cycle has been reported in Table 6.10. Note that the working fluid absorbs all the available heat provided by the HT cooling flows whereas the LT cooling flows are exploited partly. Note also that the modifications required to allow the ORC to be coupled with the cooling systems have to be realized without compromising the operation of the actual cooling systems. In particular, *H1* and *H2* have to be added in

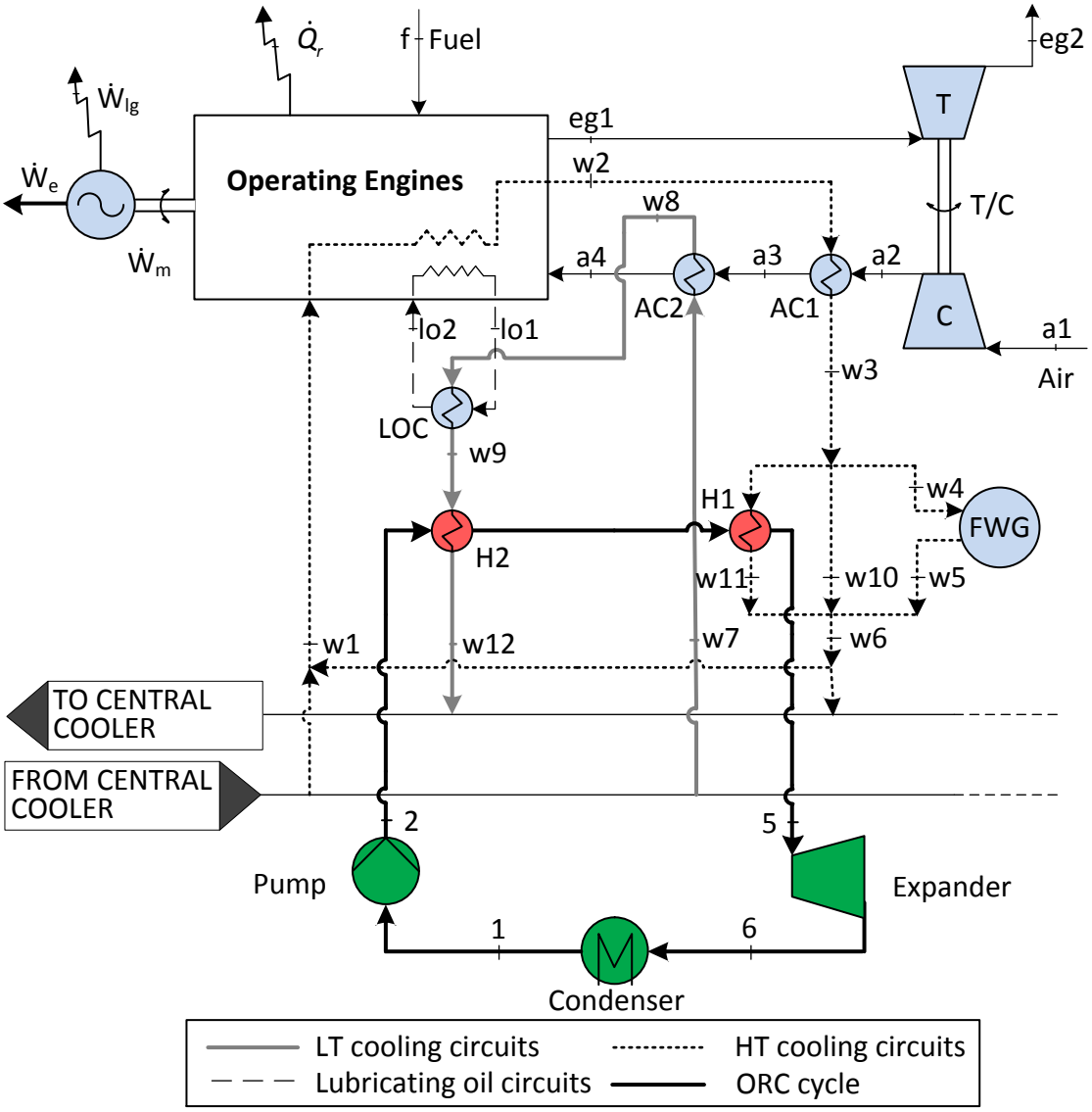

Figure 6.31 Arrangement of the simple ORC coupled with the first cooling systems configuration.

parallel to the existing coolers so that the engines can operate even when the ORC is not working.

Table 6.18 Thermal flow rates absorbed at the heat exchangers that compose the HEN.

Heat exchanger	Unit	Value
H1	kW	5367
H2	kW	406

As regards the simple cycle coupled with the second cooling systems configuration and considering R-227ea as working fluid, Figure 6.32 shows the arrangement of the HEN. It is reminded in this case LT circuits are modified so that heat can be transferred directly

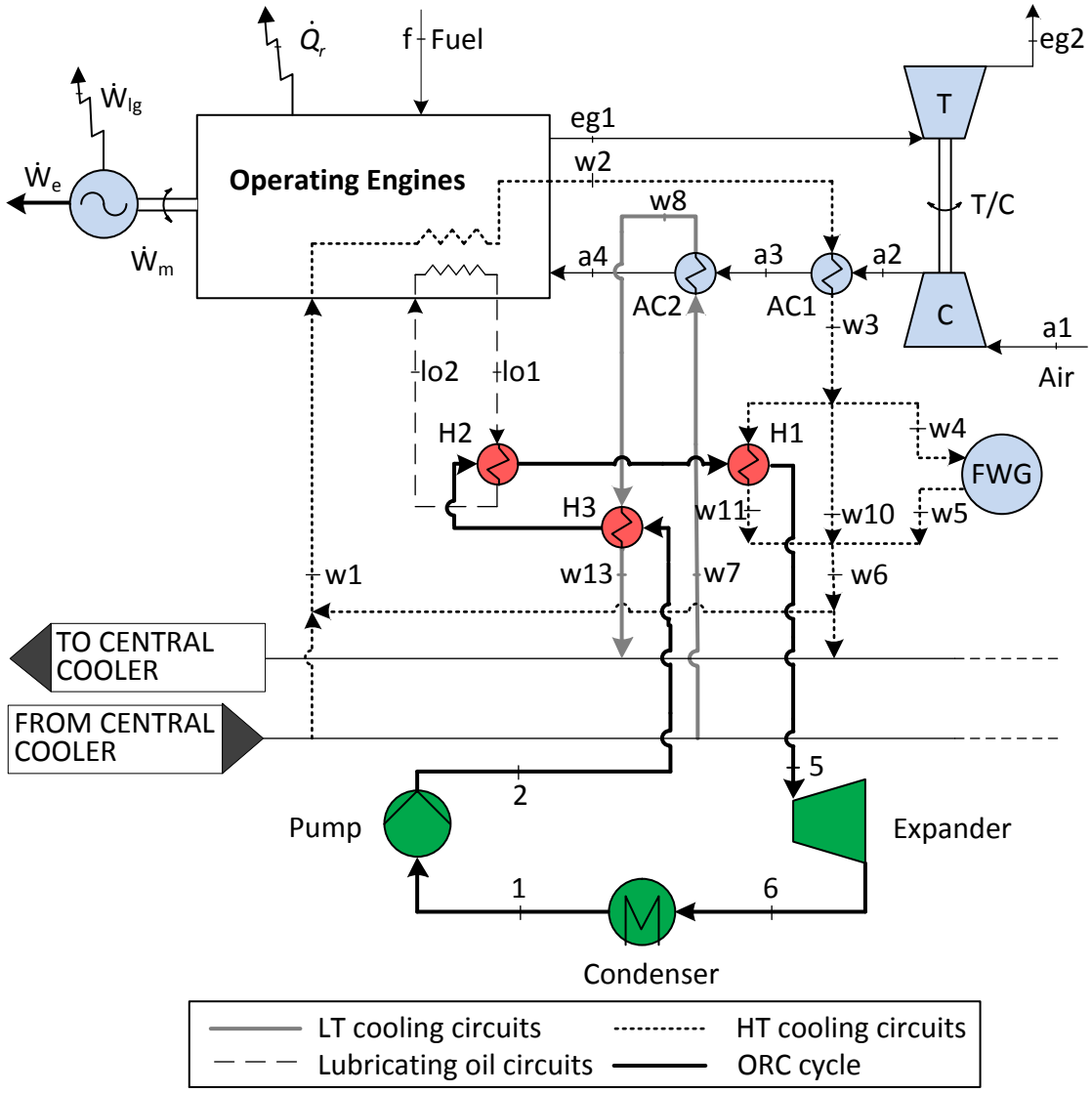

Figure 6.32 Simple cycle coupled with the second cooling systems configuration.

between lubricating oil and ORC working fluid. The HEN is composed with three heat exchangers which are *H1*, *H2* and *H3*. Table 6.19 shows the thermal flow rates transferred at these components. Note that *H1* and *H2* transfer the maximum allowed amount of heat associated with the HT circuits cooling flows and lubricating oil, respectively, whereas heat associated with the LT circuits (deprived of heat associated with the lubricating oil) is partly exploited at *H3*. Even in this case *H1*, *H2* and *H3* have to be added in parallel to the existing cooling systems heat exchangers to make free the operation of the engine-generator sets from that of the ORC system.

Table 6.19 Thermal flow rates transferred at the heat exchangers that compose the HEN.

Heat exchanger	Unit	Value
H1	kW	5367
H2	kW	1978
H3	kW	630

As regards the two-stage ORC coupled with the third cooling systems configuration, the design of the HEN is more complex than in the previous cases. Three hot streams (i.e., charge air, jacket water and lubricating oil) are overlapped in the HCC because of the charge air which covers completely the temperature interval of the HCC. Also, three cold streams (i.e., working fluid in the two stages and the water flow feeding the FWG) are overlapped in the CCC. The two-stage cycle is here considered operating with R-236fa because of the highest net power output achieved with this medium (Sub-section 6.6.3).

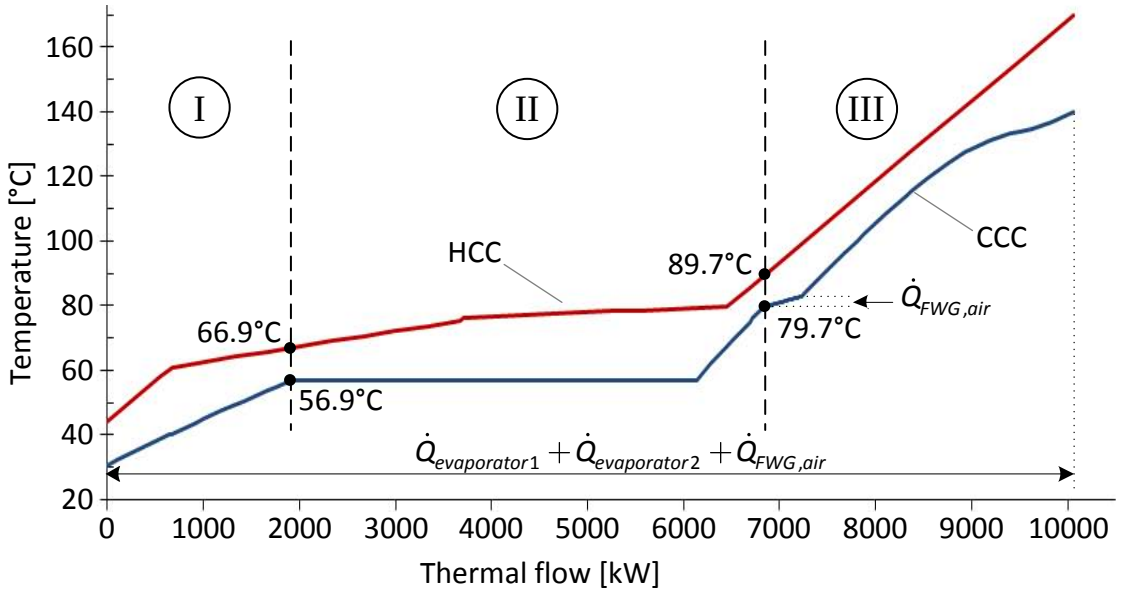

Figure 6.33 HCC and CCC of the optimized two-stage ORC operating with R-236fa and coupled with the third engines cooling systems configuration. Construction of the HEN.

Figure 6.33 reports here for convenience the matching between the HCC and CCC of the optimized cycle that has already been shown in Figure 6.29. Figure 6.33 divides the composite curves into three regions which are separated from each other by a pinch point. The HEN has to be designed to avoid heat transfer through these pinch points in accordance with MER criteria. This leads to design the HEN as three independent networks where the optimum thermal interactions occurred in each region have to be realized without interacting with the other regions. In each region the design of the HEN starts from the pinch points because of the higher occurred restrictions in the heat transfer. Figure 6.34 shows the arrangement of the designed HEN. The first three horizontal lines represent the hot streams whereas the second three are referred to the cold streams. The aforementioned three regions are presented in the figure as well as the temperatures of the hot and cold streams occurred at the pinch points. Hot and cold streams are drawn with a continuous line in the regions where they are active from the heat transfer point of view. The heat exchangers that compose practically the HEN are represented in the figure. The number reported below each heat exchanger in the cold streams area is the heat flow rate that is transferred between the joined hot-cold streams. Temperatures reported between the heat exchangers allow to follow the cooling of the heat sources. Note that in the first region (*I*), *H2'* transfers heat from the lubricating oil to the working fluid belonging to the lower stage of the ORC. The coupling between these streams continues in the second region (*II*) at the heat exchanger H2'' so

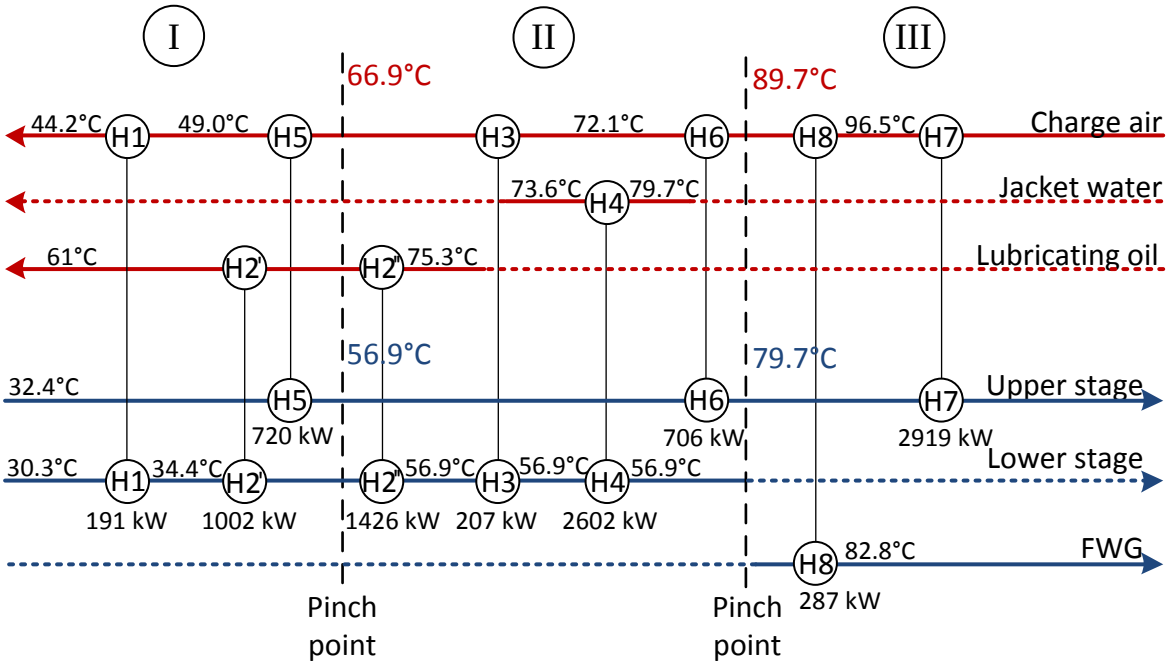

Figure 6.34 Heat exchanger network (HEN) of the two-stage ORC coupled with the third engines cooling systems configuration and operating with R-236fa.

that *H2'* and *H2''* are in fact designed as an unique heat exchanger called *H2*. Figure 6.35 shows the coupling between the two-stage ORC and third cooling systems configuration that is realized through the designed HEN.

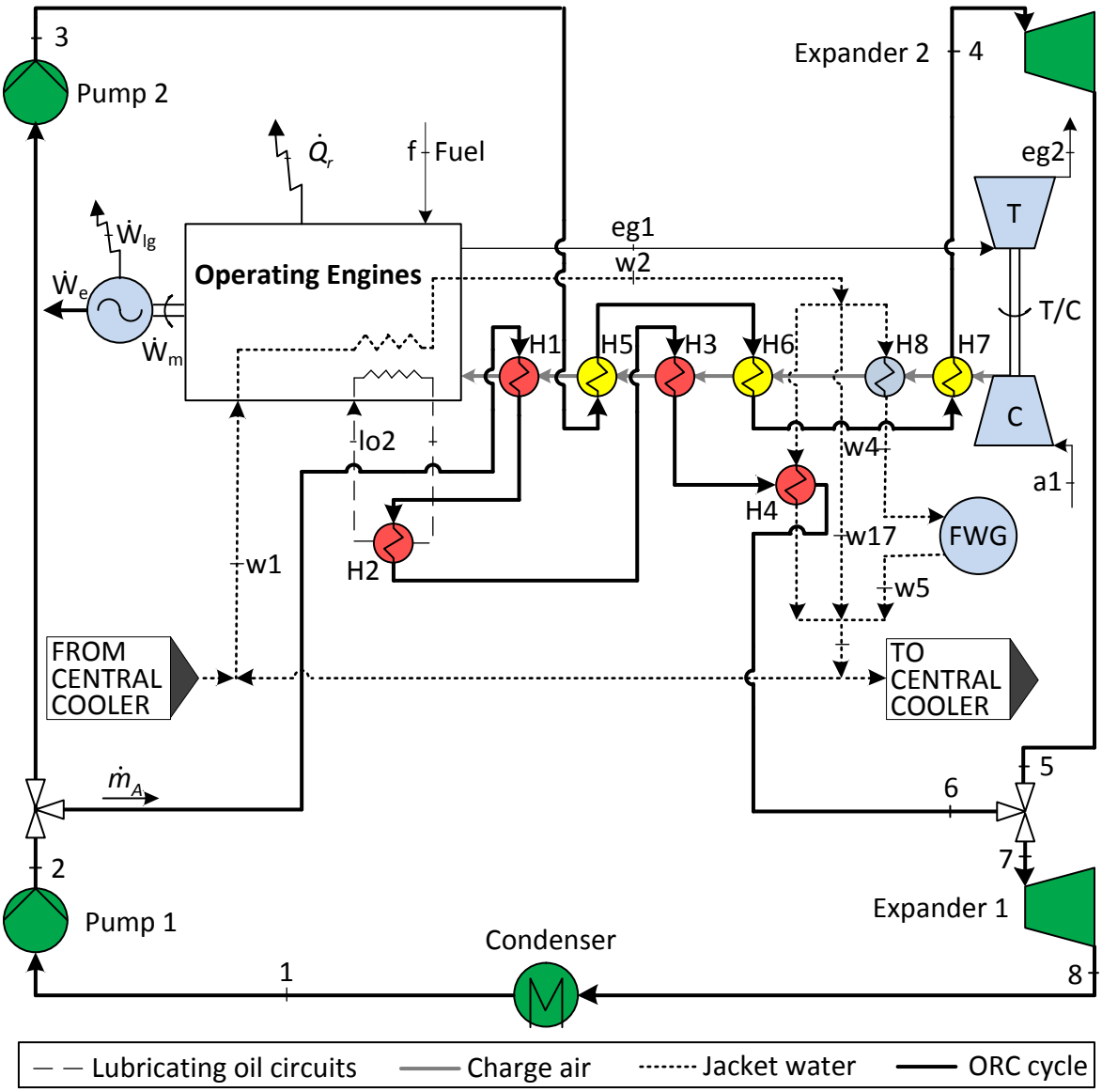

Figure 6.35 Arrangement of the two-stage ORC cycle coupled with the third cooling systems configuration.

6.8 Conclusions

Three kinds of ORCs operating with 6 different fluids each have been investigated to be coupled with the main engines of the LNG ship under study. These fluids are suitable for naval applications and have been selected among those suggested in literature for low grade heat recovery. Three cooling systems configurations of the engine-generator sets

have been taken into consideration to collect the available heat. These are the actual arrangement and other two configurations that introduce modifications aimed at a better exploitation of the available heat. An operating point for the equipment that compose the ship energy system (engine-generator sets and fresh water generators) has been selected in order to allow a comparison between different ORC-cooling systems configurations couples to be performed.

The thermal matching that maximizes the net power output of the total system including engine cooling circuits and ORC cycle is found by applying the Heatsep method, which allows the optimum heat transfer between thermal streams to be evaluated independently of the structure/number of the heat exchangers within the system. The heat transfer feasibility has been checked through Pinch Analysis rules.

The available heat provided by each cooling systems configuration has been calculated in terms of thermal flow rates and temperatures.

The thermodynamic model of each cycle has been defined as well as the simulation procedure that has allowed the results to be obtained. The calculations have been performed by using various scripts developed in MATLAB-Simulink environment.

The simple ORC has been studied coupled with all the three cooling systems configurations. The optimization problem has been solved for the maximum of net power output finding various solutions with a power level of about 430 kW, 510 kW and 580 kW, respectively for the three cooling systems configurations. These values correspond to an increase of the ship engines electric power output of about 1.83%, 2.18% and 2.48%, respectively at the operating condition selected for the comparison (i.e., electric power output of 23,375 kW). Differences from these values have been obtained considering different fluids. R-245ca and R-245fa showed best performance in case of the first cooling systems configuration whereas R-227ea and R-236fa were good choices for the second configurations. R-227ea still represented the best choice in case of third cooling systems configuration.

The regenerative ORC does not allow a higher net power output to be generated than the simple cycle because of the relevant quantity of heat that is available at low temperatures. This excess is particularly clear in case of third cooling systems configuration.

The two-stage ORC has been studied applied to the third configuration of the engine-generator sets cooling systems. The maximum net power output that is possible to achieve is around 820 kW occurred using R-236fa as working fluid. However, R-245fa has shown a good performance (790 kW) with the advantage of requiring a significantly lower evaporation pressure in the higher stage than that of the R-236fa.

The heat exchanger network (HEN) that provide the heat to the ORC has been designed for the simple cycle coupled with the first and second cooling systems

configurations and for the two-stage ORC coupled with the third cooling systems configuration. The results show that the design of these simple cycle solutions is more simple than that of the two-stage ORC. In particular, the high design and operational complexity of the two-stage ORC might reduce the advantage represented by the higher net power output. The use of the second cooling systems configuration is an interesting design solution because of the significant improvement in net power output that can be achieved with only minor changes to the existing layout.

7 ESTIMATION OF THE SAVINGS

7.1 Introduction

The previous chapter has considered some operating condition of the energy systems in the LNG ship to evaluate the net power that is possible to generate by various ORCs. No information has been provided regarding the energy that is possible to save annually if these systems are installed on board. The aim of the current chapter is to provide an approximate estimation of these savings. Moreover, an economic analysis is performed taking into consideration the capital cost of the ORC system, the annual expenses for maintenance and operation and the energy savings in terms of money.

7.2 Method of the Calculations

The operating profile of the engines has been defined in Section 5.3 considering the needs of the vessel in the laden and ballast voyage. The related information is collected in Table 5.4 and Table 5.5. Each row corresponds to an operating condition of the generation plant that is characterized by the power that has to be generated, the engine-generator sets that are working and the number of hours in the year in which the plant is operated in those conditions.

The available heat from the engines should be defined for each operating condition taking into consideration the differences in quantity (in terms of kW) and quality (in terms of temperature) of the heat rejected by the two models of engines (as made in the previous chapter). However, comparing the information of Table 4.2 related to the two models it is noted that they present the same behaviour: thermal flows available from the *Wärtsilä 12V50DF* model are approximately twice as those available from the *Wärtsilä 6L50DF* and their level of temperature is approximately the same as shown in Table 4.4. This fact allows for the following simplification in calculations: for each operating condition of the generation plant, the actual type of engines that work is neglected and the available heat is calculated by considering an equivalent number of engines *Wärtsilä 12V50DF* that allows the requested power to be generated. The choice to refer the calculations to the this type of engine is due to the fact that most of the electricity is generated by this type of engine.

Table 7.1 shows the operating conditions that are considered in the study. For each of them, the equivalent number of engines *Wärtsilä 12V50DF* is reported. Sources of the data are the aforementioned tables related to the laden and ballast voyage. The table

shows that the electric power to be generated for the conditions *1* and *2* is higher than the value selected for the investigations of Chapter 6. This means that the thermal flow rates that are made available are higher than those considered for the calculation of the design point of the ORC system. The higher load at which the engines are operated increases the temperature of the thermal flows.

The values of the parameters that define the design point of the Rankine systems considered here are assumed to be equal to those calculated in Chapter 6 as solutions of the optimization problem (maximum of the net power). The higher heat availability of the operating conditions *1* and *2* leads to assume that the net power output of the ORC in these two conditions is equal to the design value which cannot be exceeded.

The operating conditions *20*, *21* and *22* are not considered for the calculations of the energy savings, because the low quantity of heat that is available seems to be not sufficient to operate the ORC.

Table 7.1 Operating conditions of the engines and equivalent number of 12V50DF engines.

Cond.	t	$\dot{W}e$	Load	12V50DF Eq.	Cond.	t	$\dot{W}e$	Load	12V50DF Eq.
-	h	kW	%	-	-	h	kW	%	-
1	248.1	28301.5	85.8	3.0	12	386.6	10180.5	92.5	1.0
2	146.6	24315.1	88.4	2.5	13	444.1	9606.6	87.3	1.0
3	94.0	23026.7	83.7	2.5	14	180.6	8349.6	75.9	1.0
4	326.5	20710.5	94.1	2.0	15	232.3	7867.3	71.5	1.0
5	317.5	19607.1	89.1	2.0	16	211.8	6789.4	61.7	1.0
6	483.3	17513.9	79.6	2.0	17	192.8	6385.1	58.0	1.0
7	1079.8	16573.5	75.3	2.0	18	125.2	5478.3	99.6	0.5
8	766.4	14741.0	89.3	1.5	19	14.7	5139.5	93.4	0.5
9	561.4	13939.2	84.5	1.5	20	43.8	4394.6	79.9	0.5
10	357.7	12303.7	74.6	1.5	21	117.1	2822.7	51.3	0.5
11	175.5	11623.7	70.4	1.5	22	22.3	2111.7	38.4	0.5

For each operating condition, the simulation procedure looks for the optimum operating parameters of the ORC that maximize the net power output; the HCCs are built by using the methods described in Chapter 6. The calculations assume that the design values of the evaporation pressure of the working fluids in the cycles cannot be exceeded in off-design. This assumption represents an additional constraint in the optimization problem.

The steps of the simulation procedures are similar to those defined in Chapter 6. The concept of composite curves is used to provide the first estimation of the energy that

is possible to save thanks to the ORC system. Note that the results provide only an initial optimistic indication of the performance of the system. More accurate results can be obtained only by introducing an off-design model of the system in the simulation procedure.

7.3 Energy Savings

The calculation of the energy savings has been performed for the simple and the two-stage ORCs. The regenerative configuration has not been considered. The results are reported in the following sub-sections.

7.3.1. Simple ORC

The simple ORC was initially considered coupled with the first engines cooling systems configuration (Sub-section 6.5.1). Table 7.2 presents the net power output of the ORC in the various operating conditions. As stated before, these values have been obtained solving the optimization problem for the maximum of the net power.

Table 7.3 presents the values of various parameters calculated using the results of Table 7.2. E_{saved} is the energy generated by the ORC in the considered year. It is calculated by adding the contribution of each operating condition (19 conditions as aforementioned) that is given by the product of the net power output and the number of hours:

$$E_{saved}[\text{kWh}] = \sum_{i=1}^{N} \dot{W}_{net,i}[\text{kW}] \cdot t_i[\text{h}] \tag{7.1}$$

The quantity $\bar{\dot{W}}_{net}$ is the average net power output calculated by dividing the value of E_{saved} with the number of hours in which the ORC system it is kept in operation:

$$\bar{\dot{W}}_{net}[\text{kW}] = \frac{E_{saved}[\text{kWh}]}{\sum_{i=1}^{N} t_i[\text{h}]} \tag{7.2}$$

f_{load} is the annual loading factor and E is the percentage of the annual energy demand of the vessel (in terms of electricity) that is possible to be covered by the ORC.

Table 7.2 Design and off-design net power generation of the simple ORC coupled with the first cooling systems configuration.

Cond.	R-134a	R-125	R-236fa	R-245ca	R-245fa	R-227ea
	$\dot{W}_{net}$	$\dot{W}_{net}$	$\dot{W}_{net}$	$\dot{W}_{net}$	$\dot{W}_{net}$	$\dot{W}_{net}$
-	kW	kW	kW	kW	kW	kW
1	404.5	323.1	413.8	426.9	424.6	397.1
2	404.5	323.1	413.8	426.9	424.6	397.1
3	393.5	314.4	402.4	415.4	413.1	386.0
4	373.3	302.1	381.3	392.3	390.4	367.0
5	339.0	272.4	346.6	357.2	355.3	333.0
6	273.3	217.7	279.5	288.8	287.2	267.8
7	245.8	195.3	251.3	260.0	258.4	240.5
8	238.5	191.7	243.8	251.2	249.9	234.3
9	213.1	170.4	218.0	224.9	223.7	209.1
10	164.2	130.4	167.8	173.7	172.6	160.6
11	146.2	115.9	149.4	154.8	153.9	142.9
12	147.4	119.0	150.6	155.0	154.2	144.8
13	129.5	103.9	132.5	136.6	135.9	127.2
14	91.4	72.6	93.4	96.7	96.1	89.4
15	78.4	62.2	80.1	83.0	82.5	76.6
16	54.7	43.1	55.9	58.0	57.6	53.3
17	47.9	37.6	48.9	50.8	50.5	46.6
18	50.3	41.1	51.3	52.6	52.4	49.4
19	41.2	33.3	42.1	43.3	43.1	40.5

Table 7.3 Energy savings and various parameters for the simple ORC coupled with the first cooling systems configuration.

Par.	Unit	R-134a	R-125	R-236fa	R-245ca	R-245fa	R-227ea
E_{saved}	MWh	1387	1110	1418	1464	1456	1361
$\bar{\dot{W}}_{net}$	kW	219	175	224	231	229	214
f_{load}	%	54	54	54	54	54	54
E	%	1.49	1.19	1.52	1.57	1.56	1.46

The energy that is possible to save annually by installing a simple ORC depends on the substance used as working fluid. Best performance has been found with R-245ca (1464 MWh) whereas R-125 represents the worst case (1110 MWh). Note that the performance of R-245fa is close to that of R-245ca. The simple ORC allows to cover 1.57% and 1.19% of the annual energy needs of the vessel if operated with R-245ca and R-125, respectively. The loading factor of the ORC is low for all the fluids and equal to 54%.

The simple ORC has also been considered coupled with the second engines cooling systems configuration (Sub-section 6.5.2). Table 7.4 and Table 7.5 report the results of the calculations as made for the previous configuration.

Table 7.4 Design and off-design net power generation of the simple ORC coupled with the second cooling systems configuration.

Cond.	R-134a	R-125	R-236fa	R-245ca	R-245fa	R-227ea
	$\dot{W}_{net}$	$\dot{W}_{net}$	$\dot{W}_{net}$	$\dot{W}_{net}$	$\dot{W}_{net}$	$\dot{W}_{net}$
-	kW	kW	kW	kW	kW	kW
1	501.4	418.2	509.4	484.5	497.2	512.4
2	501.4	418.2	509.4	484.5	497.2	512.4
3	510.2	410.4	515.8	472.2	511.2	502.2
4	457.5	377.5	464.7	442.3	453.2	456.8
5	418.3	348.6	425.0	404.1	414.7	424.7
6	340.4	296.8	345.9	332.7	337.7	370.6
7	304.9	278.4	312.1	304.1	304.7	321.8
8	294.2	250.1	298.9	285.0	291.6	304.9
9	264.2	229.9	268.5	257.7	262.1	277.1
10	207.6	194.0	225.3	207.9	208.6	215.1
11	188.5	178.2	203.3	190.5	191.0	205.6
12	181.1	159.8	184.0	176.9	179.5	186.7
13	159.0	145.2	162.7	158.3	158.8	168.0
14	119.7	104.9	123.7	121.6	121.9	124.5
15	105.8	91.7	111.2	109.9	110.1	111.4
16	79.0	84.3	88.5	88.5	88.5	87.7
17	70.6	76.5	81.8	82.0	80.6	80.6
18	65.1	64.9	66.8	65.5	65.7	67.8
19	55.3	56.7	57.8	56.9	57.0	58.2

Table 7.5 Energy savings and various parameters for the simple ORC coupled with the second cooling systems configuration.

Par.	Unit	R-134a	R-125	R-236fa	R-245ca	R-245fa	R-227ea
E_{saved}	MWh	1729	1511	1772	1698	1726	1801
$\bar{\dot{W}}_{net}$	kW	272.5	238.2	279.2	267.7	272.0	283.8
f_{load}	%	54.4	57.0	54.8	55.2	54.7	55.4
E	%	1.86	1.62	1.90	1.82	1.85	1.93

The second cooling systems configuration allows the energy saved annually to be increased than the first configuration. Best fluid is R-227 whereas even in this case R-125

show worse performance. These fluids allow the annual energy needs to be covered in the measure of 1.93% and 1.62%, respectively. Note that R-236fa shows good performance that is close to that of R-227ea. The loading factors increase slightly from those found for the ORC system coupled with the first cooling systems configuration.

7.3.2. Two-stage ORC

The two-stage organic Rankine cycle has been considered to be coupled with the third cooling systems configuration as made in Chapter 6. The results of the calculations are reported in Table 7.6 and Table 7.7 as made for the previous cycles. This cycle allows the higher energy savings to be obtained. Best performance is shown by R-236fa which allows to save 2911 MWh annually. Thus, the ORC system can cover 3.12% of the vessel energy needs.

The loading factor increases for all the fluids than the values found for the simple ORC coupled with the first and second cooling systems configurations but still remains below 57%.

Table 7.6 Design and off-design net power generation of the two-stage ORC coupled with the third cooling systems configuration.

Cond.	R-134a	R-236fa	R-245ca	R-245fa	R-227ea
	$\dot{W}_{net}$	$\dot{W}_{net}$	$\dot{W}_{net}$	$\dot{W}_{net}$	$\dot{W}_{net}$
-	kW	kW	kW	kW	kW
1	753.1	820.3	778.1	789.0	749.3
2	753.1	820.3	778.1	789.0	749.3
3	730.0	797.6	756.6	767.9	730.2
4	704.6	759.9	749.9	769.4	692.7
5	641.1	700.6	679.1	689.6	635.4
6	518.5	556.7	533.0	532.7	518.5
7	466.9	498.1	462.2	474.8	468.5
8	464.0	507.4	494.9	502.7	459.5
9	416.3	453.0	439.4	441.1	414.2
10	325.3	347.7	326.2	331.8	326.1
11	292.3	299.0	286.9	284.3	293.1
12	304.2	333.3	329.4	332.8	300.4
13	270.6	295.6	291.5	295.3	266.1
14	200.9	216.3	207.2	208.5	200.7
15	176.7	187.6	178.6	182.4	175.7
16	127.4	133.1	130.1	128.2	133.1
17	118.2	120.7	114.4	118.7	117.1
18	134.9	151.3	149.8	149.9	130.5
19	117.8	129.2	126.8	128.3	116.2

Table 7.7 Energy savings and various parameters for the two-stage ORC coupled with the third cooling systems configuration.

Par.	Unit	R-134a	R-236fa	R-245ca	R-245fa	R-227ea
E_{saved}	MWh	2695	2911	2794	2836	2682
$\dot{W}_{net}$	kW	424.7	458.8	440.4	447.0	422.7
f_{load}	%	56.4	55.9	56.6	56.6	56.4
E	%	2.89	3.12	3.00	3.04	2.88

7.4 Economic Feasibility

The feasibility of the ORC has to be studied from the economic point of view. A simple analysis is presented here considering one of the studied cycles.

The evaluation of the investment is made by the discounted cash flow analysis and in particular by the parameter “net present value” NPV. It is defined as the sum of discounted cash inflows and outflows in order to compare the present value of an investment to the value of savings that will be obtained in the future:

$$NPV = \sum_{t=0}^{N_e} \frac{F_t}{1+d_t}^{t} \tag{7.3}$$

where

F_t net annual cash flow for the year t,

d_t market discount rate,

N_e period of the economic analysis.

The net annual cash flow for the year F_t is given by Eq. (7.4):

$$F_t = \begin{cases} -C, & t=0 \\ C_{fs,t} - C_{om,ORC,t} + C_{om,EG,t} & t=1,2,...,N_e \end{cases} \tag{7.4}$$

where

C initial investment,

$C_{fs,t}$ cost of the fuel saved,

$C_{om,ORC,t}$ cost of operation and maintenance of the ORC,

$C_{om,EG,t}$ savings of operation and maintenance of the diesel-generator sets.

The initial investment for the ORC can be considered proportional to the maximum net power of the system. The sum of the two terms of Eq. (7.4) related to the operation and maintenance cost of ORC and diesel-generator sets is given by Eq. (7.5). This value has to be subtracted from the cost of the fuel saved of Eq. (7.4). The cost of the fuel saved is given by Eq. (7.6).

$$C_{om} = C_{om,ORC,t} - C_{om,EG,t} \tag{7.5}$$

$$C_{fs,t} = E_{saved,t} \cdot \frac{b_f}{\eta_e} \cdot \bar{c}_f \cdot (1+f_t)^{t-1} \tag{7.6}$$

where

$E_{saved,t}$ energy saved in the year t,
$\bar{c}_f$ mean unit cost of the fuels,
b_f specific fuel energy consumption of the engine-generator sets,
η_e electrical efficiency of the engine-generator set,
f_t inflation rate.

The specific cost of the fuel is considered constant: the study is conducted with constant dollars and the inflation rate is not taken into account. Based on this, Eq. (7.3) can be reedited in the form:

$$NPV = F_0 + F_1 \cdot \sum_{t=1}^{N_e} \frac{1}{1+d_t}^{t} \tag{7.7}$$

The summation of Eq. (7.7) is a function of the period of the economic analysis N_y and the market discount rate i_t. It is called “present worth factor” (PWF) and for the specific case is given by Eq. (7.8):

$$PWF(N_e,d) = \frac{1}{CRF(N_e,d)} \tag{7.8}$$

$$CRF(N_e,d) = \frac{d \cdot (1+d)^{N_e}}{(1+d)^{N_e} - 1} = \frac{d}{1 - (1+d)^{-N_d}} \tag{7.9}$$

The NPV expressed by Eq. (7.7) can be defined as a function of the parameter PWF:

$$NPV = F_0 + F_1 \cdot PWF(N_e, d) \tag{7.10}$$

In addition to the NPV, other two parameters are calculated in order to complete the economic analysis. They are the “payback period” (PP) and the “internal rate of return” (IRR).

7.4.1. Two-stage ORC

The economic feasibility of the two-stage ORC is investigated here because it allows the higher net power to be generated if compared with the other cycles. It is applied to the third cooling systems configuration of the engine-generator sets. Considered working fluid is R-245ca: the low evaporation pressure in the upper stage of the optimized two-stage ORC operating with this fluid (Paragraph 6.6.3.3) makes it suitable for marine applications.

The values of the parameters that are assumed for the calculations are reported in Table 7.8. The reported value for the specific fuel energy consumption of the engine-generator sets is referred to the load 85% (Sub-section 4.2.1).

Table 7.8 Values of the constant parameters considered for the economic analysis of the two-stage ORC.

Parameter	Unit	Value
N_e	year	20
d_t	%	8
b_f	MWh/MWh	2.193
η_e	%	96.49
$\dot{W}_{net}$	kW	778.1
E_{saved}	kWh	2794
C_{om}	\$/MWh	3

Under these hypothesis, Table 7.9 presents the net present value (NPV) of the investment as a function of the specific cost of the initial investment and the fuel cost. The light-shaded cells are those that present a negative value for the NPV. Figure 7.1 presents the results in graphical form: if a value is selected for the mean unit cost of the fuel and for the specific cost of the investment, the value of the NPV is given. The investment is considered economically attractive if this value is positive. Figure 7.2 and Figure 7.3 show the payback period and the internal rate of return, respectively.

Table 7.9 NPV as a function of the specific cost of the initial investment and the mean unit cost of the fuel. Two-stage ORC coupled with the third cooling systems configuration and operating with R-245ca.

		Initial investment [$/kW]						
		1000	1500	2000	2500	3000	3500	4000
		Initial investment [k$]						
		778	1167	1556	1945	2334	2723	3112
		NPV [k$]						
Mean unit cost of the fuel [$/MMBtu]	9.0	1054	665	276	-113	-502	-891	-1280
	9.5	1161	772	382	-7	-396	-785	-1174
	10.0	1267	878	489	100	-289	-678	-1067
	10.5	1373	984	595	206	-183	-572	-961
	11.0	1480	1091	702	313	-77	-466	-855
	11.5	1586	1197	808	419	30	-359	-748
	12.0	1692	1303	914	525	136	-253	-642
	12.5	1799	1410	1021	632	243	-146	-536
	13.0	1905	1516	1127	738	349	-40	-429
	13.5	2012	1622	1233	844	455	66	-323
	14.0	2118	1729	1340	951	562	173	-216
	14.5	2224	1835	1446	1057	668	279	-110
	15.0	2331	1942	1553	1163	774	385	-4
	15.5	2437	2048	1659	1270	881	492	103
	16.0	2543	2154	1765	1376	987	598	209

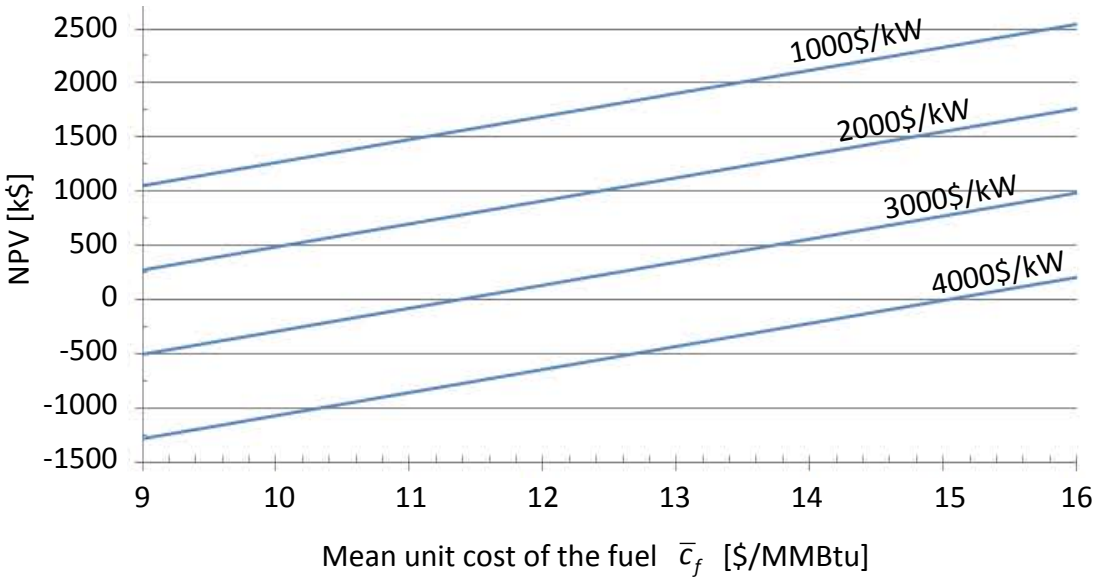

Figure 7.1 NPV as a function of the mean unit cost of the fuel with the specific cost of the initial investment as parameter. Two-stage ORC coupled with the third cooling systems configuration and operating with R-245ca.

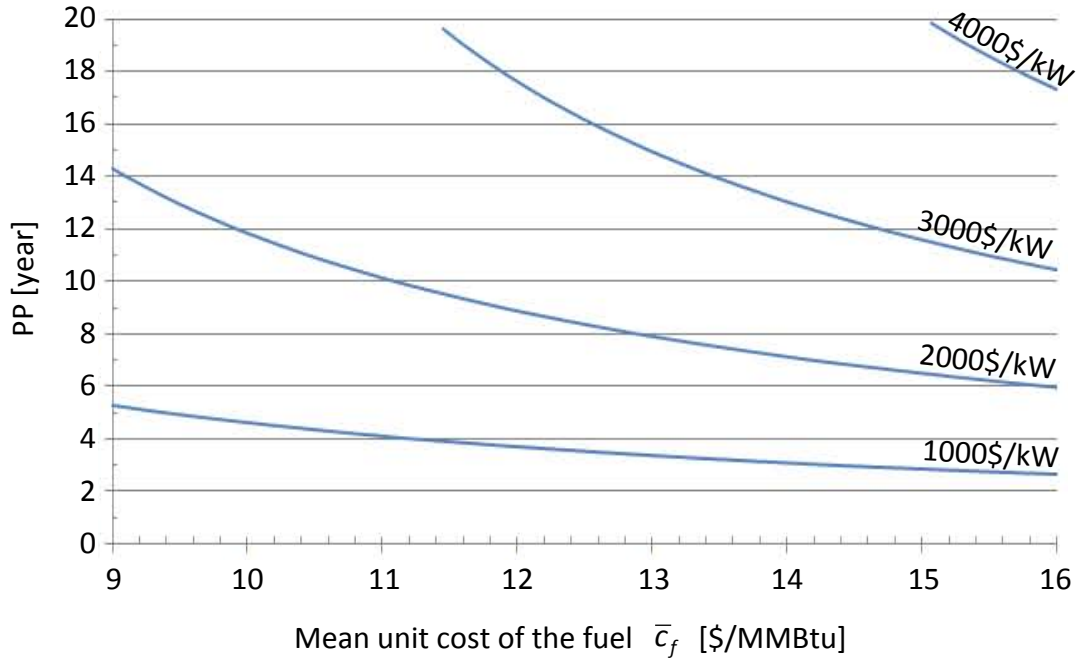

Figure 7.2 Payback period as a function of the mean unit cost of the fuel with the specific cost of the initial investment as parameter. Two-stage ORC coupled with the third cooling systems configuration and operating with R-245ca.

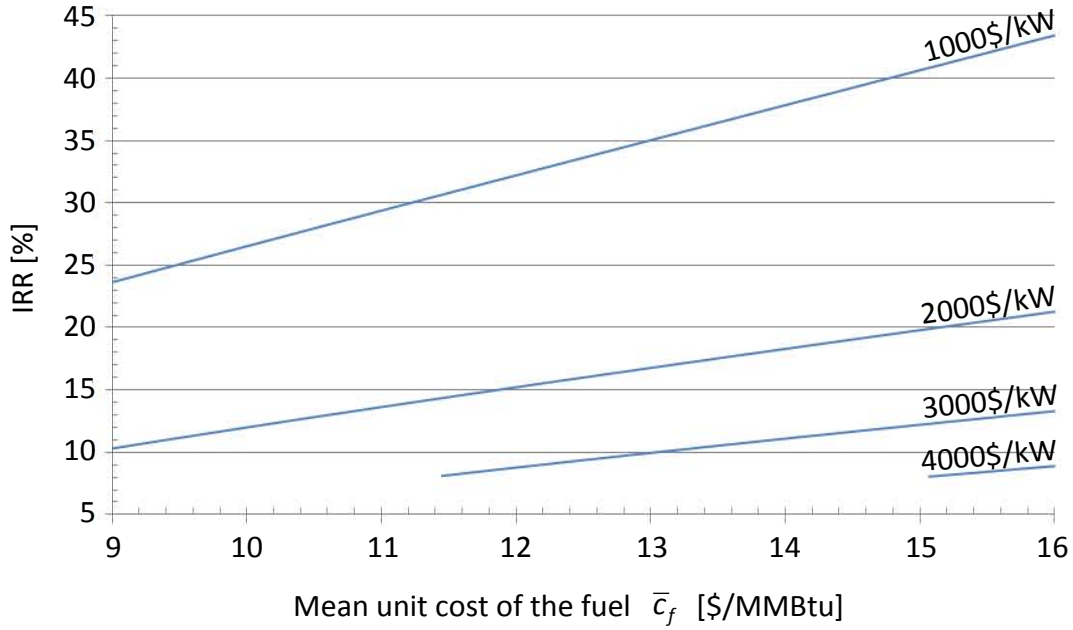

Figure 7.3 Internal rate of return as a function of the mean unit cost of the fuel with the specific cost of the initial investment as parameter. Two-stage ORC coupled with the third cooling systems configuration and operating with R-245ca.

Sub-section 7.3.2 has shown that the annual loading factor of the two-stage ORC operating with R-245ca is 56.6%. This low value is due to the fact that the design point of the ORC has been selected in order to maximize the net power output at a certain

operating condition for the energy systems of the vessel (engine-generator sets and FWG). However, most of the time the available heat is significantly lower than that in design conditions and the ORC operates in off-design. From the economic point of view, this choice is appropriate in case of low specific cost of the investment and high mean unit cost of the fuel. In the other cases a smaller ORC system might be more competitive.

In the following, a different design point is considered for the two-stage ORC operating with the same fluid and coupled with the same cooling systems configuration of the previous case. In particular, the design net power output of the ORC is considered to be equal to 439.4 kW which is the output of the optimized two-stage ORC operating at the condition "*9*" of Table 7.1. It is assumed that the net power output of the ORC is equal to design value if the heat to be exploited is higher than that available at the operating condition *"9".*

Table 7.10 shows the NPV of the two-stage ORC so designed. Table 7.11 shows the values of various constant parameters considered for the economic analysis.

Table 7.10 NPV as a function of the specific cost of the initial investment and the mean unit cost of the fuel. Two-stage ORC coupled with the third cooling systems configuration and operating with R-245ca. Optimized cycle to exploit the heat at the operating condition "*9*" of Table 7.1.

		Initial investment [k/kW]						
		1000	1500	2000	2500	3000	3500	4000
		Initial investment [k$]						
		439	659	879	1099	1318	1538	1758
		NPV [k$]						
Mean unit cost of the fuel [$/MMBtu]	9.0	1096	876	656	437	217	-3	-222
	9.5	1185	965	746	526	306	86	-133
	10.0	1274	1054	835	615	395	176	-44
	10.5	1363	1144	924	704	484	265	45
	11.0	1452	1233	1013	793	574	354	134
	11.5	1541	1322	1102	882	663	443	223
	12.0	1631	1411	1191	971	752	532	312
	12.5	1720	1500	1280	1061	841	621	401
	13.0	1809	1589	1369	1150	930	710	491
	13.5	1898	1678	1459	1239	1019	799	580
	14.0	1987	1767	1548	1328	1108	889	669
	14.5	2076	1856	1637	1417	1197	978	758
	15.0	2165	1946	1726	1506	1287	1067	847
	15.5	2254	2035	1815	1595	1376	1156	936
	16.0	2344	2124	1904	1684	1465	1245	1025

Table 7.11 Values of some parameters considered for the economic analysis of the two-stage ORC designed to exploit the heat available at the operating condition "9" of Table 7.1.

Parameter	Unit	Value
$\dot{W}_{net}$	kW	439.4
E_{saved}	kWh	2341
f_{load}	%	84.0

This two-stage ORC is compared with the ORC analysed at the beginning of the paragraph. As shown in Table 7.11, the annual loading factor (84%) is higher than that of the previous cycle (56.6%). Even if the maximum net power output of the system is significantly lower (≈-44%), the energy generated annually does not show a corresponding decrease (≈-16%). The lower cost of the investment affects differently the NPV, depending on the mean unit cost of the fuel that is considered.

Figure 7.4 presents in graphical form the results reported in Table 7.10. Figure 7.5 and Figure 7.6 give the payback period and the internal rate of return, respectively, as a function of the mean unit cost of the fuel with the specific cost of the investment as parameter.

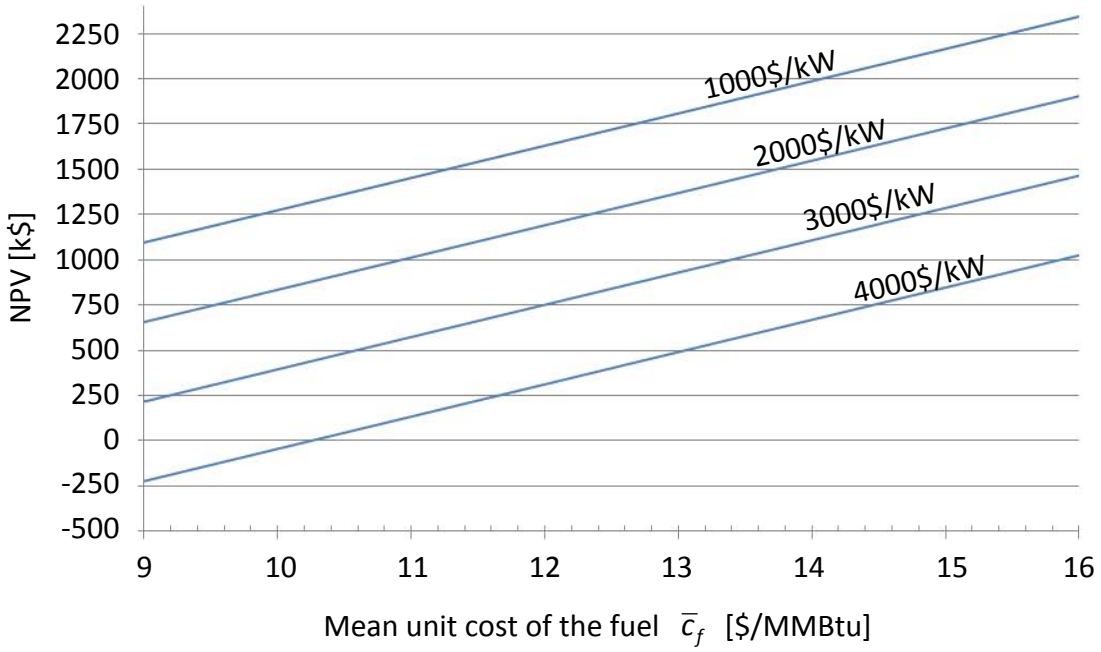

Figure 7.4 NPV as a function of the mean unit cost of the fuel with the specific cost of the initial investment as parameter. Two-stage ORC coupled with the third cooling systems configuration and operating with R-245ca. Optimized cycle to exploit the heat provided by the operating condition "*9*" of Table 7.1.

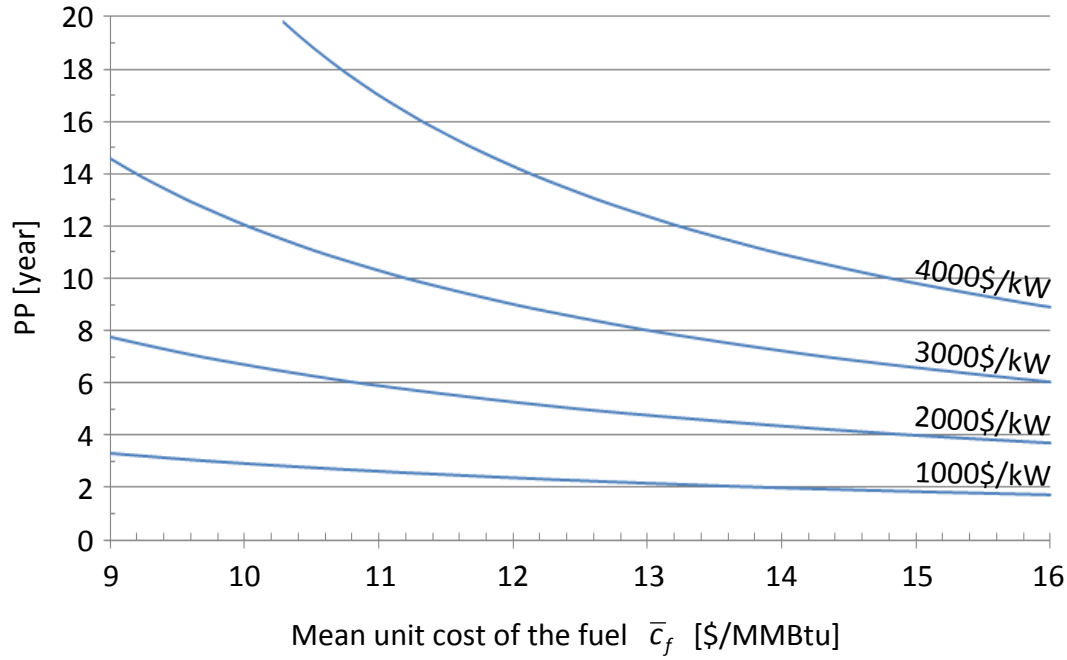

Figure 7.5 Payback period as a function of the mean unit cost of the fuel with the specific cost of the initial investment as parameter. Two-stage ORC coupled with the third cooling systems configuration and operating with R-245ca. Optimized cycle to exploit the heat provided by the operating condition "*9*" of Table 7.1.

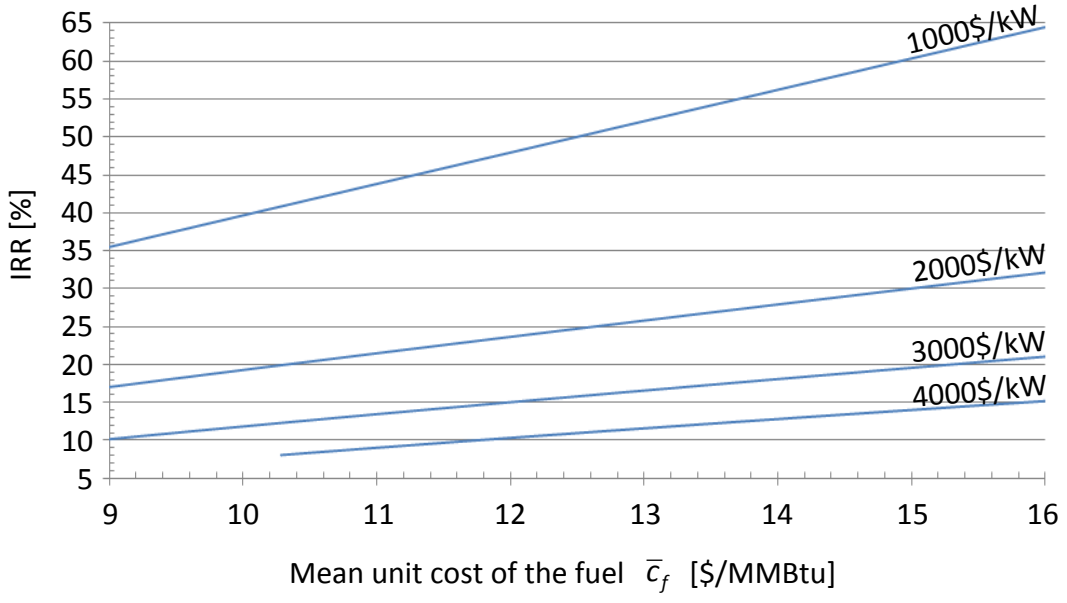

Figure 7.6 Internal rate of return as a function of the mean unit cost of the fuel with the specific cost of the initial investment as parameter. Two-stage ORC coupled with the third cooling systems configuration and operating with R-245ca. Optimized cycle to exploit the heat provided by the operating condition "*9*" of Table 7.1.

7.5 Conclusions

The evaluation of the annual energy savings (MWh) have been performed for the simple ORC applied to the first and second engine cooling systems configurations and for the two-stage ORC applied to the third configuration. The results have been obtained by using a simplified method that has allowed the calculation of the net power output of the ORCs in off-design conditions to be done. The operating conditions defined by the annual operating profile of the engines (Section 5.3) and the operation of the FWG have been taken into consideration to defined the available heat to be exploited by the ORCs.

The annual loading factor, the average net power output and the percentage of the annual energy demand of the vessel (in terms of electricity) that is covered by the ORCs have been calculated in addition to the energy savings.

The results show that the simple ORC system coupled with the first and second engines cooling systems configurations allows the 1.6% and 1.9% of the annual electrical needs of the vessel to be covered. Annual electricity savings of the two-stage ORC are about 3.1%. Best fluids have been found to be R-245ca, R-227ea, R-236fa for these three cases, respectively.

All the cycles have shown low values for the annual loading factor of the system. This result depends on the design of the ORCs that has been performed with respect to the maximization of the net power output when the available heat is that related to the vessel operating condition selected in Section 6.4. However, most of the time the ORC is operated in part load because the available heat is lower than maximum exploitable. Thus, the annual loading factor of the ORCs is about 54÷57% for all the considered cases.

The economic feasibility of the two stage ORC coupled with the third cooling systems configuration and operating with R-245ca has been investigated by the discounted cash flow analysis: the “net present value” of the investment has been calculated with respect to different values of specific cost of the ORC system (k$/kW) and mean unit cost of the fuel ([$/MMBtu). The choice of the working fluid has been based on the low evaporation pressure reached by R-245ca in the upper stage of the optimized two-stage cycle which is a critical issue for marine installations.

The analysis has been performed with respect to two sizes for the ORC system: the cycle designed for the maximization of the net power output at the aforementioned vessel operating condition selected in Section 6.4 has been considered as well as a smaller cycle which shows a lower maximum power output but higher annual loading factor. The results show that the ORC system is economically attractive in wide ranges of specific cost of the initial investment and mean unit cost of the fuel. The width of these ranges increased with the annual loading factor.

8 CONCLUSIONS

8.1 Results of the work

A waste heat recovery system based on the ORC technology has been investigated to be installed aboard a real LNG carrier. First of all, a literary review of the fluids used in ORCs has been conducted with particular reference to low temperature heat recovery applications. Properties of the fluids which affect the performance of the cycle and lead to environmental and safety issues have been presented in order to allow the selection of the appropriate mediums to be investigated in the present work. Various ORC cycles have been found in literature: heat recovery from different sources results in different best solutions for the ORC arrangement and the operating parameters so that the design process requires to consider various alternatives simultaneously.

The detailed analysis of the overall ship energy system has allowed the waste heat to be characterized both in quantity (i.e., heat flow rate of the hot streams) and quality (i.e., temperature levels of the hot streams) taking into account the operation of the engine-generator sets, fresh water generators and exhaust gas boilers. The waste heat associated with the exhaust gas of the engine-generator sets is already used for low pressure steam production. The heat associated with the jacket water, lubricating oil and charge air cooling is partly used for desalinated-water generation whereas the remaining is available for the ORC system. Three layouts for the engine-generator sets cooling systems collecting the available heat have been compared. They are the actual arrangement and two other arrangements, which enable higher temperature heat extraction by allowing the direct heat transfer from hot streams to ORC. In particular, direct heat transfer is applied to the lubricating oil only in the second cooling systems configuration whereas it is applied to all heat sources available from the engines in the third configuration.

The low temperature level and the variety of the thermal sources resulted in various design options of the heat recovery system. A systematic method (Heatsep) has therefore been applied to find all the possible thermal coupling between heat sources and ORC configurations which are optimum for the overall system. The design solutions that have been devised are very different from each other: the two-stage ORC allows the highest net power output to be achieved at the expense of high design and operational complexity; the simple ORC solution provides a lower net power output than that of the two-stage ORC but is less costly and more reliable due to the simplicity of the design. This suggests the simple ORC as the most promising solution. In particular, the simple ORC provides a net power output of 430 kW if the actual engines cooling systems arrangement

is considered whereas the power output increases to 510 kW and 580 kW if the cycle is coupled with the second and third cooling systems configurations, respectively. These values correspond to an increase of the ship engines power output (23,375 kW at the considered operating condition) of about 1.83%, 2.18% and 2.48%, respectively. Fluids R-245ca and R-245fa showed best performance in case of the first cooling systems configuration whereas R-227ea and R-236fa were good choices for the second configuration. R-227ea still represented the best choice in case of third configuration. The use of the second cooling systems layout seems to be the most promising option because of the significant improvement in net power output that can be achieved with only minor changes to the existing layout. Nonetheless the viability of this change has to be investigated in agreement with the engine manufacturer. It also appears that the further increase in net power output obtained with the third cooling system configuration it is not enough to justify the additional complexity.

The regenerative ORC does not allow a higher net power output to be generated than the simple cycle because of an excess of low grade heat made available at low temperature by the engines cooling systems which cannot be exploited by the ORC cycle.

The two-stage ORC has been studied in combination with the third engines cooling systems configuration. Using R-236fa as working fluid, the net power output of the ORC reaches 820 kW, which corresponds to a 3.5% increase in the net power produced by the ship power generating plant. This solution is interesting from the thermodynamic point of view because it properly couples the thermal sources with the heating of the working fluid in both the two pressure level circuits.

A simplified estimation of the annual energy savings has been performed for the simple cycle applied to the first and second cooling systems configurations and for the two-stage cycle applied to the third cooling systems configuration. The results showed that the ORC system allows to cover 1.6%, 1.9% and 3.1% of the annual electrical needs of vessel, respectively. The two-stage ORC has also been studied from the economic point of view. The analysis has been conducted with respect to various values of the mean unit cost of the fuel ($/MMBtu) and the specific cost of the initial investment (k$/kW). The results show that the two-stage ORC is economically attractive in wide ranges of values for these two parameters.

8.2 Recommendations and notes for further works

The present work has considered that the engine-generator sets are fuelled with natural gas (and a certain quantity of Light Fuel Oil as pilot injection) as justified in Sub-section 4.2.1. However, the engines are dual-fuel units so that they can be fuelled with fuel oil (FO) instead of natural gas. In this last case, the values of the thermal flow rates

rejected to the engines cooling systems would be higher as indicated in the “Machinery operating manual” of the ship. Exhaust gas temperature would be lower of about 40÷50°C in all engines loads if compared with the natural gas mode operation. Charge air temperature after the compressor would be higher due to the higher mass flow rate occurred in the FO mode operation. Note that the efficiency of the engine-generator sets is lower in FO mode. If the ORC system is designed to exploit the low grade waste heat rejected by the engines in natural gas mode operation but the engines operate in FO mode in some periods of the year or in certain phases of the voyage (e.g., staying in port) the ORC might still operate at equal engines power output due to the increase in available thermal flow rates to be exploited. This possibility might be interesting to be investigated.

Other analyses might consider to replace the actual FWGs with units based on different technologies (e.g., reverse osmosis) or fed by a different heat source in order to let available all the heat rejected by the engine-generator sets to the ORC system. This would simplify the design of the heat exchanger network which couples the ORC with the engines. Alternatively, a FWG might be designed to be fed by a water flow lower in temperature than that currently exploited in the ship. All these interventions would allow a higher net power to be generated by the ORC.

Section 5.3 has shown that the electric power demand of the vessel is most of the time significantly lower than the capacity of the ship power generating plant. This suggests that the LNG forced vaporizer might not be used during the laden and ballast voyage. Steam produced by the exhaust gas boilers (EGBs) might exceed the actual demand of the vessel. A further study might better investigate the actual steam needs of the vessel and the quantity provided by the EGBs. Steam might be considered as an additional thermal source for the ORC system. Moreover, the possibility to exploit the heat associated with the exhaust gas of the two main engines which are not equipped with an EGB should be investigated.

The study has investigated various ORC systems with respect to a particular operating condition of the engine-generator sets and FWGs. However, Section 5.2 has presented in detail the operating profile of the vessel which is composed of 22 operating conditions. A further study might conduct the comparison between cycles considering all the operating profile. This would require a steady-state off-design model of the ORC. The optimization problem might search for the optimum design parameters which allow the annual electricity generation to be maximized. A nested optimization problem might be defined to search for the optimum operating characteristics (e.g., speed of the pump, speed of the turbine) of the ORC which maximize the net power output in each off-design operating condition. A possible constraint for the “external” optimization problem might be the compliance of a minimum value for the ORC annual loading factor. This would allow to avoid over-sized ORC systems. A more interesting objective function that might

be considered for the “external“ optimization problem if an economic model (that include costing or cost equation) is introduced is the “present worth saving”.

The developed MATLAB scripts consider that the working fluid mass flow rate is equal to the maximum value that is allowed by pinch constraints. For each set of values assigned to the decision variables, the maximization of the ORC net power output leads to maximize the heat that is transferred from the sources to the working fluid. This approach leads to find solutions that are interesting from the thermodynamic point of view because of the close thermal coupling between hot and cold streams. However, if an accurate economic analysis is performed, the working fluid mass flow rate should be considered as a decision variable to be optimized. It might be possible to find that the optimum ORC design from the economic point of view is achieved with a mass flow rate lower than the maximum allowed. In fact, at constant evaporation pressure and temperature at expander inlet, the lower is the working fluid mass flow rate, the lower is the size of the heater (i.e., preheater, evaporator, super heater) because of the lower heat that has to be transferred and because of the higher mean temperature difference occurred in the thermal coupling.

Further studies should investigate the actual feasibility of the modifications proposed for the engines cooling systems according to the eventual limitations dictated by the manufacturer. Also, it should be considered the possibility of proposing an integrated design for the ORC cycle and the engine-generator sets.

Two documents related to the engine-generator sets state that the outlet temperature of the water flow belonging to the HT cooling circuit is 91°C when the engine load is 100%. In accordance with a third source the present work has considered a lower value for this temperature as reported in Table 4.4. However, it might be interesting to investigate the improvement in net power output of the ORC that is possible to achieve in case of the aforementioned higher heat extraction.

The work has considered that the condensation temperature of the working fluid in the various cycles is 30°C. As mentioned in Chapter 6, this value was selected considering that the sea-water temperature is equal to 25°C (ISO conditions). It might be interesting to perform a sensitive analysis of the net power output with respect to the condensation temperature.

More complex and performing heat recovery options for the ship generating plant might be found by investigating the possibility of replacing the existing waste heat recovery equipment (i.e., exhaust gas boilers, fresh water generators) with a single comprehensive heat recovery system including the ORC. These options might not be appropriate for retrofit of existing vessels but they could be considered for new installations.

References

Alfa Laval Desalt A/S (a), “Instruction manual for freshwater generator type JWP-26-C100”.

Alfa Laval Desalt A/S (b), “Installation and instruction manual for hot water loop type HWL 7-20...60-100”.

Andersen W.C., Bruno T.J. (2005), “Rapid Screening of Fluids for Chemical Stability in Organic Rankine Cycle Applications,” *Industrial & Engineering Chemistry Research*, Vol. 44, pp. 5560-5566.

Angelino G., Gaia M., Macchi E. (1984), “A review of Italian activity in the field of Organic Rankine Cycles,” *International VDI-Seminar*, Zürich, Switzerland, 10-12 September, VDI Berichte 539, pp. 465-481.

ASHRAE (2000), “ASHRAE Standard – Addenda to Designation and Safety Classifications of Refrigerants”.

Baik Y.J., Kim M., Chang K.C., Kim S.J. (2011) “Power-based performance comparison between carbon dioxide and R125 transcritical cycles for a low-grade heat source,” *Applied Energy*, Vol. 88, pp. 892–898.

Branchini L., De Pascale A., Peretto A. (2013), “Systematic comparison of ORC configurations by means of comprehensive performance indexes,” *Applied Thermal Engineering*, Vol. 61, pp. 129-140.

Calderazzi L., Colonna di Paliano P. (1997), “Thermal stability of R-134a, R-141b, R-13I1, R-7146, R-125, associated with stainless steel as a containing material,” *International Journal of Refrigeration*, Vol. 20, No. 6, pp. 381-389.

Calm J.M., Hourahan G.C. (2001), “Refrigerant data summary,” *Engineered Systems*, 18 (11), pp.74-88.

Calm J.M., Hourahan G.C. (2007), “Refrigeration data update,” *Heating/Piping/Air Conditioning Engineering*, 79 (1), pp. 50-64.

Chen H., Goswami D.Y., Stefanakos E.K. (2010), “A review of thermodynamic cycles and

working fluids for the conversion of low-grade heat," *Renewable and Sustainable Energy Reviews*, Vol. 14, pp. 3059-3067.

Choi B.C., Kim Y.M. (2013), "Thermodynamic analysis of a dual loop heat recovery system with trilateral cycle applied to exhaust gases of internal combustion engine for propulsion of the 6800 TEU container ship," *Energy*, Vol. 58, pp. 404-416.

Dai Y., Wang J., Gao L. (2009), "Parametric optimization and comparative study of organic Rankine cycle (ORC) for low grade waste heat recovery," *Energy Conversion and Management*, Vol. 50, pp. 576-582.

Desai N.B., Bandyopadhyay S. (2009), "Process integration of organic Rankine cycle," *Energy*, Vol. 34, pp. 1674-1686.

Di Genova K.J., Botros B.B., Brisson J.G. (2013), "Method for customizing an organic Rankine cycle to a complex heat source for efficient energy conversion, demonstrated on a Fischer Tropsch plant," *Applied Energy*, Vol. 102, pp. 746-754.

Dimopoulos G.D., Frangopoulos C.A. (2008), "Thermoeconomic Simulation of Marine Energy Systems for a Liquefied Natural Gas Carrier," *International Journal of Thermodynamics*, Vol. 11, No. 4, pp. 195-201.

EC (2009), "Regulation (EC) No 1005/2009 of the European Parliament and of the Council on substances that deplete the ozone layer" (recast), 16 September.

Fu W., Zhu J., Li T., Zhang W., Li J. (2013) "Comparison of a Kalina cycle based cascade utilization system with an existing organic Rankine cycle based geothermal power system in an oilfield," *Applied Thermal Engineering* Vol. 58, pp. 224-233.

Guo T., Wang H.X., Zhang S.J. (2011) "Fluids and parameters optimization for a novel cogeneration system driven by low-temperature geothermal sources," *Energy* Vol. 36, pp. 2639-2649.

He C. et al. (2012), "The optimal evaporation temperature and working fluids for subcritical organic Rankine cycle," *Energy*, Vol. 38, pp. 136-143.

Houghton T.J. et al., eds. (2001), "*Climate change 2001: the scientific basis*," Cambridge University press, Cambridge, UK. Chapter 6 "*Radiative forcing of climate change*," written by V. Ramaswamy V. et al.

Hung T.C., Shai T.Y., Wang S.K. (1997), "A Review of Organic Rankine Cycles (ORCs) for the Recovery of Low-Grade Waste Heat," *Energy*, Vol. 22, No. 7, pp. 661-667.

Invernizzi C., Iora P., Silva P. (2007), "Bottoming micro-Rankine cycles for micro-gas turbines," *Applied Thermal Engineering*, Vol. 27, pp. 100-110.

Karellas S., Leondaritis A.-D., Panousis G. (2012), "Heat transfer in organic Rankine cycle applications," Chapter 10 in "*Advances in Industrial Heat Transfer*," Minea A. A., ed., CRC Press.

Karellas S., Schuster A. (2008), "Supercritical Fluid Parameters in Organic Rankine Cycle Applications," *International Journal of Thermodynamics*, Vol. 11, No. 3, pp. 101-108.

Lakew A.A., Bolland O. (2010), "Working fluids for low-temperature heat source," *Applied Thermal Engineering*, Vol. 30, pp. 1262-1268.

Larsen U., Pierobon L., Haglind F., Gabrielli C. (2013), "Design and optimisation of organic Rankine cycles for waste heat recovery in marine applications using the principles of natural selection," *Energy*, Vol. 55, pp. 803-812.

Lazzaretto A., Manente G. (2013) "A criterion to optimize ORC design performance taking into account real turbine efficiencies," *26th International Conference on Efficiency, Cost, Optimization, Simulation and Environmental Impact of Energy Systems, ECOS 2013*, Guilin, China, 16-19 June.

Lazzaretto A., Toffolo A. (2008), "A method to separate the problem of heat transfer interactions in the synthesis of thermal systems," *Energy*, Vol. 33, pp. 163-170.

Lemmon E.W., Huber M.L., McLinden M.O. (2007), "NIST standard reference database 23: REFPROP - Reference fluid thermodynamic and transport properties," NIST, Physical and chemical properties division.

Linnhoff B. et al. (1994), "*A user guide on process integration for the efficient use of energy*," Institution of Chemical Engineers, Rugby, UK.

Liu B.T., Chien K.H., Wang C.C. (2004), "Effect of working fluids on organic Rankine cycle for waste heat recovery," *Energy*, Vol. 29, pp. 1207-1217.

Machinery operating manual of the ship

Macián V., Serrano J.R., Dolz V., Sánchez J. (2013), “Methodology to design a bottoming Rankine cycle, as a waste energy recovering system in vehicles. Study in a HDD engine,” *Applied Energy*, Vol. 104, pp. 758-771.

MARPOL (2002) Annex VI, Regulation 12 - Ozone Depleting Substances.

McNaught A.D., Wilkinson A. (1997), “*IUPAC. Compendium of Chemical Terminology, 2nd ed. (the "Gold Book)*,” Blackwell Scientific Publications, Oxford.

Mignini F. et al. (2004), “Individual susceptibility to hexavalent chromium of workers of shoe, hide, and leather industries. Immunological pattern of HLA-B8,DR3-positive subjects,” *Preventine Medicine*, No. 39, pp. 767-775.

Mikielewicz D., Mikielewicz J. (2010), “A thermodynamic criterion for selection of working fluid for subcritical and supercritical domestic micro CHP,” *Applied Thermal Engineering*, Vol. 30, pp. 2357-2362.

Öhman H., Lundqvist P. (2013), “Comparison and analysis of performance using Low Temperature Power Cycles,” *Applied Thermal Engineering*, Vol. 52, pp.160-169.

Papadopoulos A.I., Stijepovic M., Linke P. (2010), “On the systematic design and selection of optimal working fluids for Organic Rankine Cycles,” *Applied Thermal Engineering*, Vol. 30, pp. 760-769.

Quoilin S. et al. (2013), “Techno-economic survey of Organic Rankine Cycle (ORC) systems,” *Renewable and Sustainable Energy Reviews*, Vol. 22, pp. 168-186.

Saidur R., Rezaei M., Muzammil W.K., Hassan M.H., Paria S., Hasanuzzaman M. (2012), “Technologies to recover exhaust heat from internal combustion engines,” *Renewable and Sustainable Energy Reviews*, Vol. 16, pp. 5649-5659.

Sauret E., Rowlands A.S. (2011), “Candidate radial-inflow turbines and high-density working fluids for geothermal power systems,” *Energy*, Vol. 36, pp. 4460-4467.

Schuster A., Karellas S., Kakaras E., Spliethoff H. (2009), “Energetic and economic investigation of Organic Rankine Cycle applications,” *Applied Thermal Engineering*, Vol. 29, pp. 1809-1817.

Schuster A., Karellas S., R. Aumann (2010), “Efficiency optimization potential in

supercritical Organic Rankine Cycles," *Energy*, Vol. 35, pp. 1033-1039.

Shengjun Z., Huaixin W., Tao G. (2011), "Performance comparison and parametric optimization of subcritical Organic Rankine Cycle (ORC) and transcritical power cycle system for low-temperature geothermal power generation," *Applied Energy*, Vol. 88, pp. 2740-2754.

Shu G. et al. (2013), "A review of waste heat recovery on two-stroke IC engine aboard ships," *Renewable and Sustainable Energy Reviews*, Vol. 13, pp. 385-401.

Shu G., Zhao J., Tian H., Liang X., Wei H. (2012), "Parametric and exergetic analysis of waste heat recovery system based on thermoelectric generator and organic Rankine cycle utilizing R123," *Energy*, Vol. 45, pp. 806-816.

Smolen S. (2011), "Simulation and thermodynamic analysis of a two-stage organic Rankine cycle for utilisation of waste heat at medium and low temperature Levels," *Energy Science and Technology*, Vol. 1, No. 1, pp. 64-78.

Solomon S., Mills M., Heidt L.E., Pollock W.H., Tuck A.F. (1992), "On the Evaluation of Ozone Depletion Potential," *Journal of Geophysical Research*, Vol.97, No. D1, pp. 825-842.

Sprouse C., Depcik C. (2013), "Review of organic Rankine cycles for internal combustion engine exhaust waste heat recovery," *Applied Thermal Engineering,* Vol. 51, pp. 711-722.

Tchanche B.F., Lambrinos Gr., Frangoudakis A., Papadakis G. (2011), "Low-grade heat conversion into power using organic Rankine cycles. A review of various applications," *Renewable and Sustainable Energy Reviews*, Vol. 15, pp. 3963-3973.

Tien W.K., Yeh R.H., Hong J.M. (2007), "Theoretical analysis of cogeneration system for ships," *Energy Conversion and Management*, Vol. 48, pp. 1965-1974.

Toffolo A., Lazzaretto A., Manente G., Paci M. (2012), "An Organic Rankine Cycle off-design model for the search of the optimal control strategy," 25th *International Conference on Efficiency, Cost, Optimization, Simulation and Environmental Impact of Energy Systems, ECOS 2012*, Perugia, Italia, 26-29 June.

Toffolo A., Lazzaretto A., Manente G., Rossi N. (2010), "Synthesis/Design Optimization of Organic Rankine Cycles for Low Temperature Geothermal Sources with HEATSEP Method," *23rd International Conference on Efficiency, Cost, Optimization, Simulation and Environmental Impact of Energy Systems, ECOS 2010*, Lausanne, Switzerland, 14-17 June.

Vaja I., Gambarotta A. (2010), "Internal Combustion Engine (ICE) bottoming with Organic Rankine Cycles (ORCs)," *Energy*, Vol. 35, pp. 1084-1039.

Wang D., Ling X., Peng H., Liu L., Tao L.L. (2013), "Efficiency and optimal performance evaluation of organic Rankine cycle for low grade waste heat power generation," *Energy*, Vol. 50, pp. 343-352.

Wang E.H., Zhang H.G., Zhao Y., Fan B.Y., Wu Y.T., Mu Q.H. (2012), "Performance analysis of a novel system combining a dual loop organic Rankine cycle (ORC) with a gasoline engine," *Energy*, Vol. 43, pp. 385-395.

Wang T., Zhang Y., Peng Z., Shu G. (2011), "A review of researches on thermal exhaust heat recovery with Rankine cycle," *Renewable and Sustainable Energy Reviews*, Vol. 15, pp. 2862-2871.

Wang Z.Q., Zhou N.J., Guo J., Wang X.Y. (2012), "Fluid selection and parametric optimization of organic Rankine cycle using low temperature waste heat," *Energy*, Vol. 40, pp. 107-115.

Wärtsilä (2009), "Boosting energy efficiency," February.

Wärtsilä (2012), "Wärtsilä 50DF product guide," Issue 1, December.

Wuebbles D.J. (1983), "Chlorocarbon emission scenarios: potential impact on stratospheric ozone," *Journal of Geophysical Research*, Vol. 88, No. C2, pp. 1433-1443.

Yamamoto T., Furuhata T., Arai N., Mori K. (2001), "Design and testing of the organic Rankine cycle," *Energy*, Vol. 26, pp. 239-251.

Yu G., Shu G., Tian H., Wei H, Liu L. (2013), "Simulation and thermodynamic analysis of a bottoming Organic Rankine Cycle (ORC) of diesel engine (DE)," *Energy*, Vol. 51, pp. 281-290.

Zhang H.G., Wang E.H., Fan B.Y. (2013), “A performance analysis of a novel system of a dual loop bottoming organic Rankine cycle (ORC) with a light-duty diesel engine,” *Applied Energy*, Vol. 102, pp. 1504-1513.